BOOK OF ABSTRACTS

The 4th International Conference on Nanomaterials: Fundamentals and Applications

November 10-11, 2020 Online conference

Organized by:

Department of Physical Chemistry
Faculty of Natural Science
Pavol Jozef Šafárik University in Košice
&
Slovak Chemical Society

Bratislava

Edited by: Jana Shepa, Pavol Jozef Šafárik University in Košice, Institute of Chemistry, Moyzesova 11, 040 01 Košice, Slovakia, jana.hovancova@student.upjs.sk
Ivana Šišoláková, Pavol Jozef Šafárik University in Košice, Institute of Chemistry, Moyzesova 11, 040 01 Košice, Slovakia, ivana.sisolakova@upjs.sk

Reviewed by: Renáta Oriňaková, Pavol Jozef Šafárik University in Košice, Institute of Chemistry, Moyzesova 11, 040 01 Košice, Slovakia, renata.orinakova@upjs.sk
Andrea Straková Fedorková, Pavol Jozef Šafárik University in Košice, Institute of Chemistry, Moyzesova 11, 040 01 Košice, Slovakia, andrea.fedorkova@upjs.sk

Available at: https://unibook.upjs.sk
Publication date: 19.11.2020

ISBN 978-80-8152-941-2

LIST OF CONTENTS

LIST OF AUTHORS

Preface

The 4th International Symposium on Fundamentals and Application

The decision to hold the 4th symposium NFA - Nanomaterials: Fundamentals and Application in November 2020 was made because the previous three (2017, 2015 and 2012) had proved that there was a real need for giving scientists and engineers a combined forum to discuss the nanomaterials preparation and analysis of materials and associated problems from their various points of view. Another reason was that there have been many advances in chemical and physical technology, vital to the discovery, production and characterization of materials. Due to the current critical epidemiological situation, we decided to organize this year's conference online. This is why number of participant is just symbolic but with strength in presentation. Novel knowledge will be presented from a field: models in catalysis and technology use, changed of structures under electron beam, and PEGylated alginate carrier.

As with the past three symposia in the series the Slovak Chemical Society again agreed that the symposium could be held under its aegis. This organization has always supported the principle of free communication among bona fide scientists, but for the time in many years, nearly every country in the world allowed their scientists to travel to Slovakia.

We believe in virtual enthusiastic discussions, the constructive arguments and suggestions and the establishment of friendship ties between delegates from all corners of the globe.

The organizers are most grateful, not only to Slovak Chemical Society for its unfailing support over the years, but also to those people, authorities, and organizations that made it possible to hold this symposium.

I wish all participants enjoy this virtual meeting to collect new information form nanoscience. And WELCOME at the next year's conference in the High Tatras **from 10th to 13th October 2021**!

Andrej Oriňak

Turning streetwear into solar power plants

Ready-to-wear solar cells ...

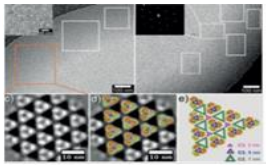

Nanopatterns of proteins detected by cryo-electron microscopy

Nanostructures for electronics, catalysis, medicine ...

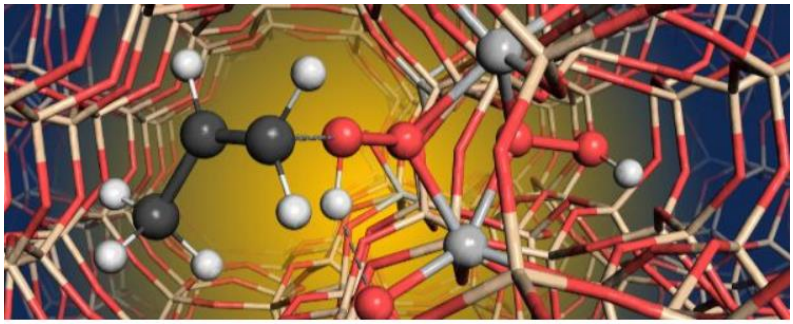

A 40-year-old catalyst unveils its secrets

Findings will help catalyst research take an important step forward

"Titanium silicalite-1" (TS-1) is not a new catalyst: It has been almost 40 years since its

First principles perspective on nanostructures in catalysis

K. Honkala[a*]

[a]Department of Chemistry, Nanoscience Center, University of Jyväskylä, Finland
[*] karoliina.honkala@jyu.fi

Density functional theory calculations (DFT) together with different multiscale strategies are nowadays extensively used to explain and predict the catalytic properties variety of nanostructures. In my presentation, I will give examples on our recent efforts in these fields.

Recent studies demonstrate that single atom catalysts can efficiently catalyze many chemical reactions. Employing DFT calculations, we have evaluated thermodynamic and kinetic stabilities of Rh and Pt single atoms with and without CO atmosphere on ZrO_2. Our results show that bae subnanoclusters are more stable than single atoms and become more so with increasing size meaning that acclomeration is always favored. CO binds strongly to the single atoms and clusters, and our atomistic thermodynamics treatment indicates that some CO will be present even at ultra-high vacuum conditions. A CO atmosphere is shown to hinder cluster growth from single atoms, and is even capable of spontaneous cluster disintegration in the case of Pt clusters.

The second example deals with the optimization of Rh and Pt clusters on ZrO_2 [2]. Herein, we combined DFT calculations with genetic algorithm to optimize cluster structures. The reactivity of these structures towards a water-gas-shift [3] reaction have been studied anlysing the binding properties of CO [2] and H_2O [4]. We find that metal-oxide perimeter sites are structurally different presenting varying Pt and Rh co-ordinations and CO adsorption energies. Our analysis shows that the presence of a support always destabilizes CO adsorption at the cluster edge but the magnitude of destabilization varies substantially from site to site. We also find that the metal-oxide interface activate water, but the dissociation behavior varies considerably between sites. It is shown that the studied clusters break scaling relationships for water dissociation, suggesting these catalysts may achieve activities beyond the maximum imposed by such relations. Overall, our results highlight the uniqueness of interfacial sites in catalytic reactions, and the need for developing new concepts and tools to deal with the associated complexity.

References

[1] M. Kauppinen, M. Melander, and K. Honkala Catal. Sci Tech. 10, 5847 (2020).

[2] A. Bazhenov and K. Honkala J. Phys. Chem. C 123, 7209 (2019).

[3] M.M. Kauppinen, M.M. Melander, A.S. Bazhenov, and K. Honkala ACS Catal. 8, 11633

(2018).

[4] M. Kauppinen, V. Korpelin, A.M. Verma, M. Melander, and K. Honkala J. Chem. Phys. 151, 164302 (2019).

Two-dimensional nanomaterials: research and applications

M. Omastová[a,*], M. Mičušík[a], N. Bugárová[a], Y. Soyka[a], A. Aniskevich[b], D. Zeleniakiene[c]

[a] Polymer Institute SAS, Dubravska cesta 9, 845 41 Bratislava, Slovakia
[b] Institute for Mechanics of Materials, University of Latvia, Jelgavas Str. 3, Riga, LV-1004, Latvia
[c] Department of Mechanical Engineering, Kaunas University of Technology, Studentu Str. 56, 51424, Kaunas, Lithuania
*maria.omastova@savba.sk

The discovery of graphene [1] motivated the scientific community to prepare and study other new two-dimensional (2D) materials. The current intense interest about 2D materials is due to their unique properties resulting from their structure. They offer highly specific surface area as well as electronic structures that can achieve new interesting properties. Graphene and/or graphene oxide particles are intensively studied as promising candidates for various applications as materials for energy storage, photovoltaics, electrical and optical sensors, etc. Graphene based biosensors, including modified graphene oxide (GO) particles are intensively studied nowadays. In particular, the hydrophilic character of GO permits the manufacture of reliable, highly sensitive and ultrafast biosensing nanoplatforms.

MXenes are a new class of 2D inorganic materials, discovered by Barsoum and his group in 2011 [2]. MXenes are prepared from MAX phases of the formula $M_{n+1}AXn$, where M is the most common transition metal, A is an element of the 13 or 14 group of the periodic table, and X is usually C and/or N. By etching of the A layers from MAX phase, MXene are formed. The process of etching caused that surface of MXenes contains functional groups e.g., -O, -F, -OH, and hydrophilicity of these 2D particles.

In this work modification of GO and MXene was studied, and application examples of these 2D fillers will be demonstrated.

A new type of graphene-oxide multifunctional nanoplatform was prepared for the detection of tumor cells. In a first step, GO nanolayers were prepared and functionalized with magnetic nanoparticles and a monoclonal antibody (MAb) specific for CA IX cancer marker. Prepared GO platforms were characterized in terms of oxidation, nanoparticle size and exfoliation, using various physical and chemical methods. Magnetic nanoparticles (MNps) were prepared by the chemical precipitation method and their surface was modified by poly-L-lysine. CA IX-specific antibody was attached via an amide bond to a modified magnetic nanoparticle that was conjugated to the GO platform again via an amide bond. After performing toxicological tests on a cell line, no effect of the cytotoxicity of the multifunctional GO platforms was found. The selectivity of GO-MNps-MAb platforms to target tumor cells has been demonstrated. The results also provided promising evidence of tumor cell targeting with a wide potential for visualization and future tumor treatment [3].

$Ti_3C_2T_z$ MXenes were prepared by the hydrochloric acid/lithium fluoride etching of MAX phase type Ti_3AlC_2. The characterisation of MXenes, and MXene coatings was carried out with XPS, AFM, and SEM analyses [4]. The stability of MXene layers was study within few months by conductivity measurement.

Experimental condition of MAX phase etching and methods of MXene preparation significantly influence the final electrical conductivity of MXenes [5]. It is found that the high electrical conductivity and mobility of MXene can accelerate the charge transfer, what opened opportunities for the use of MXene as potential materials solar cell applications, in batteries and supercapacitors**.**

Acknowledgements

This project has received funding from the European Union's Horizon 2020 research and innovation programme under the Marie Skłodowska-Curie grant agreement No 777810, and by project APVV 14-0120 (Slovakia).

References

[1] K.S. Novoselov, A.K. Geim, S.V. Morozov, D. Jiang, Y. Zhang, S.V. Dubonos, I.V. Grigorieva, A.A. Firsov. Science. 306 (2004) 666-669.

[2] M. Naguib, M. Kurtoglu, V. Presser, J. Lu, J. Niu, M. Heon, L. Hultman, Y. Gogotsi, M. W. Barsoum. Adv. Materials, 23 (2011) 4248-4253.

[3] N. Bugárová, Z. Špitálsky, M. Mičušík, M. Bodík, P. Šiffalovič, M. Koneracká, V. Závišová, M. Omastová, et.al. Cancers, 11 (2019) art. no. 753.

[4] V. Gajdošová. L. Lorencová, M. Procházka, M. Mičušík, M. Omastová, S. Procházková, F. Kvetoň, M. Jerigová, D. Velič, P. Kasák, J. Tkáč. Microchimica Acta. 187, (2020) art. no. 52.

[5] K. Zukiene, G. Monastyreckis, S. Kilikevicius, M. Prochazka, Micusik, M. Omastova, A. Aniskevich, D. Zeleniakiene. Mat. Chem. Phys. 257 (2021) 123820.

On the use of the ICA technique for EV-battery SOH estimation

D-I. Stroe[a*], A. Gismero[a], E. Schaltz[a]

[a]Department of Energy Technology, Aalborg University, 9220 Aalborg Øst, Denmark
*dis@et.aau.dk

Introduction

Electric vehicles (EVs) have developed as a key technology in the transition to a sustainable and fossil fuel-free future. Because of their advantages in terms of energy density, power capability, and lifetime in comparison to other battery technologies, Lithium-ion batteries are powering the majority of the EVs available in the market. Nevertheless, as in the case of all energy storage devices, the performance of Li-ion batteries (e.g., capacity, power capability etc.) is degrading in time during long-term operation [1]. In the case of a Li- ion battery-powered EV, this will result in reduced range and acceleration capability. Furthermore, the battery is the most expensive component of the EV and subsequently the value of the EV is given by the state of the battery. Thus, it becomes obvious that the state-of-health (SOH) of the battery has to be estimated from both technical and economic perspectives.

Different methods for battery SOH estimation have been proposed [2]; each of them with their advantages and drawbacks. However, in this work we propose the incremental capacity analysis (ICA) technique for estimating the SOH of EV -batteries because it requires only the current and voltage signals measured during constant-current charging of the battery. Thus, there is no need for special measurement equipment as it is the case of the electrochemical impedance spectroscopy.

Dubarry et al. firstly proposed the ICA technique, as a method for identifying aging mechanisms, which cause the capacity fade of the battery [3]. The method relies in differentiating the battery charging capacity against the voltage. In the newly obtained incremental capacity (IC) curve, the voltage plateaus, which are characteristic to the charging voltage curve, are transformed into visible IC peaks and valleys as illustrated in Fig. 1.

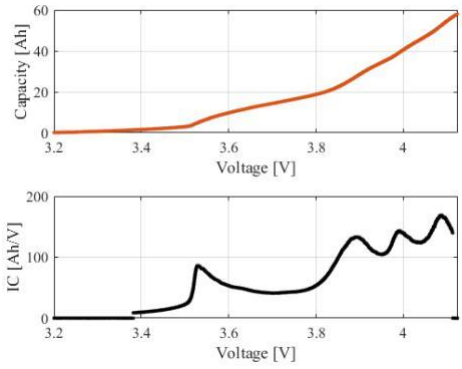

Figure 1 Battery capacity (top) and IC (bottom) as a function of voltage.

In this paper, we demonstrate the applicability of the ICA technique as a method for SOH estimation of EV Li-ion batteries by successfully comparing the ICA results obtained at both cell- and car-level.

Experimental Set-Up

A Li-ion battery pack (see Fig. 2) from a market available EV was dissembled and the twelve NMC-based Li-ion batteries were aged at various calendar and cycle aging conditions. the aging tests were stopped and the capacity of each cell was measured at 25°C using a 0.2C-rate current (i.e., 12.6 A), as presented in Fig. 3. For more details regarding the calendar aging tests, the reader is referred to [4].

Figure 2 Disassembeled EV battery pack.

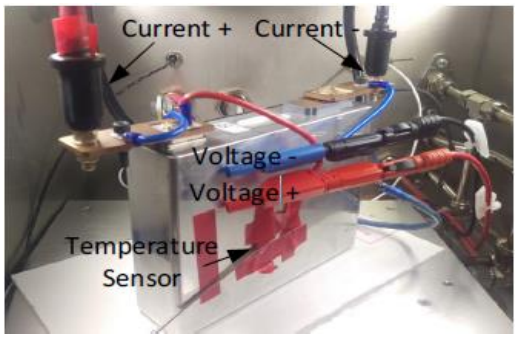

Figure 3 EV battery cell during capacity measurement.

Results at cell level

The ICA technique was applied to all the charging capacities measured on the twelve cells during the aging tests. An example of the ICA plots behavior obtained during 12 months of calendar aging at 50% SOC and 40°C is presented in Fig. 4. Similar results were obtained for all the other cells.

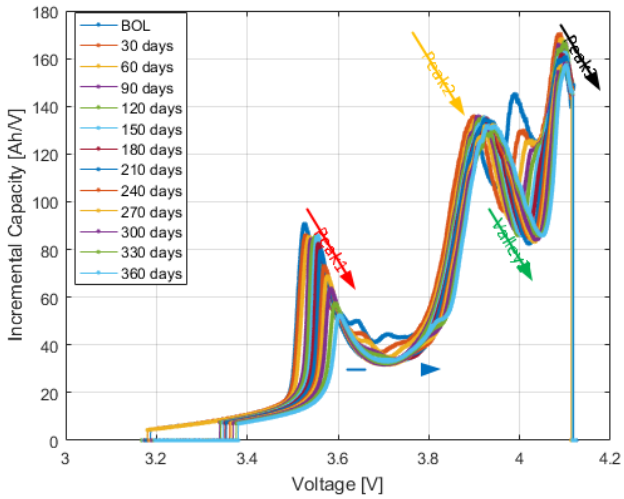

Figure 4 Evolution of the IC plots during 12 months of calendar aging.

As it can be observed in Fig. 4, different metric points (i.e., IC peaks and IC valleys) are highlighted. The position of all these metric points is changing, while the aging process evolves. Thus, they can be considered as features, which can be used for battery SOH estimation.

The relationship between the capacities of the calendar and cycling aged cells and the coordinates of the IC Peak 1 are presented in Fig. 5 and Fig. 6. There is a good correlation between the capacity fade of the cells, and the evolution of the location of both the voltage coordinate (see Fig. 5) and IC coordinate (see Fig. 6.), in the case of Peak 1; however, the voltage coordinate estimates better the battery capacity, which was measured with 0.2C.

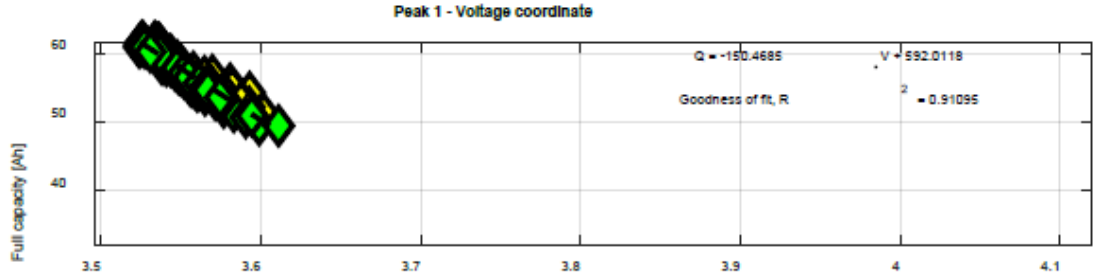

Figure 5 Battery capacity fade as a function of the voltage coordinate corresponding to Peak 1.

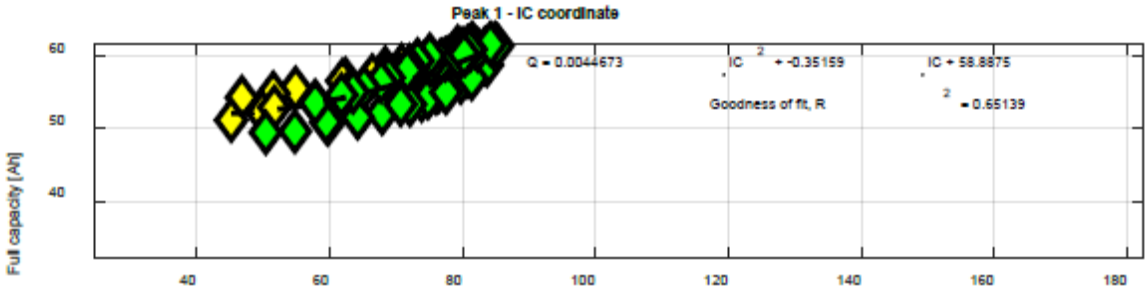

Figure 6 Battery capacity fade as a function of the IC coordinate corresponding to Peak 1.

Similar investigations were performed for all the observed peaks and valleys and we found out that it is mainly the voltage coordinate of the IC metric points (i.e., peaks and valleys) that estimates with higher accuracy the capacity of the tested NMC-based EV battery cells.

Results at car level

The ICA technique was also applied at car level as presented in Fig. 7. Due to the limitations imposed by the battery management systems (BMS), the allowed voltage interval for performing the capacity measurement was 3.55 V – 4.1 V (while at cell level 3 V – 4.125 V). The obtained ICA plots for five measurements at car level are presented in Fig. 8. In order to be able to compare the results at cell and care level, the voltage at car level was down scaled to the values at cell level. A good agreement between ICA results obtained at car and cell level can be observed.

Figure 7 Test setup for capacity measurement on EV battery.

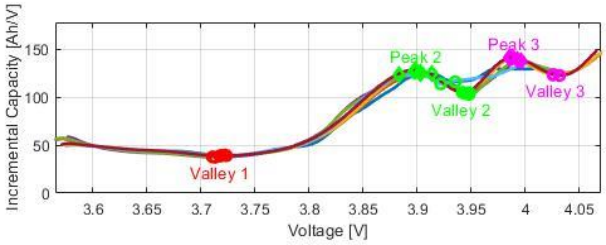

Figure 8 IC as a function of voltage obatined for EV battery (voltage scaled to cell level).

Conclusions

In this work, we demonstrate the feasibility of applying the ICA technique for the SOH estimation of EV batteries. Very similar IC plots can be obtained at both cell and car level, even though the BMS of the EV battery does not allow a full charging of the battery (as it can be performed in laboratory conditions).

Acknowledgements

This work has been part of the Adaptive Battery Diagnostic Tools for Lifetime Assessment of EV batteries (BATNOSTIC) research and development project, project no. 64015-0611. The authors gratefully acknowledge EUDP Denmark for providing the financial support necessary for carrying out this work.

References

[1] M. Ecker et al., Journal of Power Sources 215 (2012) 248-257.

[2] M. Berecibar et al., Renewable and Sustainable Energy Reviews 56 (2016) 572-587.
[3] M. Dubarry, V. Svoboda, R. Hwu, and B. Yann Liaw, Electrochem. Solid-State Lett. 9 (2006) A454–A457.
[4] D.-I. Stroe, E. Schaltz, IEEE Trans. Ind. Appl. 56 (2020) 678-685.

 ISBN 978-80-8152-941-2

Nonenzymatic sensor for determination of glucose modified by gold nanoparticles

V. Niščáková[a]*, J. Shepa[a], R. Oriňaková[a]

[a] Department of Physical Chemistry, Faculty of Science, P. J. Šafarik University in Košice, Moyzesova 11, 041 54, Košice
*veronika.niscakova@student.upjs.sk

Worldwide, diabetes is the most common disease. To avoid complications with this disease, patients monitor and control their blood glucose levels [1]. The key goal of reducing problems with diabetes is to measure the patient´s blood glucose concentration, based on which a significant number of enzymatic and non-enzymatic electrochemical glucose sensors have been investigated [2].

In this work we prepared a sensor for the glucose determination and we subsequently characterized surface and electrochemical performance of this sensor. We prepared this sensor by a simple electrochemical deposition of gold nanoparticles on Au microelectrode. The surface morphology of this modified electrode was studied by a scanning electron microscopy and atomic force microscopy. We observed the formation of spike-like nanostructures, which were homogeneously distributed on the surface (Fig. 1), increased the surface area of electrode, and showed the best catalytic activity. We used three different methods to study performance of electrodes: cyclic voltammetry, chronoamperometry and electrochemical impedance spectroscopy. Modified electrode exhibited good electrocatalytic activity toward oxidation of glucose in two linear ranges from 0.1 mM to 0.5 mM and from 0.5 mM to 30 mM, high sensitivity for both linear ranges 1.7 μA/mM and 2.4 μA/mM, and stability. Moreover, the modified electrode showed a good selectivity and suitability for use in real samples.

14

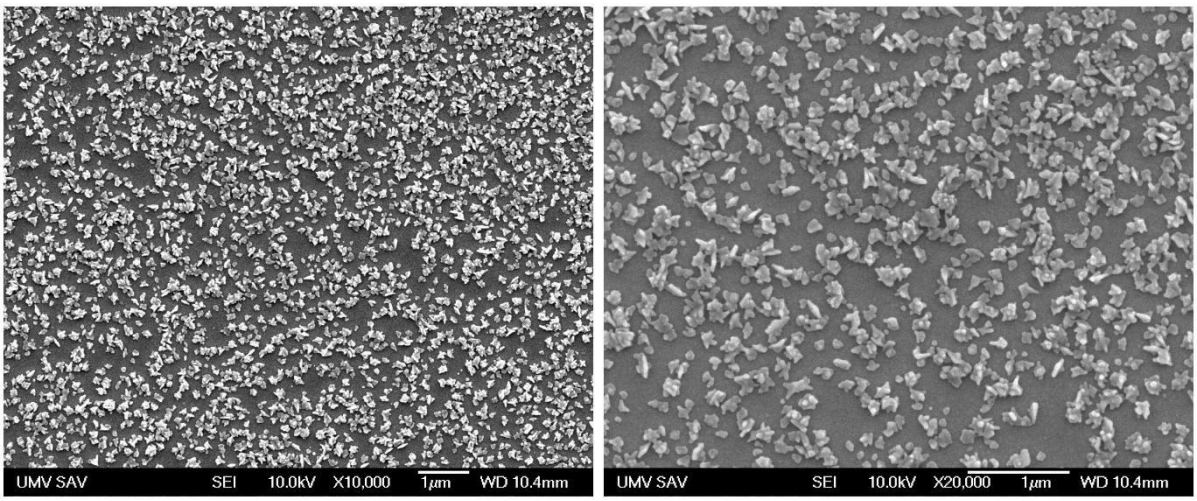

Figure 1 SEM images of Au microelectrodes modified with spike-like nanostructures deposited at -0.2V potential,

Magnification: 10,000x and 20,000x scale: 1μm.

 ISBN 978-80-8152-941-2

Acknowledgements

This work was supported by the projects VEGA 1/0074/17 of the Slovak Scientific Grant Agency, and APVV-16-0029 of the Slovak Research and Development Agency.

References

[1] K.J. Cash, H.A. Clark, Trends Mol. Med. 16 (2010) 584–593.

[2] R.J. Forster, L.R. Cumba, Optimizing glucose sensing for diabetes monitoring, in: Bioelectron. Med. Devices, Elsevier Ltd, 2019: pp. 765–778.

 ISBN 978-80-8152-941-2

NiAg nanocavity films for SERS detection of organic dyes

O. Petruš[a]*, J. Macko[b], R. Oriňaková[b], V. Socha[c]

[a] Institute of Materials Research, Slovak Academy of Sciences, Watsonova 47, 040 01 Košice, Slovakia
[b] Department of Physical Chemistry, University of P. J. Šafárik in Košice, Moyzesova 11, 040 01 Košice, Slovakia
[c] Department of Air Transport, Czech Technical University in Prague, Horská 3, 128 03, Prague, Czech Republic
*opetrus@saske.sk

Since the 1980s, the USA, EU, China, and other countries have been making efforts to reduce the utilization of organic dyes in the industry; however, they are still illegally used in many countries due to their low cost and high efficiency [1]. Nowadays, the industry produces many contaminants such as the by-products during the production of paper, textile but also pharmaceutical products. About 200 tonnes of organic dyes per month are still used as a feedstock in these industries [2]. Surface Enhanced Raman Spectroscopy (SERS) is a suitable technique to detect a very low concentration of organic molecules using nanostructured films or nanoparticles to enhancement analytical signal. In our study, we prepare the NiAg nanocavity films by colloidal lithography using 518 nm polystyrene sphere mask followed by two steps electrochemical deposition of Ni film and Ag nanoparticles. As probe analytes, we selected rhodamine 6G (R6G), crystal violet (CV), methylene blue (MB), and malachite green oxalate (MGO) which are used in many industries as dyes, fungicides etc. NiAg nanocavity films show high hydrophobicity with contact angle 140.2° ± 6.1°. Due to this fact, the analytes can be preconcentrated to the small spot on the sample. SERS activity was tested with 532 nm laser excitation source with different concentrations of dyes. Figure 1 shows concentration dependence range from 1.10^{-5} to 1.10^{-12} mol.dm^{-3} for R6G and from 1.10^{-5} to 1.10^{-10} mol.dm^{-3} for CV, MB and MGO. The RSD for R6G, CV, MB, and MGO was 20.1%, 13.8%, 16.7%, and 19.3%, and the detection limit was 1.3×10−12, 1.5×10−10, 1.4×10−10, 7.5×10−11 mol.dm-3, respectively. Finally, we performed the principal component analysis to extract the differences in complex spectra of the dyes where the first and second PCs carry 42.43 % and 31.39 % of the sample variation, respectively. The achieved results demonstrated the suitability of AgNi nanocavity films for the SERS-based detection of organic dyes, with a potential in other sensing applications.

16

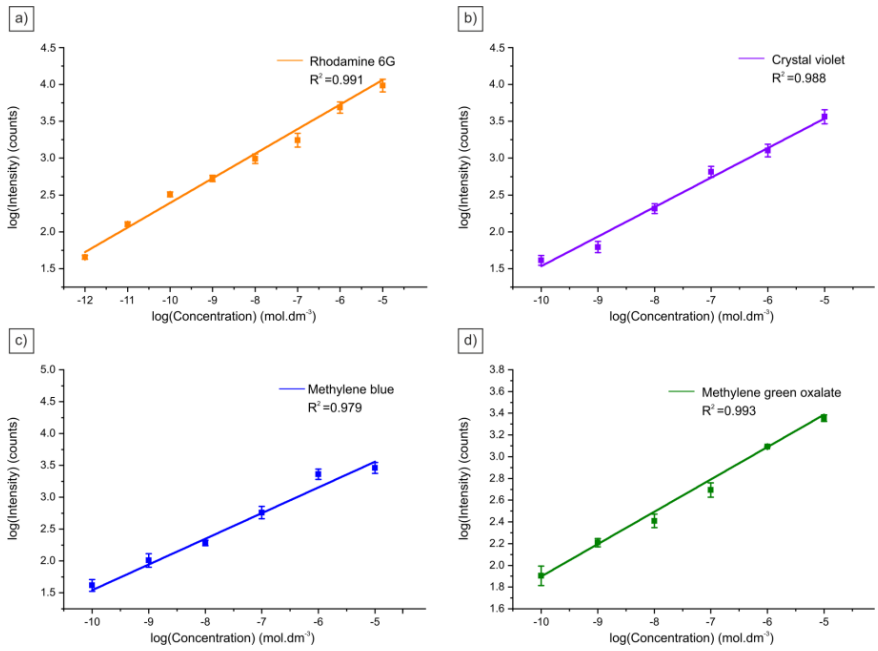

 ISBN 978-80-8152-941-2

Figure 1 Plot of logarithmic signal intensity vs. logarithm of dyes concentration for the characteristic peaks of R6G, CV, MB, and MGO at 1646, 1175, 1617, and 1615 cm-1, respectively.

Acknowledgements

This research was financially supported by projects VEGA 1/0074/17 of the Slovak Scientific Grant Agency, APVV-16-0029 of the Slovak Research and Development Agency.

References

[1] L. Pei, Y. Huang, C. Li, Y. Zhang, B.A. Rasco, K. Lai, J. Nanomater. 2014 (2014) 8.

[2] R.S. Lodhi, N. Lal, Int. Res. J. Eng. Technol. 4 (2017) 121–131.

 ISBN 978-80-8152-941-2

New approach to TiO_2 based glucose sensors

J.Shepa[a]*, I. Šišoláková[a], R. Oriňaková[a]

[a] Pavol Jozef Šafárik University in Košice, Moyzesova 11, 040 01 Košice, Slovakia
*jana.hovancova@student.upjs.sk

Diabetes mellitus is group of metabolic diseases which growing prevalence is certainly to be one of the most challenging problems in the 21st century [1]. A stable and cost-effective detection of glucose is of significant importance in medicine and industry [2]. Titaniun dioxide is widely used material, its properties depend on the morphology, crystallinity, and polymorph type [3]. However, from the sensors point of view, the most important ability is the formation of ligant-to-metal charge transfer complex with glucose molecule [4]. According to this property, one could expect that TiO_2 nanostructure could have comparable selectivity to an enzymatic sensor, but overcome the typical drawbacks accompanying these sensors. It can be stated that TiO_2 is the most promising material for non-enzymatic glucose sensors development.

The aim of this work was to study properties of TiO_2 nanotubes as a very promising material for glucose detection. The principle of TiO_2 glucose sensors is shown in the figure1. The TiO_2 – glucose ligant-to-metal charge transfer complex formation was proved via infrared, Raman, and X-ray photoelectron spectroscopy. The electrochemical impedance spectroscopy was applied as a promising analytical method to study surface phenomena and the bulk properties [5]. To the best our knowledge, this kind of sensor has never been studied especially in the case of non-enzymatic glucose detection. TiO_2 sensor displays wide linear range from 1 to 15 mM in a pH neutral condition. The sensors display good reproducibility and repeatability. Moreover, TiO_2 sensors show good sensitivity 8.3 $k\Omega.mM^{-1}$ and low limit of detection 1.2 mM. Therefore, this kind of sensors is promising candidate for blood glucose sensing and could replace the enzymatic glucose sensors.

 ISBN 978-80-8152-941-2

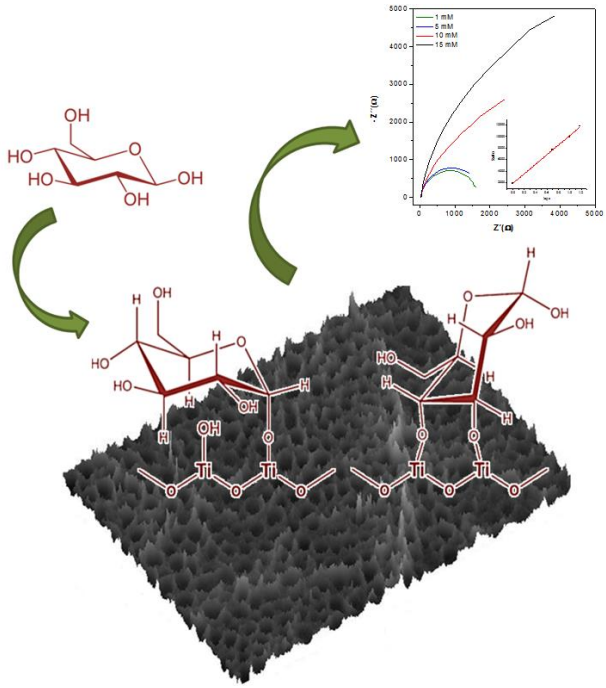

Figure 2 Graphical interpretation of TiO_2 non-enzymatic glucose sensor principle.

Acknowledgements

This work has been supported by the projects VEGA 1/0074/17 of the Slovak Scientific Grant Agency, APVV-16-0029 and APVV-PP-COVID-20-0036 of the Slovak Research and Development Agency, and Visegradfund project number 22020140.

References

[1] S.Y. Tee, C.P. Teng, E. Ye, Mater. Sci. Eng. C. 70 (2016) 1018–1030.

[2] J. Hovancová, I. Šišoláková, R. Oriňaková, A. Oriňak, J. Solid State Electrochem. 21 (2017) 2147–2166.

[3] G.K. Mor, O.K. Varghese, M. Paulose, K. Shankar, C.A. Grimes, Sol. Energy Mater. Sol. Cells. 90 (2006) 2011–2075.

[4] W. Macyk, K. Szaciłowski, G. Stochel, M. Buchalska, J. Kuncewicz, P. Łabuz, Coord. Chem. Rev. 254 (2010) 2687–2701.

[5] Y. Ram, T. Yoetz-Kopelman, Y. Dror, A. Freeman, Y. Shacham-Diamand, Electrochim. Acta. 200 (2016) 161–167.

 ISBN 978-80-8152-941-2

Electrochemical determination of insulin on nanomodified screen printed carbon electrodes

I. Šišoláková[a]*, J. Shepa[a], F. Chovancová[a], R. Oriňaková[a]

[a] [a] Department of Physical Chemistry, Faculty of Science, Pavol Jozef Šafárik University, Moyzesova 11, 04011 Košice, Slovak Republic
*ivana.sisolakova@upjs.sk

Diabetes mellitus (DM) is a heterogeneous metabolic disease characterized by chronic hyperglycemia. Often, the symptoms are not sufficiently observable at early stages and so hyperglycemia causes that pathological and functional changes take place in advance, before the diagnosis of the disease. Therefore, the development of sensors that are time saving, accurate, instrumentally undemanding are currently unavoidable. Currently, third generation of glucose sensors are udes for diabetes diagnosis. The huge disadvantage of these sensors are pH and temeprature stability limitation arising from the properties of the used enzyme. Mentioned senosrs are stable only in pH range 4-8 and they are unstable at the temperature over 40°C. Therefore, research is currently focused on the development of a new sensor for insulin determination withou biological component. Screen printed carbon electrodes (SPCEs) can be considered as a most suitable material for diabetes diagnosis because of the small size of working electrode leads to analysts volume reduction [1-3]. The surface of bare SPCE was modified by combination of chitosan, multi walled carbon nanotubes (MWCNTs), and zinc nanoaprticles (ZnNPs). ZnNPs were electrochemically deposited on the chitosan.MWCNTs/SPCE surface via pulse depoition method. Thereafter, insulin was determined on the prepared electrode using chornoamperometry method (Figure 1). The measurement was performed by adding a constant amount of insulin in 0.1 M NaOH and PBS (2 µl) with the same concentration (2 µM) and the current response of the system was monitored after a gradual increase in concentration. Subsequently, the limit of detection of the prepared electrode was determined via Randles-Ševčík equtaion. The LOD was calculated as 0.47 µM. This value make the ZnNPs/chitosan-MWCNTs/SPCE as a potential candidate for future insulin determination.

20

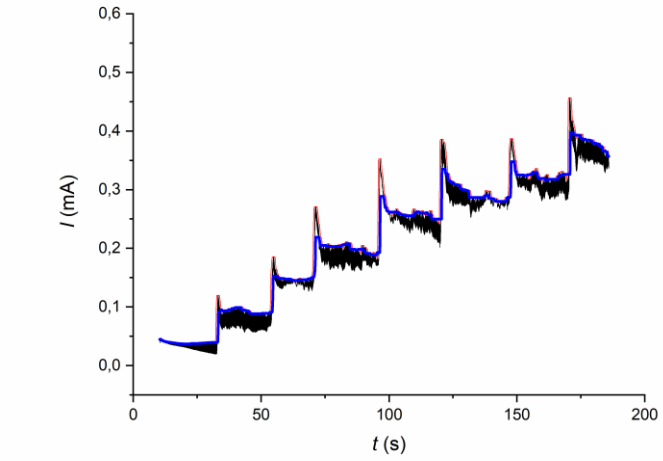

Figure 1 The current-time response curve for the successive addition of 2 µM insulin in 0.1 M NaOH and PBS.

 ISBN 978-80-8152-941-2

Acknowledgements

This work has been supported by the projects VEGA 1/0074/17 of the Slovak Scientific Grant Agency, APVV-16-0029 and APVV-PP-COVID-20-0036 of the Slovak Research and Development Agency, and Visegradfund project number 22020140.

References

[1] I. Šišoláková, J. Hovancová, R. Oriňaková, A. Oriňak, L. Trnková, I. Třísková, Z. Farka, M. Pastucha, J. Radoňák, J.Electroanal. Chem. 860 (2020).

[2] I. Šišoláková, J. Hovancová, R. Oriňakova, A. Oriňak, L. Trnková, D. R. García, J. Radoňák, Bioelectrochemistry. 130 (2019).

[3] J. Hovancová, I. Šišoláková, R. Oriňaková, A. Oriňák, J Solid State Electrochem. (2017) 2147-2166.

 ISBN 978-80-8152-941-2

Surface morphology of the compacted metallic materials after immersion in simulated body fluids

R. Gorejová[a]*, Z. Orságová Králová[a], R. Oriňaková[a], R. Macko[a], A. Oriňak[a]

[a] Department of Physical Chemistry, Faculty of Science, Pavol Jozef Šafárik University in Košice, Moyzesova 10, 040 01 Košice
*radka.gorejova@student.upjs.sk

Different corrosion products are formed on the surface of the metallic samples after immersion into a corrosive medium. Their appearance may be influenced by different factors, such as medium composition, sample composition, immersion time, pH, etc [1]. Morphology of the sample surface can also bring information about the corrosion mechanism. The type of corrosion is a crucial factor that needs to be addressed during the preparation of biodegradable metals. In this work, we have compared iron and zinc powders compressed at 350 MPa into the form of pellets with 1 cm diameter (Figure 1a,b) and immersed in simulated body fluids (SBF) for 3 hours at 37 °C. After immersion, pellets were gently rinsed in ethanol and dried at 65 °C for 20 minutes. Morphology of the metallic surface was observed by means of optical microscopy (Dino-Lite Premier AM4013MT, 1.3 MPx, 200× Magnification). Iron and zinc samples were compared (Figure 1). In the case of pure iron, brown corrosion products (iron hydroxides) (Figure 1c) are formed inhomogeneously over the whole sample. On the other hand, the Zn sample was completely covered with a thin layer of zinc oxides (Figure 1d) suggesting that most of the products passed into the corrosive medium. Localized corrosion can cause a sudden change in properties after a relatively long period of stagnation. These findings suggest different corrosion behavior of iron and zinc in SBF which needs to be taken into account when choosing proper potential implant biomaterial.

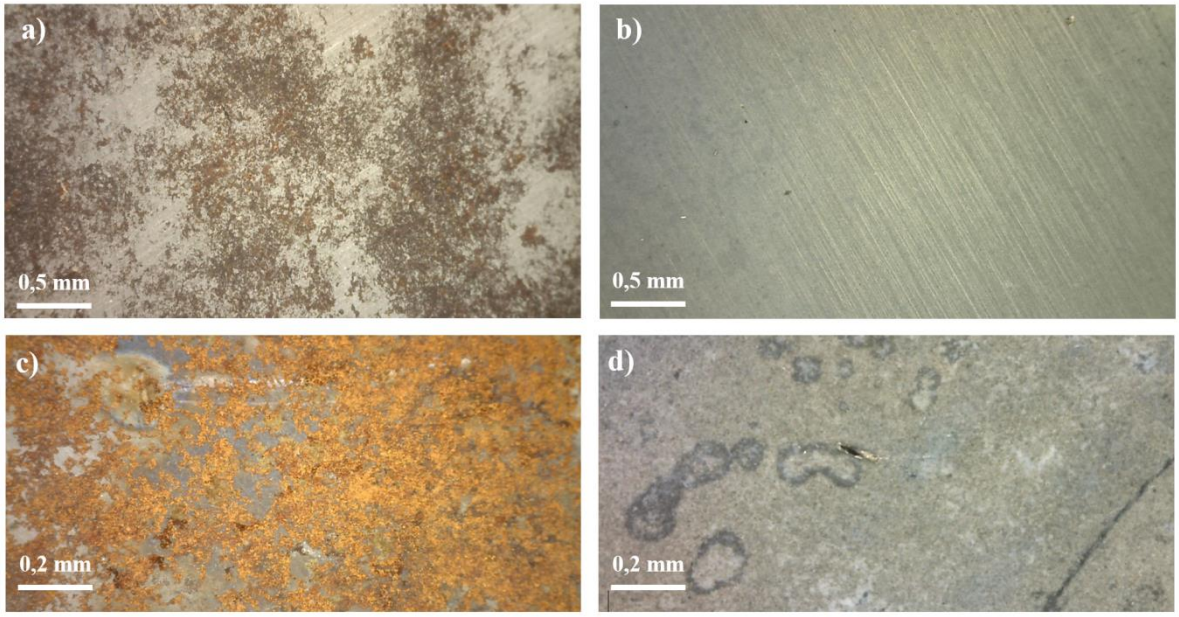

Figure 1 a) Fe and b) Zn pellet surface before corrosion (50 × magnification); c) Fe and d) Zn pellet surface after 3 hours of corrosion (250 × magnification).

 ISBN 978-80-8152-941-2

Acknowledgments

This work was supported by the projects APVV-16-0029 of the Slovak Research and Development Agency, VEGA 1/0074/17 of the Slovak Scientific Grant Agency, and VVGS-PF-2019-1049 of the Internal Research Grant System of Faculty of Science of P. J. Šafárik University.

References

[1] J. P. Weimer et al. Appl. Environ. Microbiol. 54 (2) (1988) 386-396.

 ISBN 978-80-8152-941-2

Corrosion characteristics of heterogeneous materials composed of metal and metal oxide

M. Kupková[a]*, M. Kupka[b]

[a] Institute of Materials Research of SAS, Watsonova 47, Košice, Slovakia
[b] Institute of Experimental Physics of SAS, Watsonova 47, Košice, Slovakia
*mkupkova@saske.sk

Besides the continuing quest for still better bioinert, practically incorrodible metallic materials for the use in permanent implants, an interest in bioabsorbable or biodegradable, quite corrodible metallic materials has emerged in context with their possible future use as biomaterials in temporary implants [1,2].

Bioabsorbable implants have to satisfy a number of engineering and medical requirements. The possibility of adjusting the degradation rate of implant in order to match the application needs is one of them. In that context, the ability to control the corrosion rate of involved metallic biomaterials is important.

One of interesting ways is to fabricate metal - matrix composites filled with micro- and nano-particles from appropriately chosen semiconducting metal oxides. To manipulate the corrosion rate, the dependence of corrosion parameters on geometric, electrochemical and physical characteristics of the composite and its constituents can be used [3,4].

To gain a preliminary insight on how the oxides in metal-matrix composite can affect its corrosion behaviour, a simple mathematical representation of corrosion of a two-component, metallic-oxidic specimen in an electrolyte simulating human body fluids was analysed [5]. The model has assumed [6-10]:

1. At a steady-state corrosion, there is one oxidation reaction - the oxidation of metal, and one reduction reaction - the reduction of oxygen dissolved in electrolyte.

2. The oxidation of metal takes place only on the metallic surface of the specimen, while the reduction of oxygen takes place on the entire surface of the specimen. In general, the rate of oxygen reduction on a metallic surface differs from that on an oxidic surface.

3. The transport of electroactive species by diffusion through the electrolyte is sufficiently fast, so the electrode reactions are purely activation-controlled.

4. The electrolyte and all participating solids conduct electricity sufficiently well to almost eliminate any ohmic potential drop when the current flows through them. The significant potential drop is only that across the electrode-electrolyte interface.

If a two-component specimen freely corrodes in an electrolyte, it is gaining an electric charge until some distribution of local values of electric potential is established. Under the above mentioned assumptions, these local values are practically equal to each other and the potential of the electrode is established at some value common for the whole specimen - the corrosion potential E_{corr}. After the corrosion potential is established, the total current flowing from the electrode (specimen) to the electrolyte (the total corrosion current) is balanced by the total current flowing from the electrolyte to the electrode (specimen). Using the equality of currents flowing from and to the specimen, choosing the appropriate relationships between current density and electrode potential and accepting the above assumptions, the following relationships for the corrosion potential E_{corr} and corrosion current density i_{corr} can be found

$$E_{corr} = E^0_{corr} + \frac{b_a b_c}{b_a + b_c} \ln\left(1 + \frac{i^0_{c,oxide}}{i^0_{c,metal}} \frac{A_{oxide}}{A_{metal}}\right) \quad (1)$$

 ISBN 978-80-8152-941-2

$$\frac{i_{corr}}{i^0_{corr}} = \frac{A_{metal}}{A_{metal}+A_{oxide}}\left(1+\frac{i^0_{c,oxide}}{i^0_{c,metal}}\frac{A_{oxide}}{A_{metal}}\right)^{\frac{b_c}{b_a+b_c}} \quad (2)$$

Here A_{metal} is the area of the specimen surface region occupied by a metal and A_{oxide} is the area of specimen surface region occupied by an oxide. The total area of the specimen surface is $A_{metal}+A_{oxide}$. $b_a$ln10 and $b_c$ln10 are Tafel slopes for the anodic reaction (oxidation of metal) and the cathodic reaction (reduction of oxygen). $i^0_{c,metal}$ is the exchange current density for the reduction/evolution of oxygen on the surface of metal, $i^0_{c,oxide}$ is the exchange current density for the reduction/evolution of oxygen on the surface of oxide. E^0_{corr} and i^0_{corr} is the corrosion potential and the corrosion current density for purely metallic specimen (A_{oxide} = 0).

Equations (1) and (2) show that corrosion characteristics of the specimen depend on the concentration of oxides determining the value A_{oxide}.

If the ratio of area of surface region occupied by oxide to the area of surface region occupied by metal A_{oxide}/A_{metal} increases, the corrosion potential of the specimen increases too (Fig.1). If $b_c i^0_{c,oxide} < (b_a + b_c) i^0_{c,metal}$, corrosion current density decreases with increasing ratio A_{oxide}/A_{metal}. Otherwise, the corrosion current density first increases, reaches its maximum value, then decreases and approaches zero when A_{oxide}/A_{metal} tends to infinity (Fig.2).

But for a large enough ratio A_{oxide}/A_{metal}, it is necessary to take equations (1) and (2) with a grain of salt. If the ratio A_{oxide}/A_{metal} increases to such an extent that the value of corrosion potential approaches closer than about 100 mV the value of reversible potential of oxygen reduction/evolution reaction, it is necessary to take into consideration another oxidation reaction, namely the reverse reaction to the oxygen reduction. In such a situation, analysed simple model becomes insufficient and a more exact model is needed.

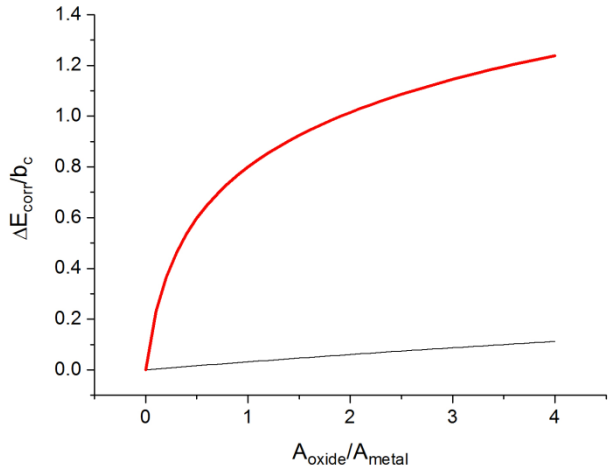

Figure 1 Corrosion potential calculated by means of equation 1. Figure demonstrates the change in $(E_{corr} - E^0_{corr})/b_c$ with the change in the A_{oxide}/A_{metal} ratio. The curves presented were calculated for b_c=2b_a, $i^0_{c,oxide}/i^0_{c,metal}$=10 (top curve) and $i^0_{c,oxide}/i^0_{c,metal}$=0.1 (bottom curve).

ISBN 978-80-8152-941-2

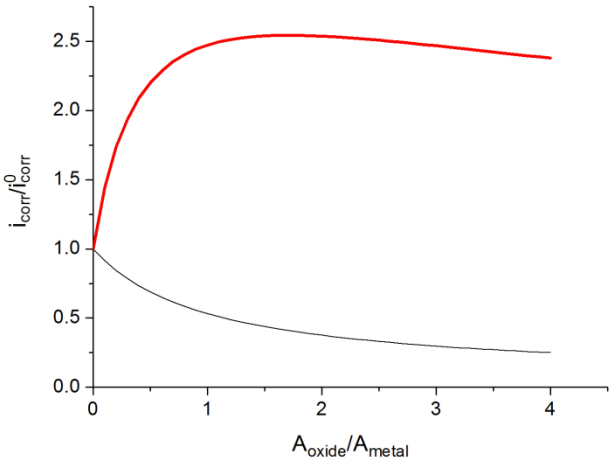

Figure 2 Corrosion current density calculated by means of equation 2. Figure demonstrates the change in i_{corr}/i^0_{corr} with the change in the A_{oxide}/A_{metal} ratio. The curves presented were calculated for $b_c=2b_a$, $i^0_{c,oxide}/i^0_{c,metal}=10$ (top curve) and $i^0_{c,oxide}/i^0_{c,metal}=0.1$ (bottom curve).

Acknowledgements

This work was supported by the Slovak Research and Development Agency (project APVV-16-0029) and Scientific Grant Agency of the Ministry of Education, Science, Research and Sport of the Slovak Republic (project VEGA 1/0074/17).

References

[1] Hermawan, H. Biodegradable Metals: From Concept to Applications; Springer: Heilderberg, 2012.

[2] Zheng, Y. F.; Gu, X. N.; Witte, F. Biodegradable metals. Mater. Sci. Eng. R. Rep. 2014, 77, 1–34.

[3] Cheng, J.; Huang, T.; Zheng, Y. F. J. Biomed. Mater. Res. Part A 2014, 102 (7), 2277–2287.

[4] Kupková, M.; Kupka, M.; Hrubovčáková, M.; Oriňaková, R; Morovská Turoňová, A.; Puchý, V. Int. J. Electrochem. Sci. 2018, 13, 11839–11852.

[5] Kupková, M.; Kupka, M.; Oriňaková, R.; Gorejová, R. Koroze a ochrana materiálu, accepted for publication

[6] Heusler, K. E.; Lorenz, W. J. Iron. In Standard Potentials in Aqueous Solution; Bard, A. J., Parsons, R., Jordan, J., Eds.; Marcel Dekker, Inc.: New York, 1985; pp 391–412.

[7] Hoare, J. A. Oxygen. In Standard Potentials in Aqueous Solution; Bard, A. J., Parsons, R., Jordan, J., Eds.; Marcel Dekker, Inc.: New York, 1985; pp 49–66.

[8] Lemire, R. J.; Berner, U.; Musikas, C.; Palmer, D.A.; Taylor, P.; Tochiyama, O.; Perrone, J. Chemical Thermodynamics of Iron-Part 1-Chemical Thermodynamics.Volume 13a (No. NEA-6355), Data Bank; OECD Publications: Paris, 2013.

[9] Talbot, D. E.; Talbot, J. D. Corrosion Science and Technology, 3rd ed.; CRC press: Boca Raton, 2018.

[10] Revie, R. W.; Uhlig, H. H. Corrosion and Corrosion Control. An Introduction to Corrosion Science and Engineering, 4th ed.; John Wiley & Sons, Inc.: Hoboken New Jersey, 2008.

 ISBN 978-80-8152-941-2

Fe-based biodegradable implant material cytotoxicity

J. Macko[a]*, R. Gorejová[a], Z. Orságová-Králová[a], V. Huntošová[b], R. Oriňaková[a]

[a] Department of Physical Chemistry, P. J. Šafárik University in Košice, Moyzesova 11, 041 54, Košice, Slovakia
[b] Center for Interdisciplinary Biosciences, Technology and Innovation Park, P. J. Safarik University in Kosice, 041 54, Kosice, Slovakia
*jan.macko@upjs.sk

Degradation of metallic biomaterials for implants with temporary function represents a new concept of bioactive biomaterials used. They should support the tissue during the healing process for a certain period of time. The corrosion resistant metal implant materials currently used for orthopaedic, cardiovascular, and paediatric implants could be potentially replaced by degradable metallic materials in some cases. The major constituent of these degradable materials could be iron for its low toxicity. However, the cytotoxic effect of iron nanoparticles *in vitro* on some cell lines was confirmed [1]. Zhu et al. [2] have shown that only iron concentration over 50 μg ml^{-1} expresses in vitro toxicity to endothelial cells (ECs). In this study, we have examined the influence of extract dilution to the viability of human brain glioblastoma astrocytoma cell culture U87MG. Extracts were prepared by leaching of an iron sample in a certain amount of culturing media in a thermostat at 37°C simulating human body temperature. We have observed a significant dependence of cell viability to the final extract dilution. In case of pure undiluted extract relatively low cell viability was observed. Cell viability in case of 10% extract content was about the same as in the case of the control sample, thus significantly low toxicity was observed. When considering permanent circulation and renewal of body fluids, prepared iron cellular material could be suitable for implant use.

Acknowledgements

This research has been financially supported by APVV-16-0029 of the Slovak Research and Development Agency and VEGA 1/0074/17 of the Slovak Scientific Grant Agency.

References

[1] S. Salah. Iraqi J. Cancer. Med. Genet. 10(1) (2018) 71–77

[2] S. Zhu, N. Huang, L. Xua, Y. Zhang, H. Liu, H. Sun, Y.Leng, Mater. Sci. Eng. C 29 (2009) 1589–1592

 ISBN 978-80-8152-941-2

Mechanical properties and degradation performance of biodegradable Fe-based materials containing MgO and ZnO nanoparticles

A. Morovská Turoňová[a*], M. Kupková[b], M. Džupon[b], M. Hrubovčáková[b]

[a]Institute of Chemistry, Faculty of Science, P. J. Šafárik University, 040 01 Košice, Slovakia,
[b]Institute of Materials Research, Slovak Academy of Sciences, 040 01 Košice, Slovakia
*andrea.morovska.turonova@upjs.sk

The development of appropriate degradable materials with the ability to improve the repair and regeneration of human bones and tissues is constantly advancing. The reliability of implantable biomaterials depends on their mechanical and degradative properties and certainly the biocompatibility of such biomaterials plays a role in their success in medical applications [1].

In many cases, material sintered from powdered Fe is used as the biodegradable metal. It can be modified with various additives, which leads to a change in the properties of this material. Inorganic metal oxides such as MgO and ZnO are attractive for corrosion resistance control. The effect of reducing bacterial contamination has also been reported using these specific nanoparticles [2].

Powdered carbonyl iron and MgO or ZnO nanoparticles were treated by powder metallurgy. The powders were mixed, compressed and sintered by spark plasma sintering (SPS) method.

One of the requirements Fe-based biomaterials must meet is that the material has to be mechanically resistant. The material should have the same or greater mechanical stability as the replaced body part to ensure its high reliability. The physical properties of materials depend on their microstructure, which can be characterized in terms of the number and types of phases present and the relative amount of each.

The microstructure of samples was examined in more detail using a scanning electron microscope. The flexural strength of Fe-MgO and Fe-ZnO composites prepared by SPS was measured, and their Young's modulus was determined.

Fe-MgO and Fe-ZnO rectangular bars (25×5×4 mm) were subjected to three-point bending tests. These tests were performed at room temperature using a TiraTest 2300 (Germany) universal loading machine. Deformation rates were 0.8 mm/min, span of 16mm. Ultimate flexural strengths (UFS) were determined. The modulus of elasticity was determined by the dynamic resonant method. The natural frequency of the fundamental bending mode was measured utilizing the equipment BUZZ-O-SONIC 5.9.6. (BuzzMac International, LLC, U.S.A), and the corresponding modulus of elasticity was subsequently calculated using the equipment software. The test results are summarized in Table 1. The addition of nanoparticles to the iron powder results in an improvement of the mechanical properties of the sintered products in case of MgO nanoparticles, while it results in an deterioration of these properties in the case of ZnO nanoparticles. A more homogeneous distribution of MgO and ZnO in sintered products plays a decisive role.

 ISBN 978-80-8152-941-2

specimen	*Young's modulus [GPa]*	*UFS [MPa]*
Fe	198.8	697
Fe-1.0ZnO	199.0	688
Fe-5.0ZnO	185.4	616
Fe-0.5MgO	201.4	703
Fe-1.0MgO	214.1	735

Table 1 Mechanical properties of the biomaterials

Degradation performance of the materials was evaluated by potentiodynamic measurements and electrochemical impedance spectroscopy method in Hanks' solution.

Corrosion measurements showed that a small addition of MgO or ZnO nanoparticles to the iron matrix caused an increase in the degradation rate and the corrosion potential shift to more negative values. But as the content of nanoparticles increased, the corrosion rate of the composite decreased. The corrosion rate fell even below the level of pure iron prepared by spark plasma sintering. This reduction in the corrosion rate was most likely due to the low electrical conductivity of the oxide phase, which led to the ohmic potential drops along the galvanic current paths in the ZnO regions. In order to reduce undesired ohmic potential drops and thus accelerate corrosion, the current paths in the oxide regions should be as short as possible and/or the conductivity of the oxidic regions should be as high as possible [3]. It turns out that in the case of samples treated with SPS, the shift of the corrosion potential and the degradation rate depend on the amount of nanoparticles present. In these cases, the material appears to be more compact, the surface is more homogeneous.

In the last step, the hemocompatibility of the prepared samples was determined. Different amounts of added nanoparticles led to a reduction in hemolytic activity compared to pure iron. A slight decrease in thrombus formation was also observed. The samples were evaluated as hemocompatible.

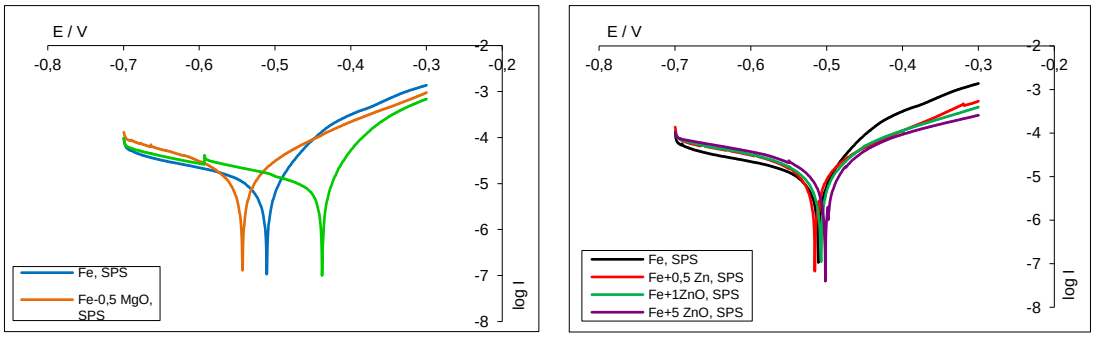

Figure 1 Tafel plots for Fe-MgO and Fe-ZnO composites in Hanks' solution.

Acknowledgement

This work was supported by the Slovak Grant Agency VEGA under project VEGA 1/0074/17 and by the project APVV-16-0029.

 ISBN 978-80-8152-941-2

References

[1] Wang L., Wang C., Wu S., Fan Y., Li X., Biomater. Sci. 8 (2020) 2714-2733.

[2] Sawai, J., Journal of Microbiological Methods 54 (2003) 177-182.

[3] Kupková M., Kupka M., Hrubovčáková M., Oriňaková R., Morovská Turoňová A., Puchý V., Int. J. Electrochem. Sci. 13 (2018) 11839 – 11852.

 ISBN 978-80-8152-941-2

Study of nanocrystalline hydroxyapatite coatings electrochemically deposited on titanium implant material

Z. Orságová Králová[a]*, R. Gorejová[a], R. Oriňaková[a], M. Schnitzer [b], R. Hudák [b], M. Kozák[b], T. Sopčák[c], K. Kovaľ[c], A. Oriňak[a]

[a]Department of Physical Chemistry, Faculty of Science, Pavol Jozef Šafárik University in Košice, Moyzesova 11, 041 54 Košice, Slovakia
[b]Department of Biomedical Engineering and Measurement, Faculty of of Mechanical Engineering, Technical University of Košice, Letná 9, 042 00 Košice, Slovakia
[c]Institute of Materials Research, Slovak Academy of Sciences, Watsonova 47, 040 01 Košice, Slovakia
*zuzana.orsagova.kralova@upjs.sk

Hydroxyapatite ($Ca_{10}(PO_4)_6(OH)_2$) (HAp) has been used for a plenty of biomedical applications such as matrix for drug release control and bone tissue engineering materials. HAp deposited on to the implant surface led to improved adhesion of osteoblasts and enhanced calcium deposition in the case of nanocrystalline HAp coating compared to microstructural HAp coating [1]. The low mechanical strength of regular HAp biocoatings limits its use to low load-bearing purpose. To overcome these limitations nanocrystalline HAp was developed which exhibits improved densification due to larger surface area [2].

Samples of certified Ti-6Al-4V material were prepared by additive manufacturing. Their porous structure imitated cancellous bone structure. Titanium prismatic samples had regularly arranged pores with a rage of diameter from 200, 400 to 600 μm. (Fig.1). The samples were etched for 30 min in 1M H_2SO_4 to improve the adhesion of the deposited HAp coating. The electrolyte used in deposition process was composed of $Ca(NO_3)_2$, $NH_4H_2PO_4$ with the addition of hydrogen peroxide. Optimization of the most appropriate electrochemical HAp deposition procedure involves galvanostatic and potentiostatic methods.

The morphology, arrangement and composition of HAp coatings were characterized by scanning electron microscope with EDX elemental analysis (Fig. 1). Resulting coatings were detected and identified by XRD analysis, which confirmed the nanocrystalline structure of HAp. The HAp coating was distributed homogenously with a formation of three-dimensional longitudinal crystals (Fig. 1B). Thus, using the mentioned methods, we evaluated that the most suitable electrochemical method for deposition of HAp coating onto the titanium implants is galvanostatic deposition for 40 min (-5mV) with consequent leaching in NaOH for 2 hours. Compared to other application method, such as spray procedure, the HAp coating was deposited also in the inner surface of the porous structure.

 ISBN 978-80-8152-941-2

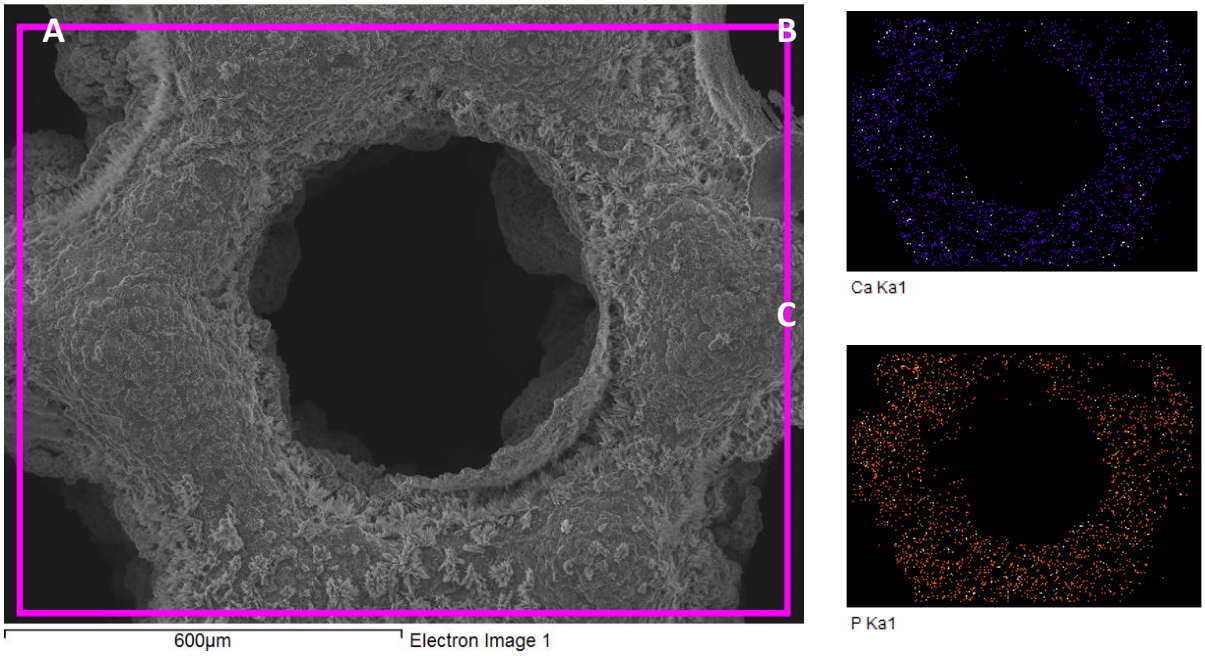

Figure 1 A) SEM image of HAp coating electrochemically deposited onto Ti porous material (600 µm). EDX analyses of the surface chemical composition of the studied HAp coatings B) calcium B) phosphorus.

Acknowledgements

This work was supported by the Slovak Research and Development Agency (APVV-16-0029) and Scientific Grant Agency of the Ministry of Education, Science, Research and Sport of the Slovak Republic (project VEGA 1/0074/17).

References

[1] S. Anil, E.P. Chalisserry, S.Y. Nam, J. Venkatesan, Biomaterials for craniofacial tissue engineering and regenerative dentistry, Elsevier Ltd, 2019. https://doi.org/10.1016/b978-0-08-102476-8.00025-6.

[2] P. Choudhury, D.C. Agrawal, Hydroxyapatite (HA) coatings for biomaterials, Woodhead Publishing Limited, 2012. https://doi.org/10.1533/9780857096449.1.84.

 ISBN 978-80-8152-941-2

Influence of polymeric coating on corrosion properties of iron-based biodegradable materials

M. Petráková[a]*, R. Oriňaková[a], R. Gorejová[a], A. Oriňak[a]

Department of Physical Chemistry, Institute of Chemistry, Faculty of Science, P. J. Šafarik University in Košice, Moyzesova 11, 040 01 Košice
*martina.petrakova@student.upjs.sk

Metallic biomaterials are used for various medical purposes due to their excellent mechanical properties. Depending on the application a suitable surface treatment method may lead to an increase or decrease in the rate of degradation [1]. The properties of metallic biomaterials are highly influenced by production treatments, such as chemical treatment or electrochemical and biochemical treatments [2]. One of the new approaches in the treatment of biomaterials is the application of nanocoatings to metallic biodegradable materials to improve the degradation properties of the biomaterials and biocompatibility.

This work deals with the preparation and testing of the degradation behaviour of iron-based biomaterials. Iron-based cellular samples were prepared by sintering of iron-impregnated polyurethane (PUR) foam. In order to increase the corrosion rate and improve the mechanical properties and biocompatibility of the samples, a polymeric polyethylene glycol (PEG) coating was applied to the porous samples. To study the degradation, the open circuit potential (OCP) of the samples was measured at 37 °C in Hanks' solution. A Nyquist plot of cellular samples before immersion in Hanks' solution is shown in Figure 1. The diameter of the semicircle for uncoated samples indicates increased resistance and increased susceptibility to corrosion of polymer coated samples. Corrosion properties of coated and uncoated samples were studied using an anodic polarization method in Hanks´ solution. The samples coated with polymeric layer corroded faster than uncoated samples.

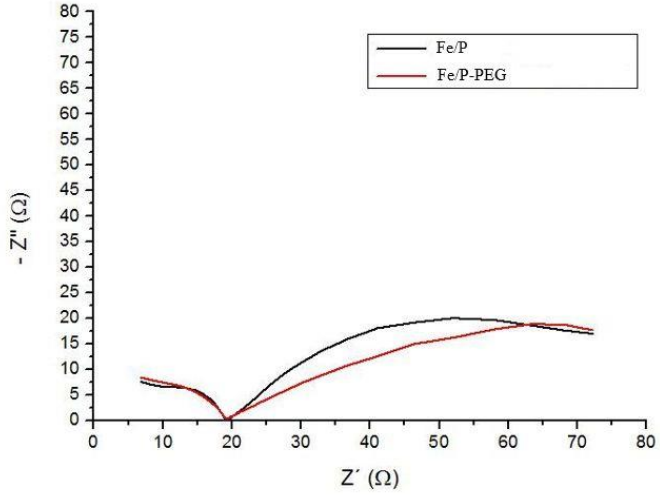

Figure 1 Nyquist diagram of Fe/P and Fe/P-PEG samples before degradation.

 ISBN 978-80-8152-941-2

Acknowledgments

This work was supported by the projects APVV-16-0029 of the Slovak Research and Development Agency and VEGA 1/0074/17 of the Slovak Scientific Grant Agency.

References

[1] A. Nouri, C. Wen, Introduction to surface coating and modification for metallic biomaterial; in Surface Coating and Modification of Metallic Biomaterials, Cambridge: Elsevier, 2015, 3–60.

[2] S. Dharadhar, A. Majumdar, Biomaterials and Its Medical Applications; in Application of Biomedical Engineering in Neuroscience, 3 (2019) 355–380.

 ISBN 978-80-8152-941-2

In particular, research on an encapsulated drug carrier using alginate acid as an outer shell coating: Encapsulation research of ultrafine particles using PEGylated alginate acid and its application. Development and research of drug-encapsulated PEGylated alginate carrier

K. Yagi[a], A. Oriňak[b]

[a] Tokyo Metropolitan University Graduate School of Human Health Sciences, 7-2-10, Higashi-ogu, Arakawaku, Tokyo. Japan.
[b] Faculty of Science, Pavol Jozef Safarik University. Moyzesova 11, 04154 Kosice, Slovakia. Slovakia.
*yagi@tmu.ac.jp

Stage 1：

Basic research on the development of PEGylated alginate carrier（：Experiment completed and ongoing）

：Development and research of drug-encapsulated PEGylated alginate carrier

Stage 2：

Application example to new drug development（：Experiment completed and ongoing）

: New drug synthesis using drug-encapsulated PEGylated alginate carrier

Specific example-A new drug containing ultrafine particles

：Application to the development of new MRI contrast agents.

Composite synthesis of PEGylated alginate-coated magnetic ultrafine particles（：Experiment completed）

Alginate acid were used to our research, it succeeded a little more waited to undertake research using.

In our research group, the use of ultrafine particle outer shell coating material of alginate acid has been successful with a little ingenuity from the research experience of the past 35 years.

So, it synthesized almost successfully by performing research and development of ultrafine particles agents using Alginate acid in place of glycose coating. It is where the product has been characteristics and evaluation. Since Alginate acid is a polymer having very much a carboxyl group, it was able to bind very strongly and polyethylene glycol and iron oxide, Zn-iron oxide particles. Since alginate acid is also a polymer having a large number of carboxyl groups, it would be able to bind.

Stage 3：

Animal experiment research on PEGylated alginate acid-coated magnetic ultrafine particles（：During the experiment）

 ISBN 978-80-8152-941-2

Using 7.0T-MRI (Bruker Co. Ltd) for animals of the Experimental Animal Central Research Institute in Japan, we administered a newly developed and manufactured MRI contrast medium to rats and evaluated MRI angiography and intra-organ accumulation of contrast medium.

Stage 4：

Study of alginate composite gel structure（：During the experiment）

Specific example

Study of Isopropyl-acrylamide-Hydroxyethyl methacrylate-alginate composite gel（：During the experiment）

Applied research

Application and development of artificial organs alginate composite gel structure (not the start of the experiment)

Stage 5：

In vitro studies in cultured cells (not the start of the experiment)

：Evaluation of intracellular uptake rate of alginate complex gel structure in vitro study.

 ISBN 978-80-8152-941-2

Corrosion processes in Li-accumulator systems with non-aqueous electrolytes

R. Apostolova[a*], E. Shembel[a]

[a]Scientific Research Laboratory of Chemical Power Sources of Ukrainian State University of Chemical Technology, Dnipro, 49005, Ukraine
*apostolova.rd@gmail.com

In the presentation, some new data about corrosion processes in Li-battery systems with non-aqueous electrolytes are presented. Corrosion and side processes in lithium power sources are considered: (1) electrochemical corrosion of the positive and negative electrodes, (2) electrochemical and chemical decomposition of a non-aqueous electrolyte that occurs in parallel with the main electrochemical processes.

Corrosion of materials in an aquatic environment has been extensively and deeply studied, while in a non-aqueous environment it has received much less attention from researchers. Along with the general laws of corrosion processes in non-aqueous and aqueous media, there are specific features of corrosion processes inherent only in non-aqueous media. Corrosion in a battery system is defined as a chemical or electrochemical reaction between a material and the environment, resulting in deterioration of material properties [1]. A rechargeable lithium-ion battery (LIB) is a system in which the potentials of the electrodes often go beyond the stability of the electrolyte. As a result, in contrast to a thermodynamically stable system, corrosion can easily occur in LIB. In LIB, current collectors of positive and negative electrodes must be electrochemically stable in contact with the components of the power source within the window of electrochemical resistance. In practice, prolonged corrosion of current collectors leads to a gradual increase in the internal resistance of the power source and a gradual decrease in capacity. Corrosion of the current collector can short-circuit the power supply, affecting its safety. Formation of a compact, protective passive film on the metal surface of the current collector is very important for battery performance and safety. Depending on the nature of salts and electrolyte additives, different types of protective films are formed. The solubility of these surface layers in the electrolyte is a determining factor in the overall stability of the current collector. The review [2] presents the electrochemical behavior and processes of the formation of a protective film on various metal current collectors in typical Li-containing electrolytes.

In a lithium battery on the positive electrode side with an aluminum current collector, the dissolution of aluminum and the formation of a cathode surface film (CEI) are processes associated with corrosion. One of the two processes that leads to the dissolution of aluminum is anodic dissolution. Another reason leading to the chemical dissolution of aluminum is an insufficient protective layer on its surface. Aluminum with a standard redox potential of (–1.68 V) vs. (H^+/H_2) can react chemically with the environment and be oxidized, which leads to its dissolution and formation of pitting without the need for external current/voltage imposition. The formation of surface films on the positive and negative electrodes in a lithium-ion battery (LIB) and a lithium battery (LA) is considered as a corrosion phenomenon. For cathode materials of a lithium power source, the CEI film, usually induced by an external current/voltage is characterized by oxidation of the electrolyte components with the formation of a Li^+-permeable surface coating. Similar processes are known for anode materials (graphite), where an electronically insulated Li^+-conductive SEI surface layer is formed. While SEI on graphite in LIB forms when an external current/voltage is applied, for aircraft with a lithium anode such surface layers arise spontaneously, caused by a very low standard redox potential of lithium (–3.04 V) vs. H^+/H_2-electrode. In the case of a lithium electrode, the formation of SEI is accompanied by the reduction of electrolyte components and lithium oxidation [3]. A lot of research has been devoted to the dissolution of the aluminum current collector, the formation of CEI and SEI, while the deterioration of conversion in LIB and aircraft associated with galvanic corrosion did not attract close attention of battery researchers until recently.

 ISBN 978-80-8152-941-2

Lithium electrode corrosion processes. Recently Lin et al. showed that the difference in the kinetics of electrolyte reduction on two contacting metals Li/Cu leads to the degradation of lithium deposits on a metal base [4]. Galvanic corrosion is defined here as an electrochemical reaction involving a galvanic pair of two metals and an electrolyte, resulting in accelerated oxidation of the metal with a lower standard potential in the presented galvanic pair. In aircraft such galvanic corrosion occurs at the Cu-collector/Li interfaces especially intensively when thin lithium electrodes are used. Although it has long been believed that lithium corrosion in electrolytes involves direct transfer of charge across the lithium-electrolyte interface, it has been found that the observed corrosion is due to a galvanic process between lithium and a copper substrate. The observations are confirmed by a detailed analysis of films formed on copper and lithium, where differences in the kinetics of electrolyte reduction on two surfaces can explain the rapid galvanic process [5].This path is largely ignored by previous research on battery corrosion.

Lithium-based (LA) batteries have ten times the theoretical capacity of graphite-based batteries. However, lithium metal is very sensitive to corrosion due to its low redox potential, which is one of the dominant factors that determine the stability of lithium during cycling. Further, a systematic understanding of the evolution of the corrosion process after the initial formation of SEI is needed.

Several strategies can be used to suppress galvanic corrosion. First, the passivation of the current collector is required for low electrolyte permeability, which has become an intensively studied topic of homogeneous deposition of lithium [6]. Second, the deposition of dense compact lithium is necessary to isolate the substrate from the electrolyte in order to block the path of galvanic corrosion. Third, the development of an all-solid-state battery can help stabilize the interface to avoid excessive side reactions.

Corrosion properties of current collectors of the positive electrode

The authors of this publication in the studies of thin-layer electrochemically obtained electrodes for lithium batteries have repeatedly observed manifestations of galvanic corrosion. We are talking about thin-layer vanadium oxides V_2O_5 and manganese dioxide MnO_2, deposited on a 18N12Kh9T stainless steel substrate. These oxide materials have a high potential, in excess of 3.7 V vs. Li/Li^+ electrode in an aprotic environment. The potential of the stainless steel electrode can be 3.0–.3 V vs. Li/Li^+electrode. After a long stay of the V_2O_5/steel18N12X9T electrode with an active mass of less than 0.3-0.4 mg/cm^2 in a lithium-containing alkyl carbonate electrolyte without current, its initial potential decreases to values close to 3.4 V vs. Li/Li^+electrode.. This leads to a loss of discharge capacity in the redox reaction with lithium, since the V_2O_5/Li discharge curve has a phase transition region in V- pentoxide at a potential undercurrent of about 3.4 V, which is lost during storage of a thin-layer V_2O_5/ stee1 18N12X9T electrode due to galvanic corrosion leading to a decrease in potential without current to 3.4 V.

The anodic behavior of austenitic stainless steel SUS 304 as a positive electrode current collector in a lithium-ion battery/capacitor has been studied in organic electrolyte solutions based on a mixed alkyl carbonate solvent with various lithium salts [7]. Stable passivating characteristics were determined for stainless steel in a $LiPF_6$ solution, but pitting corrosion or active dissolution of steel is observed in solutions containing the anions BF_4^-, $(CF_3SO_2)_2^{N-}$, $(TFSA)^-$ and ClO_4^-. The mass ratios of dissolved metal particles in Li-TFSA and $LiClO_4$ solutions are equivalet to the ratios of the alloy composition mass, which indicates that during anodic polarization in these electrolyte solutions, the predominant dissolution of one of the steel components does not occur. Anodic corrosion in a Li-TFSA solution is partially suppressed by the addition of a PF^-_6-containing salt or HF to the electrolyte.

In our studies of electrochemically prepared thin-layer NiS electrodes in lithium-perchlorate electrolytes with a solvent 1,3-dioxolane, the reason for the drop in the discharge capacity of a NiS/Li battery during cycling was established [8]. Changes in the surface morphology of the NiS electrode after 14-fold cycling are manifested in the formation of a pronounced surface film on the electrode. The adhesion and cohesion of NiS particles is weakened. With further cycling, the active component loses its mechanical integrity, peels off from the base. An analysis of the FTIR spectra of the electrodes revealed a satisfactory stability of the spectral region, which characterizes the vibration of bonds in NiS (in the region of wave numbers around 400 cm^{-1}). After a 14-fold discharge of the NiS electrode to 0.9 V in the

 ISBN 978-80-8152-941-2

spectral region 1200–600 cm^{-1}, the intensity of the bands attributed to surface impurities increases as a result of electrochemical interaction of the base (stainless steel) with electrolyte with the formation of a surface film that prevents the effective passage of the electrode process. Metal sulfides based on stainless steel can initiate corrosion processes in the base. Since the redox potential of the base, the predominant component of which is iron, is more negative than the potential of the metal sulfide, anodic dissolution of the base is carried out in a corrosive galvanic metal-sulfide/iron pair. In this case, the corrosive effects of the base can contribute to weakening the adhesion of metal sulfide to the base, leading to a decrease in the discharge capacity of the battery.

Now the interest to the galvanic corrosion in Li batteries increases. However, the authors of this publication drew attention earlier to galvanic corrosion in lithium power sources with cathode materials FeS_2 (pyrite) and SO_2. In the Li-FeS_2 power source, the following processes were investigated: (1) electrochemical corrosion in a short-circuited pair active material (FeS_2 – a material of a current collector from the series Pb, Cd, Zn, Al, Ni, Ti, Cu, Pt, graphite, steel 0.6 KhN28MDT) [9–12]; (2) electrochemical and chemical decomposition of a non-aqueous electrolyte, which occurs in parallel with the main electrochemical reaction in the power source [11]. The direction of corrosion processes, their rate, and the nature of the products formed can change depending on the nature of the active material, the composition of the electrolyte, the nature of the material of the current collector, the degree of cathodic reduction,. Side processes can be carried out on the active material and the electrically conductive filler of the cathode. They should be considered for power sources with a discharge voltage near 1.5 V, since most non-aqueous electrolytes are reduced in the region close to 1.5 V. Corrosion processes have been investigated by us in the initial FeS_2 (pyrite) and reduced to a stable potential of 1.6–1.8 V in the electrolyte 1 M $LiBF_4$, PC, diglyme. The rate of corrosion processes in reduced FeS_2 (pyrite) is higher than that of the initial one. It has been found that the highest polarization is observed on aluminum and, accordingly, the lowest corrosion current. Aluminum is recognized as the best material for the FeS_2 cathode current collector.

A potentiodynamic study of various metals in electrolytes (PC, diglyme, $LiBF_4$) and (PC, DME, $LiClO_4$) on various materials showed that in the series Al <Ni <Ta <Ti <glassy carbon <Zn <Cu <Pd, the corrosion current increases. The rate of gas evolution on FeS_2 (pyrite) during decomposition of the electrolyte depends on the composition of the electrolyte and can vary from 8×10^{-3} to 2×10^{-5} cm^3/min in the investigated series of 1M $LiBF_4$/ γ-butyrolactone, 1.6 M $LiBF_4$/sulfolane, 1M $LiBF_4$/diglyme, 1M $LiBF_4$/PC, 1M $LiBF_4$/γ-butyrolactone, tetrahydrofuran (1: 1), 1M $LiBF_4$/ PC, DME (1: 1), 1M $LiBF_4$/PC, DG (1: 1), 1M $LiBF_4$/PC, dioxolane (1: 1), 1M $LiClO_4$/PC, acetonitrile (1: 1), 1 M $LiClO_4$/dimethyl sulfoxide, 1 M $LiClO_4$/PC [12]. During the cathode reduction of the solid-phase oxidizer FeS_2, the electrochemical and chemical decomposition of electrolytes occurs. The electrolyte 1M $LiBF_4$/PC, DG (1: 1) has advantages in corrosion resistance in the studied series of electrolytes. Conductive additives graphite and carbon black are used in the composition of the porous FeS_2 electrode. The potentials of unreduced pyrite and graphite with a surface oxidized in air are close (3.7 and 3.6 V vs. Li^+/Li electrode, respectively) and the magnitude of the corrosion current is small. In a partially discharged electrode, particles of a conductive filler become cathodes and gas evolution is possible on them.

In the study [13], a number of metals (Al, Zn, Pb, Cu, Sn, oxidized Al, Ni, Ti, stainless steel 18N12X9T, Pt, graphite) were tested for the cathode current collector in order to select the most corrosion-resistant materials of the SO_2/Li power source in the electrolyte composition of PC, AN (1: 3), LiBr (1 M), SO_2 (2.2 M). The values of the stationary potential of metals are lower than the potential of graphite, which is used as the cathode matrix of the SO_2 depolarizer. In corrosive metal-graphite pair in the initial state, oxidation processes on the metal are possible. However, the cathode potential changes in the range 3.14–2.00 V during the operation of the power sources due to the passivating of the cathode surface caused by the formation of lithium dithionite. The comparative rate of electrochemical processes on various metals is evidenced by potentiodynamic curves in the redox reaction with lithium. The magnitude of the cathode current at a potential scan rate of 0.05 V/s reaches about 10^{-5} A/cm^2 for all metals. The exception is aluminum, in which the current is 1.0–1.5 orders of magnitude lower. It is known that the products of cathode reduction of SO_2 in PC electrolyte, $LiClO_4$ (1 M), SO_2 (2.2 M) are oxidized on platinum,in two stages with maxima at potentials 3.14 V (oxidation of SO_2^-) and 3.9 V (oxidation dithionite ion). In the electrolyte PC, AN, LiBr (1 M), SO_2 (2.2M), the

 ISBN 978-80-8152-941-2

peak near 3.9 V is absent in the potentiodynamic curves of all studied metals due to the instability of the anodically oxidized bromide. The smallest cathode peak in the used electrolyte in the group of metals under study is observed for aluminum. By the nature of the anodic processes on metals, the latter can be divided into two groups. On metals of the first group (Ni, Ti, Cu, Pb, Zn, Sn), the oxidation processes proceed at a rate of 10^{-4}–10^{-2} A/cm^2 and more with a tendency to increase from cycle to cycle. At equal polarization of metals, the anode current increases in the series Ni <Ti <Cu <Zn <Pb <Sr. The second group of metals includes aluminum and tantalum with a maximum current of 10^{-5} A/cm^2. In studies of corrosion pairs (cathode matrix SO_2 – metal), the data on the lowest rate of processes on aluminum and tantalum were confirmed. The experimental results made it possible to unambiguously resolve the question of the best corrosion-resistant material for the cathode current collector of the SO_2 – Li cell with the electrolyte PC, AN, (1: 3), LiBr (1M), SO_2 (2.2 M). It is aluminum. To solve the problem of a cathode current collector in a secondary Li-SO_2 power source, the electrochemical behavior of nickel [14] and a number of metals [15] in the PC electrolyte, $LiClO_4$ (1 M), SO_2 (2.2 M) was studied. It was shown that the rate of electrochemical transformations on nickel depends on the properties of oxide films formed in air and during the electrochemical performance of the electrolyte. In the range of working potentials of the primary Li-SO_2 cell (2.0–3.3 V), the rate of electrochemical transformations on nickel is no more than 0.1–0.5% of the rate of the main current of the power source on the carbon graphite electrode. This gives reason to consider nickel as a suitable material for the cathode current collector of primary Li–SO_2 cell. Nickel is unsuitable for the cathode current collector of the secondary Li-SO_2, since at a potential of 4.3 V, which is reached in the charge cycle, anodic dissolution of the metal occurs according to the reaction $Ni - 2\bar{e} \rightarrow Ni^{2+}$.

To suppress corrosion of the aluminum collector, corrosion inhibitors are introduced into the electrolyte [16], and super concentrated electrolytes are used in power sources [17]. Progress has been made in defining the mechanisms for overcoming corrosion, using new electrolytes, and new materials for current collectors [18–21].

References

[1] V.Cicek, B. Al-Numan. Corrosion Chemistry, Scrivener Publishing, Salem, MA, USA, 2011.

[2] S.-T.Myung, Y.Hitoshi, Y.-K. Sun, J. Mater. Chem., 21 (2011) 9891–9911.

[3] J.Becking, A.Gröbmeyer, M.Kolek, U.Rodehorst, S.Schulze, M.Winter, P.Bieker, M.C.Stan, Adv. Mater. Interfaces, 4, (2017), 1700166.

[4] D.Lin, Y.Liu, Y.Li, Y.Li, A.Pei, J.Xie, W.Huang, Y.Cui, Nature Chemistry, 11 (2019) 382–389.

[5] A. Smigelskas, E.Kirkendall, Trans. Metall. Soc. AIME, 171 (1947) 130–142.

[6] Y Liu, D.Lin, P.J.Yuen, K.Liu, J.Xie, R.Dauskardt, Y.Cuis, Advanced Materials, 29 (2017) 1605531.

[7] K.Furukawa, N.Yoshimoto, M.Egashira, M.Morita, Electrochim. Acta, 140 (2014) 125–131.

[8] R.Apostolova, E..Shembel, B.Markovsky, D.Aurbach, Electron Processing Materials, 56 (2020) № 5.

[9] R.D.Apostolova, E.M.Shembel, A.S. Strizhko, Journal of Applied Chemistry, 10 (1989) 2232–2236.

[10] R.D.Apostolova, E.M.Shembel, G.P.Petrunin, Journal of Applied Chemistry, 9 (1990) 2069–2073.

[11] R.D.Apostolova, E.M.Shembel, Yu.S. Berlizov, Journal of Applied Chemistry, 1 (1991) 58–64.

[12] R.D.Apostolova, E.M.Shembel, A.S. Strizhko et al., J. Power Sources, 54 (1995) 421–424.

[13] R.D.Apostolova, E.M.Shembel, L.I.Neduzhko, J. Applied Chemistry, 9 (1991) 540–546.

[14] R.D.Apostolova, E.M.Shembel, Electrochemistry, 27 (1991) 140–148.

[15] R.D.Apostolova, E.M.Shembel, J. Applied Chemistry, 10 (1991) 2063–2068.

[16] Patent US 9.263,731 B2 Feb. 16, 2016, K.Tikhonov, T.Johnson, J. Chau, K. Yip, M.Juzkow.

 ISBN 978-80-8152-941-2

[17] J.Zheng, J.A.Lochala, A.Kwok, Z.D.Deng, J.Xiao, Adv. Sci., (2017) 1700032.

[18]. T.Ma, G.Xu, Y.Li, L.Wang, X.He, J.Zhen, et al., J. Phys. Chem. Lett. 8 (2017) 1072–1077.

[19] S.Wang, K.V.Kravchyk, A.N.Filippin,et al., ACS Appl. Energy Mater., 2 (2019) 974−978.

[20] M.Kuenzel, D.Bresser, G.T.Kim, et al., ACS Appl. Energy Mater., 3 (2020) 218−230.

[21] C.M.Julien, A.Mauger, Materials Science, 6 (2019) 406–440.

 ISBN 978-80-8152-941-2

Electrochemical performance of specific composites as electrodes for supercapacitors

L. Q. Bao[a,b], H. Fei[a], N. Bugarova[a,c,*], M. Omastova[c], N. E. Kazantseva[a], P. Saha[a]

[a] Centre of Polymer Systems, Tomas Bata University in Zlín, Tř. T. Bati 5678, 760 01, Zlín, Czech Republic.
[b] Conducting Polymers in Composites and Applications Research Group, Faculty of Applied Sciences, Ton Duc Thang University, Ho Chi Minh City, Vietnam.
[c] Polymer Institute, Slovak Academy of Science, Dubravska cesta, 9, 845 41 Bratislava, Slovakia.
*bugarova@utb.cz

Supercapacitors (SC) receive considerable attention due to their capabilities such as power density, long cycle life, and a wide range of operating temperatures. However, there are still many obstacles to their application that have not yet been overcome. One of the potential promising is the use of composite for preparation of SC electrode, where the advantages of one material complement the disadvantages of another. The composite consisting of carbon-based materials, transition metal oxides or hydroxides, and conductive polymers can improve capacity, due to the Faradaic reaction and separation of charge between the electrode-electrolyte interfaces [1,2].

Several conductive polymers have been studied for application in supercapacitors. In this work, the polyaniline (PANI) has been chosen. PANI has long been condemned for its poor cyclic stability, despite its strong advantages such as good resistivity, electrical conductivity, and especially pseudocapacitance [3].

This work describes the improvement of cyclic stability of PANI through a combination of reduced graphene oxide (rGO) and copper-metal-organic framework (MOF). Crystalline porous MOFs as organic units that link metal ions to clusters are characterized by a large surface area, high stability, large pore volume, and organic functionality and these properties predetermine them for the preparation of the electrode in supercapacitors [4]. Many articles have been written and even more, work has been done using carbon materials. Graphite aroused great interest, especially after its discovery. Its oxidized form - graphene oxide (GO) offers a wide range of uses in different fields of interest. Compared to pure graphite, GO is more reactive due to the oxygen functional groups on its surface and edges, but it is also less conductive. However, this can be remedied by reducing it and decreasing the oxygen content [5,6].

In this study, the composites of rGO, PANI, and Cu-MOF were prepared via the one-step co-assembly method, i.e., PANI was supported on the composite structure of rGO and Cu-MOF via chemical polymerization process. The properties of the prepared electrode materials were examined by X-ray diffraction techniques (XRD), ATR-FTIR spectroscopy, scanning electron microscope (SEM), and X-ray Photoelectron Spectroscopy (XPS). The first results showed a combination of composite hardening as promising.

Acknowledgements

This work was supported by the M-era.Net 2019 call project "LiBASED Li-ion BAttery-SupErcapacitor Hybrid Device" grant No. M-ERA.NET 2/2019/966/LiBASED from Slovak Academy of Sciences and International mobility of TBU researchers in Zlín, grant No. CZ.02.2.69/0.0/0.0/16_027/0008464.

References

C. Xu, B. Xu, Y. Gu, Z. Xiong, J. Sun, X.S. Zhao, Energy Environ. Sci. 6 (2013) 1388.

N. Kumar, P.K. Sahoo, H.S. Panda, Energy Technol. 5 (2017) 253–266.

H.P. Cong, X.C. Ren, P. Wang, S.H. Yu, Energy Environ. Sci. 6 (2013) 1185–1191.

Z. Wang, J. Huang, Z. Guo, X. Dong, Y. Liu, Y. Wang, Y. Xia, Joule. 3 (2019) 1289–1300.

 ISBN 978-80-8152-941-2

Pei S, Cheng HM., Carbon N. Y. 50(9), (2012), 3210–3228.

N. Kumar, P.K. Sahoo, H.S. Panda, Energy Technol. 5 (2017) 253–266.

 ISBN 978-80-8152-941-2

Carbonized MIL-101(Fe)-NH_2 as sulphur host for Li-S battery

D. Capková[a]*, T. Kazda[b], M. Almáši[c], N. Király[c], A. Straková Fedorková[a]

[a]Department of Physical Chemistry, Faculty of Sciences, Pavol Jozef Šafárik University in Košice, Moyzesova 11, 041 154 Košice, Slovak Republic
[b]Department of Electrical and Electronic Technology, Faculty of Electrical Engineering and Communication, Brno University of Technology, Technická 10, 616 00 Brno, Czech Republic
[c]Department of Inorganic Chemistry, Faculty of Sciences, Pavol Jozef Šafárik University in Košice, Moyzesova 11, 041 154 Košice, Slovak Republic
*dominika.capkova@upjs.sk

Carbonized metal-organic framework (MOF) MIL-101(Fe)-NH_2 was used as a host for sulphur in lithium-sulphur batteries. MOF effectively captured and encapsulated sulphur and lithium polysulphides. Consequently, the cathode showed at 0.5 C high initial discharge capacity of 705 mAh g^{-1} and after 200 cycles of 476 mAh g^{-1}, with fading rate of 0.162 % per cycle. Columbic efficiency during the whole cycling procedure at 0.5 C was around 95 %.

Introduction

The demand for high energy density batteries has increased in the last decade, mainly by electric vehicles, portable electronic devices and military applications. Commercial lithium-ion batteries can not satisfy the energy density for such extensive applications [1, 2]. Lithium-sulphur (Li-S) batteries represent a very promising battery energy storage because of their high theoretical specific capacity (1675 mAh g^{-1}) and energy density (~2600 Wh kg^{-1}) [3]. The main advantages of sulphur are nontoxicity, natural abundance, as a cathode material might reduce the battery cost and environmental concerns [4].

Nevertheless, Li-S battery system has some obstacles that block the successful commercial production. Sulphur and discharge products (Li_2S/Li_2S_2) must overcome low conductivity at the insulator level. The cathode material must contain conductive material and the amount of active material reduced. Next drawback is the volumetric expansion during cycling up to 80 %, which leads to instability of the electrode structure [5]. A lower-order (Li_2S, Li_2S_2) and a higher-order (Li_2S_4, Li_2S_6, Li_2S_8) polysulphides are produced during cycling. The higher-order polysulphides are soluble in the organic electrolyte, which leads to irreversible loss of capacity. A migration process of polysulphides is known as polysulphide shuttle; the higher polysulphides diffuses to lithium anode and react cations of lithium, the results of this reaction are lower polysulphides, and they deposit on the lithium anode. Loss of active material, low columbic efficiency and capacity fading are consequences of polysulphide shuttle [6, 7].

A conductive host with high porosity can resolve the issues mentioned above [8]. Porous materials with unique structure containing carbon are metal-organic frameworks (MOFs). MOFs are materials having metal ions on ‘robust’ framework with large surface area, modifiable pores, and cavities [9]. This work deals with application of carbonized MIL-101(Fe)-NH_2 as a host for sulphur in Li-S batteries.

Experimental

The carbonization of MIL-101(Fe)-NH_2 was executed in a tubular oven at 600 °C for 1 hour in a nitrogen atmosphere. Sulfur, carbon Super P and carbonized MIL-101(Fe)-NH_2 were grinded in a planetary ball mill for 30 min at 500 rpm. Electrode material slurry was prepared by stirring of sulfur, Super P, carbonized MIL-101(Fe)-NH_2 and PVDF (polyvinylidene fluoride) in NMP (in N-methyl-2-pyrrolidone). After 24 hours of sttiring the electrodes were fabricated on aluminum foil by a coating bar, dried in the oven at 60 °C for 24 hours and pressed with a pressure of

 ISBN 978-80-8152-941-2

315 kg cm^{-2}. The electrochemical test cells (El-Cell®) were assembled in argon-filled glove box (Jacomex). The electrolyte consisted of 0.25 M of lithium nitrate ($LiNO_3$), 0.7 M of lithium bis(tri-fluoromethanesulfonyl) imide (LiTFSI) solution in 1,2-dimethoxyethane (DME) and 1,3-dioxolane (DOL) with the volume ratio 2:1. As a counter electrode was used metal lithium and electrolyte was impregnated into the glass fiber separator.

Results and Discussion

Electrochemical investigation of the prepared electrode was realized using cyclic voltammetry (CV) and galvanostatic cycling. CV curves of the S + Super P + MIL-101(Fe)-NH_2 + PVDF electrode in a potential window from 1.8 V to 3.0 V measured at a 0.1 mV s^{-1} are shown in Figure 1. Two cathodic peaks and one anodic peak are clearly visible. The first cathodic peak observed at 2.38 V corresponds to the reduction of elemental sulphur to higher-order polysulphides. The second cathodic peak located at 2.0 V is attributed to the transformation of higher-order to lower-order polysulphides and the discharge product. Stable cathodic and anodic peaks indicating fast redox kinetics, optimal cycle stability and better utilization of the active materials.

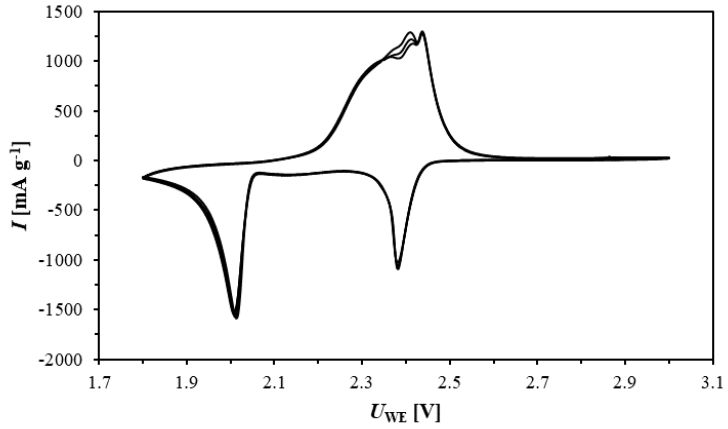

Figure 1 CV curves of the S + Super P + MIL-101(Fe)-NH_2 + PVDF electrode at scan rate 0.1 mV s^{-1}.

Galvanostatic long-term cycling measurements were performed with the S + Super P + MIL-101(Fe)-NH_2 + PVDF electrode at 0.5 C (see Figure 2). The initial discharge capacity reached the value of 705 mAh g^{-1} and after 200 test cycles, the capacity decreased to 476 mAh g^{-1} with a total efficiency of 95 % during the whole cycling procedure. The capacity decay was 0.162 % per cycle, due to strong physical capture of polysulphides. This result indicates that carbonized MIL-101(Fe)-NH_2 possess stable structure and strong chemical interaction with polysulphides, resulting in the efficient encapsulation of the polysulphides in the support.

 ISBN 978-80-8152-941-2

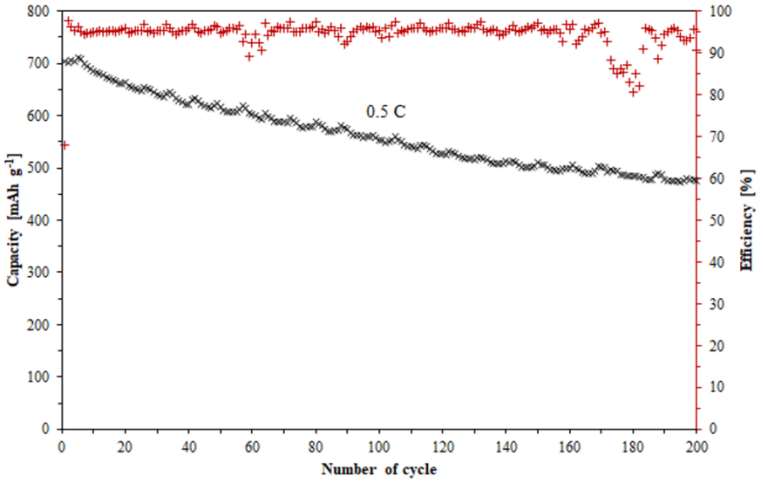

Figure 2 Galvanostatic cycling of the S + Super P + MIL-101(Fe)-NH_2 + PVDF electrode at 0.5 C.

Conclusions

It was proven that carbonized MIL-101(Fe)-NH_2 can be used as a conductive support for sulphur electrodes in Li-S batteries. The unique structure of MOF can efficiently mediate the redox reaction to stable structure of cathode and faster kinetic reaction. The initial discharge capacity at 0.5 C was 705 mAh g^{-1} and after 200 cycles the specific capacity reached the value of 476 mAh g^{-1}, which is 67.6 % of original discharge capacity. The efficiency during long-cycling was around 95 % with fading rate of 0.162 % per cycle. To sum up, it can be concluded that carbonized MOF MIL-101(Fe)-NH_2 is an appropriate support for sulphur and lithium polysulphides. The S + Super P + MIL-101(Fe)-NH_2 + PVDF electrode described in this work is a promising material for application in Li-S batteries.

Acknowledgements

This research was sponsored by project iCoTS No. 313011V334, Innovative Solutions for Propulsion, Power and Safety Components of Transport Vehicles and by specific graduate research of the Brno University of Technology No. FEKT-S-20-6206.

References

[1] J.B. Goodenough, K.S. Park, J. Am. Chem. Soc, 135 (2013) 1167.

[2] E.C. Cengiz, A.A. Hamedani, A.H. Soytas, R. Demir-Cekan, Dalton Trans., 48 (2019) 12598.

[3] X. Ji and F. Nazar, J. Mater. Chem., 20 (2010) 9821-9826.

[4] K. Cao, H. Liu, Y. Li, Y. Wang, L. Jiao, Energy Storage Materials, 9 (2017) 78-84.

[5] Z.W. Seh, W. Li, J.J. Cha, G. Zheng, Y. Yang, M.T. McDowell, Y. Cui, Nature communications, 4 (2013) 1-6.

[6] G. Ma, Z. Wen, M. Wu, C. Shen, Q. Wang, J. Jin, and X. Wu, Chemical Communications, 50 (2014) 14209-14212.

[7] D. Gueon, J.T. Hwang, S.B. Yang, E. Cho, K. Sohn, D.K. Yang, and J.H. Moon, ACS nano, 12 (2018) 226-233.

[8] R.Q. Pang, X. Liang, C.Y. Kwok, L.F. Nazar, Nat. Energy, 1 (2016) 16132.

[9] M. Almasi, V. Zelenak, J. Kuchar, S. Bourrelly, P.L. Llewellyn, Eng. Aspects, 496 (2016) 11.

 ISBN 978-80-8152-941-2

Cathode material based on sulfur-MWCNTs-PPy-nanopipes for Li-S batteries

K. Gavalierová[a]*, A. Straková Fedorková[a], D. Rueda[b], P. Gómez-Romero[b]

[a] Department of Physical Chemistry, Faculty of Science, Pavol Jozef Safarik University in Košice, Moyzesova 11, 040 01 Košice, Slovakia

[b] Catalan Institute of Nanoscience an Nanotechnology, UAB Campus, Bellaterra (Barcelona) 08193, Spain

*katarina.gavalierova@gmail.com

Nowadays, there is a huge demand for energy due to the population growth and technological progress. The researchers pay an intensive attention to the devices able to produce and store energy. Li-S batteries play a significant role in a development of rechargeable batteries. They are attractive adept due to their high theoretical capacity of sulfur (1672 mAh g^{-1}), abundance and non-toxicity of sulfur and low cost of sulfur. Li-S battery belongs to the conversion type of battery; it means new chemical compounds during electrochemical reactions are formed [1, 2].

We report the synthesis of S-MWCNTs-PPy-nanopipes as a cathode material for Li-S batteries. The synthesis was accomplished using a simple chemical oxidative polymerization of pyrrole monomer by adding the anions azo dye methyl orange (MO) and $FeCl_3$. To characterize the cathode material cyclic voltammetry, galvanostatic charge/discharge measurements or electrochemical impedance spectroscopy were carried out.

As shown in Fig. 1, MWCNTs formed agglomerates among the PPy-nanopipes. Our goal was to accommodate sulfur inside these agglomerates to control volumetric increase during the charge/discharge process. Homogeneous sulfur distribution in PPynanopipes and also in MWCNTs agglomerates was confirmed by EDX elemental map analysis and by TEM. STEM analysis confirmed a presence of sulphur inside the MWCNT tube. The improved electrochemical performance of S-MWCNTs-PPy-nanopipes was attributed to the stable network between the sulfur and MWCNTs-PPy-nanopipes that effectively facilitates Li^+ ion diffusion which inhibited shuttle effect. Combination of PPy-nanopipes and MWCNTs provides additional conductivity and delivers extra capacity.

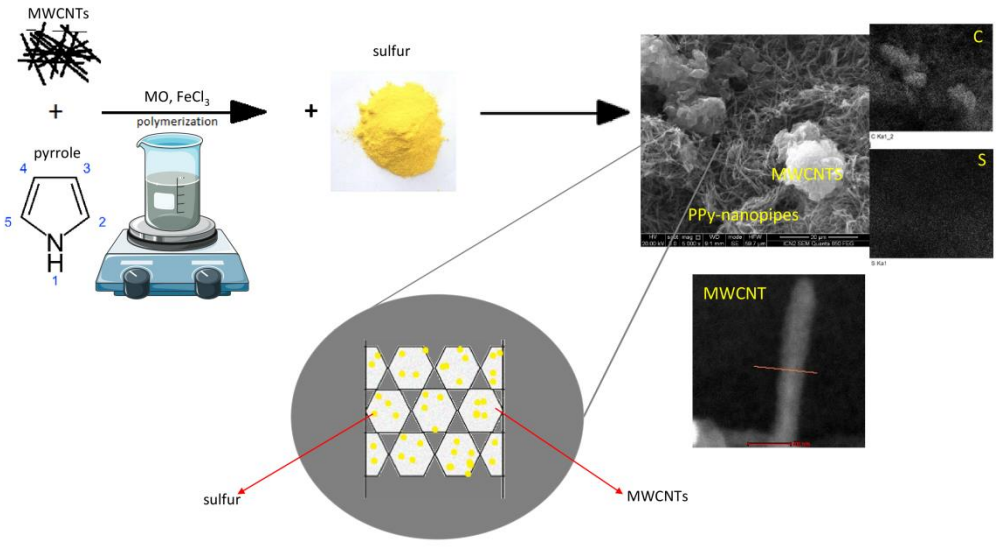

Figure 1 Schematic representation of sample preparation and characterization, SEM image and elemental map of carbon and sulfur distribution for S-MWCNTs-PPy-nanopipes sample.

ISBN 978-80-8152-941-2

Acknowledgements

This research was sponsored by the NATO Science for Peace and Security Programme under grant 985148 and by the project VEGA 1/0074/17.

References

[1] Y. Yin, S. Xin, Y. Guo and L. Wan, Angewandte Chemie, 52, (2013) 13186.

[2] A. Strakova Fedorkova, T. Kazda, K. Gavalierova, P. Gomez-Romero and E. Shembel, Int. J. Electrochem. Sci., 13, (2018) 551.

 ISBN 978-80-8152-941-2

Carbon fibers modified with cobalt phosphide nanoparticles as efficient electrocatalysts for hydrogen evolution

A. Gubóová [a]*, R. Oriňaková[a], M. Strečková[b], J. Shepa[a]

[a] Department of Physical Chemistry, Faculty of Science, P.J. Šafarik University in Košice, Moyzesova 11, 041 54, Košice

[b] Institute of Materials Research, Slovak Academy of Sciences, Watsonova 47, 040 01 Košice

*alexandra.guboova@student.upjs.sk

Hydrogen, as a renewable and clean energy source, is proposed as a potential fuel candidate for the future due to its high gravimetric energy density and environmental friendliness [1]. Electrochemical water splitting is a simple, clean, and convenient method of producing hydrogen, but its sustainable production is highly dependent on efficient and inexpensive catalysts. However, commonly used catalysts such as platinum or other noble metals are relatively expensive, therefore great emphasis is put on finding a suitable substitute [2].

Needle-less electrospinning technology (NLE) was used to prepare carbon fibers based electrocatalysts modified with cobalt phosphide nanoparticles. Two cobalt salts, nitrate $Co(NO_3)_2$ and oxalate CoC_2O_4, were used as cobalt sources. Co_2P nanoparticles are considered as the most active among transition metal phosphides with high catalytic efficiency. The fibers were heat treated in controlled sintering furnace in argon atmosphere or in argon atmosphere followed by hydrogen reduction atmosphere. SEM images revealed a continuous and regular fibrous morphology (fiber diameter 1-10 μm). The apparent porous structure was evident in both cases of used atmosphere (Ar and Ar/H_2), however, the change in the sintering method determined different porosity in the carbon fiber matrix. While the use of pure argon atmosphere caused a higher value of internal microporosity with isolated pores, the hydrogen environment led to the formation of surface micropores. The design of carbon fibers with incorporated Co2P nanoparticles for samples with highest cobalt content is shown in Fig. 1. Electrocatalytic activity was evaluated by polarization curves. The most significant potential shift to more positive values was observed for samples with the highest cobalt content (3g), which provided the current density of 10 mA cm^{-2} at an overpotential of −300 mV. The Tafel slopes were calculated form the Tafel plots derived from the polarization curves. The smallest Tafel slope and fastest HER kinetics were found in the samples with highest cobalt content and highest specific surface area. The durability and stability of the most effective fibrous catalysts was proved by means of long-term stability tests.

 ISBN 978-80-8152-941-2

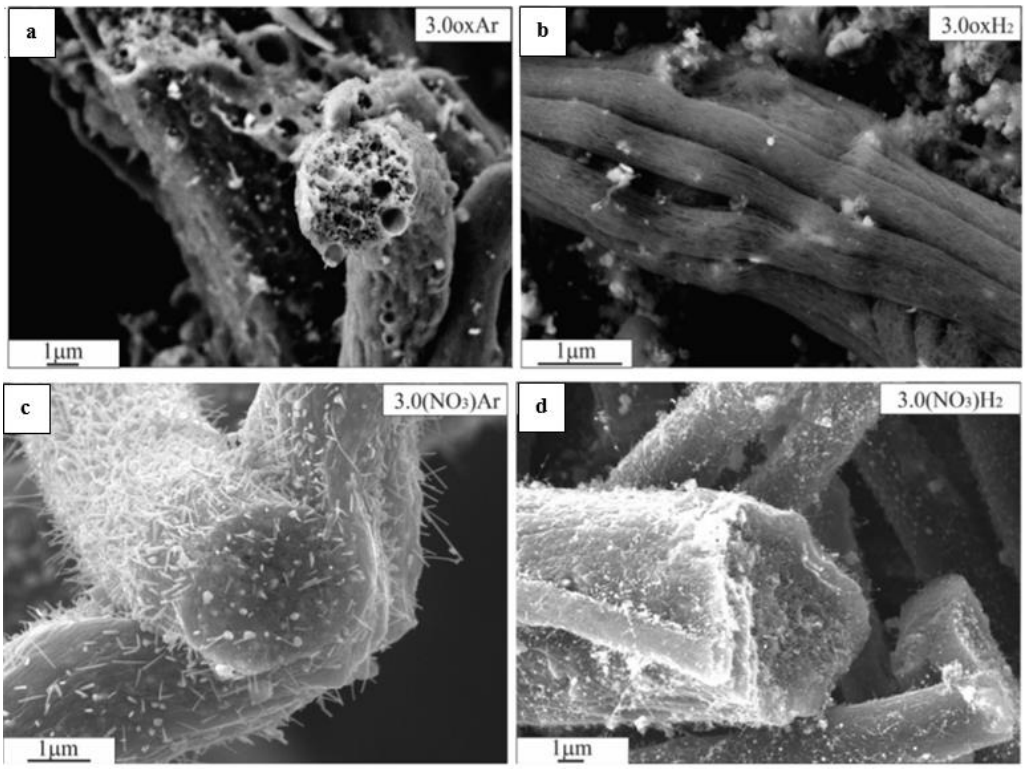

Figure 2 SEM images of carbon fibers with incorporated Co_2P nanoparticles prepared from 3.0 g Co(II) oxalate/30 ml DMF (a, b) and 3.0 g $Co(NO_3)_2$/30 ml DMF (c, d).

Acknowledgement

This work was supported by Grant Agency of Slovak Academy of Sciences, projects No. VEGA 2/0036/20, 1/0074/17 and Slovak Research and Development Agency under the contract no. APVV 15- 0115.

References

[1] A.P. Murthy, J. Madhavan, K. Murugan, J. Power Sources. 398 (2018) 9–26.

[2] T.R. Cook, D.K. Dogutan, S.Y. Reece, Y. Surendranath, T.S. Teets, D.G. Nocera, Chem. Rev. 110 (2010) 6474–6502.

 ISBN 978-80-8152-941-2

Electrode materials for post-lithium ion batteries based on advanced carbon structures

T. Kazda [a]*, D. Škoda[b]

[a]Department of Electrical and Electronic Technology, Faculty of Electrical Engineering and Communication, Brno University of Technology, Technická 10, 616 00 Brno, Czech Republic
[b]Centre of Polymer Systems, Tomas Bata University in Zlin, Tr. Tomase Bati 5678, Zlin, CZ-76001, Czech Republic
*kazda@feec.vutbr.cz

Today's world is dependent on modern technologies that are related to freely available connectivity by rapid transfer of information from anywhere and also on the fast transport of goods and people. However, transport of people and goods brings the environmental burden caused by the combustion of fuels which is from environmental point of view unsustainable from the long term perspective. Modern communication technologies, on the other hand, work without an internal combustion engine but they need some compact portable source of power. The answer solving both problems are modern Li-ion batteries, which enable the operation of portable devices and the implementation of efficient electrical transport. This technology also has its limits, and in the future, it will be necessary to look for other types of batteries for energy storage. One of the further possibilities of development are post-lithium ion batteries.

Introduction

Modern technologies such as mobile phones, laptops and other wearable electronics would be unfeasible without the use of today's Li-ion battery technologies. In the case of modern technologies in transport such as drones or electromobility, whether personal, freight transport or in the future air transport is need for high energy density batteries even higher. The currently used Li-ion batteries have undergone considerable development in the past years since its introduction into practice [1][2]. Their gravimetric energy density has thus increased more than three times to the current approximately 260 Wh/kg [3][4]. However, some applications will require even higher gravimetric energy densities in excess of 400 Wh/kg. Likewise, dependence on one type of battery using lithium as the active element may lead to a shortage of lithium sources in the distant future. Solutions for the future can be post-lithium ion batteries, which offer in the case of some technologies related to this group a higher gravimetric energy density (Li-S batteries) or independence from the use of lithium (Na-ion batteries) [5]. However, these technologies suffer from a number of problems that limit their lifespan and thus the possibility of future application in practice [6]. One of the groups of materials that can be used to solve the problems connected with this modern battery systems are the so-called metal-organic frameworks. In the following text, will be described their possible application for individual post-lithium ion technologies.

Li-S batteries

Li-S batteries are one of the most promising battery technology from the gravimetric energy density point of view. In addition to the advantage of using cheap and ecological friendly sulfur, they offer the main advantage of high theoretical capacity of the sulfur 1675 mAh/g. Thanks to the working potential against lithium around 2.1 V, it offers a high theoretical gravimetric energy density exceeding 3000 Wh/kg [7]. Main disadvantage of this battery technology is highly limited cyclelife. This is caused by high volumetric expansion of sulfur during battery cycling ~80% and by shuttle effect. Shuttle effect is connected to main electrochemical reactions occur during cycling. Original S_8 during discharging form lithium polysulfides and some part of this polysulfides are soluble in electrolyte which leads to significant capacity drop related to loss of the actime mass from electrode. Those lithium polysulfide are subsequently

 ISBN 978-80-8152-941-2

deposited on the surface of the lithium negative electrode which increase internal resistance and decrease active surface area on the negative electrode [8]. One of the effective method how we can prevent this polysulfide dissolution is their active capture in the mass or in the surface of the positive electrode [9]. One from the effective way to achieve this capture of lithium polisulfides in the electrode structure can be to use metal-organic frameworks [10]. These structures, which combine a carbon porous matrix with metals or their oxides, exhibit a number of interesting properties for Li-S battery application. When carbon-based materials are used as polysulfide scavenger, polysulfides are trapped in the porous structure of the carbon particles [11]. However, this process of the lithium polysulfide capture has its limitations. It was found that polar materials, such as nanostructured transition-metal oxides, sulfides or N-doped materials have high affinity to lithium polysulfides, becouse of the strong interaction between polar species and lithium polysulfides [12][13]. An interesting way to combine these properties of carbom materials and metal oxides is the use of metal-organic frameworks which, after their calcination, form a carbon matrix in which the transition-metal oxides are uniformly distributed. Based on these findings, an MnO/C composite structure obtained by calcination of Mn-Bpdc MOF at 700 ° C under a nitrogen atmosphere was formed. MnO was selected based on its high affinity for lithium polysulfide binding. MnO/C composite was deposit on the surface of the Li-S positive electrode based on 60% sulfur, 30% Super P and 10% poly(vinylidenefluoride) (PVDF). It was observed that MnO/C composite electrode coating leads to improvement of the electrode stability and to better capacity utilization see Figure 1. [14]

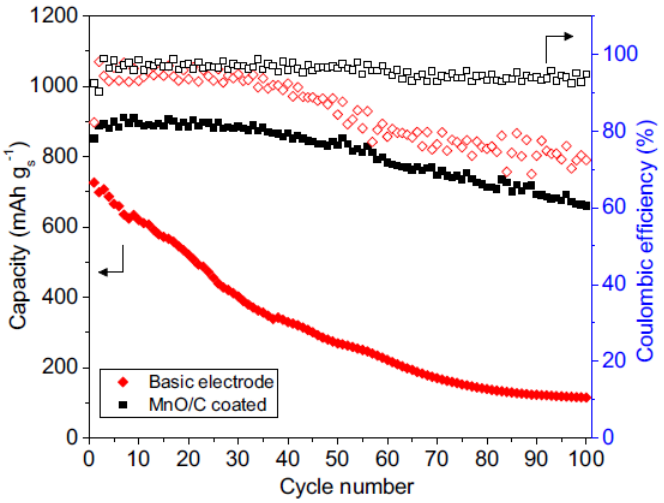

Figure 1 Capacity comparison of basic and MnO/C coated electrode during long-term cycling at 0.2 C [14].

Na-ion batteries

Na-ion battery systems are very attractive because of sodium used as active element. Sodium, the sixth most common material in the earth's crust, is cheap and ecological. Another advantage of sodium usage is the possibility of using aluminum as a current collector on both electrodes. However, sodium has higher potential against standard hydrogen electrode -2.71 V compare to lithium -3.04 V and theoretical capacity of the sodium is significantly lower 1166 mAh/g compare to lithium 3860 mAh/g [15]. These properties limit Na-ion batteries in terms of the achievable gravimetric energy density and which will be lower than in the case of Li-ion batteries. However, this limitation would not be significant for less demanding applications or for stationary energy storage and the main prerequisite for a successful market application would be price and a sufficiently long cycle life. However, the short cycle life of anode materials in particular is one of the main shortcoming of this battery system. Compared to Li-ion batteries, use of the graphite as anode material is in the case of Na-ion batteries not possible. Diameter of sodium ions is about 34% higher compare to lithium ions which leads to decomposition of graphite layers during sodium intercalation and the consequent

 ISBN 978-80-8152-941-2

capacity loss [16]. This is a main reason why the research focuses on the development of anode materials that would have a sufficiently high cycle life and at the same time high capacity. One of the promising possibilities is the use of composite carbon materials combined with metal oxides based on metal-organic frameworks. An example could be the use of the Co-C nanocomposite based on Co-Bpdc MOF after treatment at 800°C in N_2 atmosphere. The Co-C nanocomposite exhibit high electrochemical activity at low potential against sodium and capacity over 200 mAh/g see Figure.2 [17].

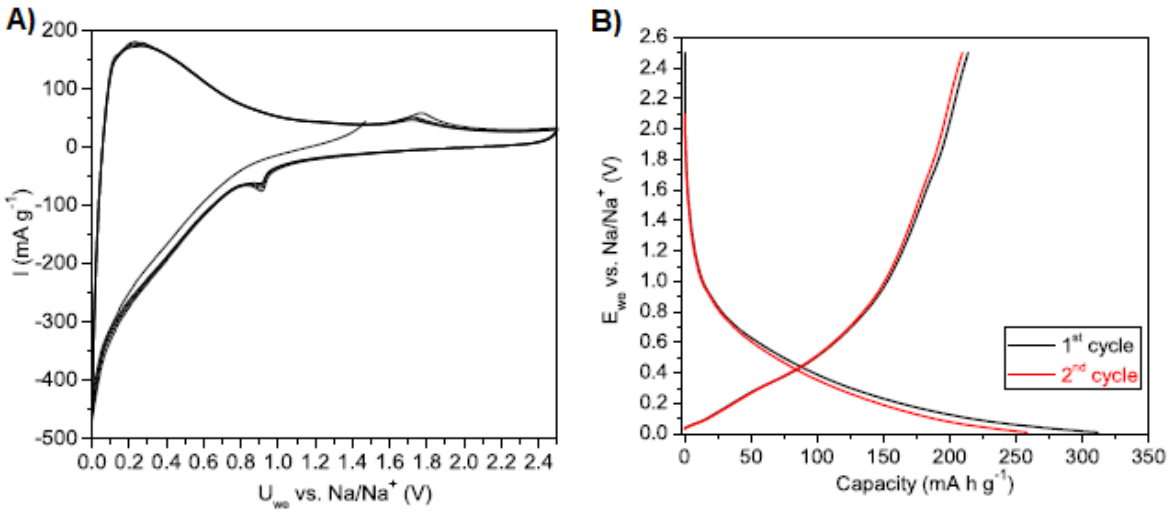

Figure 2 A) CV of the Co-C nanocomposite electrode at scan rate 0.5 mV/s, B) Charg and discharge cycles of the Co-C nanocomposite electrode [17].

Conclusions

This article serves as a brief review of post-lithium ion technologies and the possibilities of using metal-organic frameworks to improve the properties of Li-S and Na-ion batteries. It is clear from the text that different properties of active material are required for each battery technology. However, these properties can be achieved by the correct modification of the active material by selecting the metal or its oxide and if necessary by adjusting the annealing temperature and the used atmosphere.

Acknowledgements

This work was supported by the specific graduate research of the Brno University of Technology No. FEKT-S-20-6206. This work was supported by the Ministry of Education, Youth and Sports of the Czech Republic - Program DKRVO (RP/CPS/2020/006).

References

[1] ADOPTION OF THE PARIS AGREEMENT. In:. Paříž: United Nations, 2015, 21 setkání, FCCC /CP/2015/L.9/Rev.1

[2] Technology Roadmap: Energy storage. 1. Francie: OECD/IEA, 2014.

[3] Kokam_Cell_Brochure_V.4. In: *Kokam* [online]. Korea: Kokam, 2015 [cit. 2019-08-16]. http://kokam.com/data/Kokam_Cell_Brochure_V.4.pdf

 ISBN 978-80-8152-941-2

[4] YOSHINO, Akira. Development of the Lithium-Ion Battery and Recent Technological Trends. Lithium-Ion Batteries. Elsevier, 2014, 1(1), 1-20.

[5] H.D. Yoo, E. Markevich, G. Salitra, D. Sharon, D. Aurbach, On the challenge of developing advanced technologies for electrochemical energy storage and conversion, Materials Today. 17 (2014) 110-121.

[6] J.W. Choi, D. Aurbach, Promise and reality of post-lithium-ion batteries with high energy densities, Nature Reviews Materials. 1 (2016) 1-16.

[7] W. Lu, J.-B. Baek, L. Dai, Carbon Nanomaterials for Advanced Energy Systems: Advances in Materials Synthesis and Device Applications, 1st ed., John Wiley & Sons, USA, 2015.

[8] N. Nitta, F. Wu, J.T. Lee, G. Yushin, Li-ion battery materials: present and future, Materials Today. 18 (2015) 252-264.

[9] Wang Y, Huang X, Zhang S, Hou Y (2018) Sulfur Hosts against the Shuttle Effect. Small Methods 2:1700345.

[10] Wu F, Zhao S, Chen L, et al (2018) Metal-organic frameworks composites threaded on the CNT knitted separator for suppressing the shuttle effect of Lithium sulfur batteries. Energy Storage Mater 14:383–391.

[11] Juhl AC, Schneider A, Ufer B, et al (2016) Mesoporous hollow carbon spheres for lithium–sulfur batteries: distribution of sulfur and electrochemical performance. Beilstein J Nanotechnol 7:1229–1240.

[12] Liu X, Huang J-Q, Zhang Q, Mai L (2017) Nanostructured Metal Oxides and Sulfides for Lithium-Sulfur Batteries. Adv Mater 29:1601759.

[13] Q. Pang, L.F. Nazar, Long-Life and High-Areal-Capacity Li–S Batteries Enabled by a Light-Weight Polar Host with Intrinsic Polysulfide Adsorption, Acs Nano. 10 (2016) 4111–4118.

[14] Skoda D, Kazda T, Munster L, et al. (2019) Microwave-assisted synthesis of a manganese metal–organic framework and its transformation to porous MnO/carbon nanocomposite utilized as a shuttle suppressing layer in lithium–sulfur batteries. Journal of Materials Science 54:14102-14122.

[15] Yabuuchi N, Kubota K, Dahbi M, Komaba S (2014) Research Development on Sodium-Ion Batteries. Chemical Reviews 114:11636-11682.

[16] Nayak PK, Yang L, Brehm W, Adelhelm P (2018) From Lithium-Ion to Sodium-Ion Batteries: Advantages, Challenges, and Surprises. Angewandte Chemie International Edition 57:102-120.

[17] Skoda D, Kazda T, Munster L, et al. (2020) Microwave-assisted synthesis of platelet-like cobalt metal-organic framework, its transformation to porous layered cobalt-carbon nanocomposite discs and their utilization as anode materials in sodium-ion batteries. Journal of Energy Storage 27:1-20.

 ISBN 978-80-8152-941-2

RuO_2-(IrO_2) films for silicon-based photoelectrochemical water splitting

P. P. Sahoo[a]*, M. Mikolášek[b], K. Hušeková[a, c], E. Dobročka[c], J. Šoltýs[c], V. Řeháček[b], L. Harmatha[b], K. Fröhlich[a, c]

[a] Centre for Advanced Materials Application, Slovak Academy of Sciences, Dúbravská cesta 5807/9, 845 11 Bratislava, Slovakia
[b] Institute of Electronics and Photonics, Slovak University of Technology, Ilkovičova 3, 812 19 Bratislava, Slovakia
[c] Institute of Electrical Engineering, Slovak Academy of Sciences, Dúbravská cesta 9, 841 04, Bratislava, Slovakia
*prangya.sahoo@savba.sk

We describe the photoelectrochemical properties of silicon-based metal-insulator-semiconductor photoanodes for water splitting comprising thin RuO_2 and RuO_2-IrO_2 films as top catalytic layers. RuO_2 and IrO_2 offer low resistivity, high optical transparency, work function as well as high catalytic efficiency. RuO_2 and IrO_2 films with a thickness of 5 nm were grown using liquid injection metal-organic chemical vapour deposition, MOCVD. A thin SiO_2 layer was prepared by ozone treatment of the Si-n substrate at 300 °C. These samples were then subjected to photoelectrochemical water splitting reactions.

RuO_2/SiO_2/n-Si photoanode exhibited a photovoltage of 0.5 V and was able to generate photocurrent with a density up to 10 mA/cm^2 (Fig. 1, left) at a thermodynamic water oxidation potential (1.23 V vs. normal hydrogen electrode, NHE) in H_2SO_4, pH=0 solution under 1 Sun light intensity with AM 1.5 spectrum. Lower photovoltages and photocurrents were achieved in Na_2SO_4, (pH=6), and KOH (pH=14) solutions.

55

IrO_2-RuO_2/SiO_2/n-Si photoanode exhibited a lower photovoltage and lower photocurrent compared to the RuO_2 analogue. A photovoltage of 0.4 V and up to 5 mA/cm^2 (Fig. 1, right) photocurrent was achieved for the IrO_2-RuO_2/SiO_2/n-Si photoanode at a thermodynamic water oxidation potential in H_2SO_4, pH=0 solution. Similar to the RuO_2 based silicon photoanodes, these IrO_2-RuO_2 photoanodes achieved lower photocurrent at near-neutral and basic conditions.

The stability of the RuO_2/SiO_2/n-Si photoanode was examined in 1 M H_2SO_4 and 1 M KOH solutions. The RuO_2/SiO_2/n-Si photoanode in the 1M H_2SO_4 solution showed a current density of 10 mA/cm^2 under an applied voltage of 1.23 V vs. NHE. Degradation occurred after 1.5 h of operation. Similar behaviour was observed for an applied bias of 1.5 V vs NHE in 1M H_2SO_4 for the RuO_2 based photoanodes. The RuO_2/SiO_2/n-Si photoanode was found to be more stable in the KOH solution. Using an applied voltage of 0.674 V vs. NHE (0.27 V above the thermodynamic water splitting potential) in 1M KOH resulted in a current density of 2 mA/cm^2 after 10 h. Similarly, stability measurements were performed on IrO_2-RuO_2/SiO_2/n-Si photoanodes in 1 M H_2SO_4 and 1 M KOH solution. In 1M H_2SO_4 solution, at an applied bias of 1.5 V vs NHE (0.27 V above thermodynamic water oxidation potential) a photocurrent of ~20 mA/cm^2 was observed which was stable for 5 h followed by gradual degradation of the photoanode. In 1M KOH solution, at an applied bias of 0.404 V and 0.674 V vs NHE (thermodynamic water oxidation potential and 0.27 V above, respectively) lower photocurrents stable for several hours were observed.

In summary, the RuO_2/SiO_2/n-Si photoanodes provided higher photovoltage and photocurrent and were prone to rapid degradation under solar irradiation whereas the IrO_2-RuO_2/SiO_2/n-Si photoanodes exhibited lower photocurrent and photovoltage but higher stability under studied conditions.

This study was performed during the implementation of the project Building-up Centre for advanced materials application of the Slovak Academy of Sciences, ITMS project code 313021T081 supported by Research & Innovation Operational Programme funded by the ERDF. The research was funded also by APVV (project APVV-17-0169).

 ISBN 978-80-8152-941-2

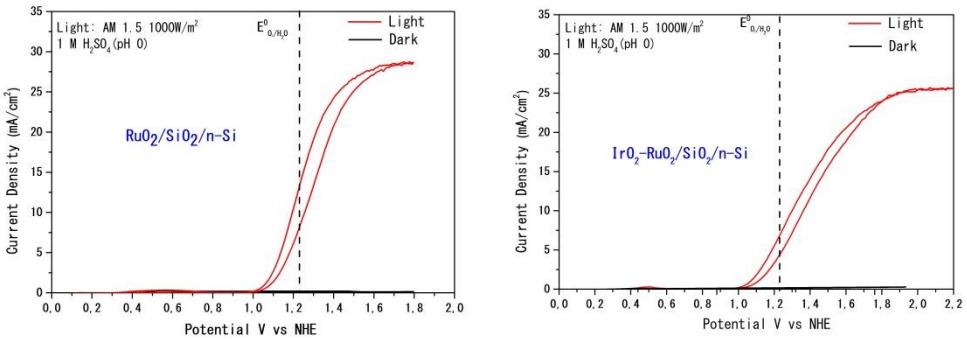

Figure 1 Cyclic voltammetry in dark and under solar light AM 1.5 1000 W/m^2 for (left) RuO_2/SiO_2/n-Si and (right) IrO_2-RuO_2/SiO_2/n-Si MIS structures measured in 1 M H_2SO_4 with pH 0. Dashed line represents the water oxidation potential.

 ISBN 978-80-8152-941-2

Influence of oxide nanoparticles on gel polymer electrolyte based on tetraethyl Ammonium tetrafluoroborate

I. Veselkova[a]*, M. Sedlaříková[a]

[a] Department of Electrical and Electronic Technology, Faculty of Electrical Engineering and Communication, Brno University of Technology, Technická 10, Brno 616 00, Czech Republic
*xgrach00@vutbr.cz

Introduction

The use of solid electrolytes is the ideal way to solve the safety problem of liquid electrolytes, but this advantage comes with a considerably reduced conductivity. To combine the advantages of liquid and solid polymer electrolytes, gel polymer electrolytes have been introduced [1]. Gel polymer electrolytes (GPEs) have a practical interest for the electrochemical power sources because they usually exhibit ionic conductivities higher than 10^{-3} S/cm and have a higher stability than solid and liquid electrolytes [2]. Furthermore, compared to liquid electrolytes, the main advantages of GPEs are their non-leakage nature and higher thermal stability, so they can be used to prepare flexible, thinner, and smaller electrochemical devices [3].

Good mechanical strength of gel polymer electrolyte can be achieved by adding nanoparticles. Generally, the addition of nanoparticles into the polymer electrolyte system slows down the re-crystallization kinetics of polymer chains and reduces the degree of crystallinity. This reduction in crystallinity in turn improves ion transport in the composures [4]. The addition of nanoparticles can improve the conductivity of electrolyte due to the ion interactions and increases the ionic transport at room temperature. Due to this addition, the potential window of electrolyte increases too.

57

Materials

For the preparation of gel electrolytes based on methacrylate, tetraethylammonium tetrafluoroborate (TEA BF_4), ethylene carbonate (EC), diethyl carbonate (DEC), methyl methacrylate (MMA), ethylene glycol dimethacrylate (EDMA) and benzoin ethyl ether (BEE) were chosen.

For the experiments the following nanoparticles were chosen: aluminium oxide (Al_2O_3), tungsten(VI) oxide (WO_3), zirconium oxide (ZrO_2) and lanthanum oxide (La_2O_3) [5]. All nanoparticles and other materials were purchased from Sigma-Aldrich.

Preparation of GPEs

The first step is the preparation of precursor solution. Precursor solution consists of conductive salt, which dissolved in organic solvent. A monomer, a cross-linked agent and an initiator of UV-light polymerization were also added into the precursor [6]. Nanoparticles were added into the electrolyte solution in the amount of 2 wt%.

The second step is determined by obtaining a gel structure. After stirring the solution with all materials, the precursor was exposed to UV irradiation to obtain self-standing gel polymer electrolyte.

Experiment

 ISBN 978-80-8152-941-2

During the experiment gel polymer electrolytes with nanoparticles were prepared. Electrical conductivity was measured by impedance spectroscopy in temperatures from 30 °C to 60 °C.

Figure 1 presents values of electrical conductivity of gel polymer electrolytes, which were measured at room temperature (23 °C).

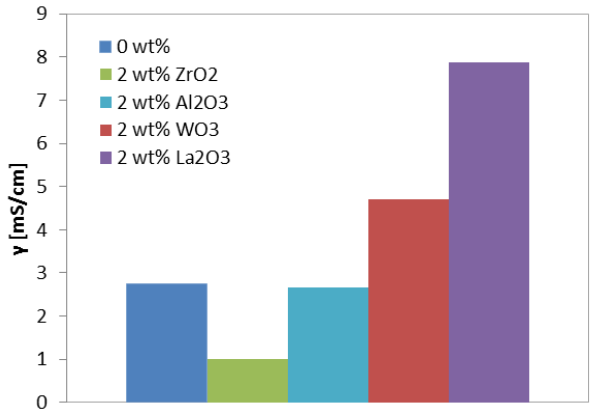

Figure 1 Electrical conductivity of gel electrolytes at room temperature.

Figure 2 presents the Arrhenius plot, which shows electrical conductivity depending on temperature.

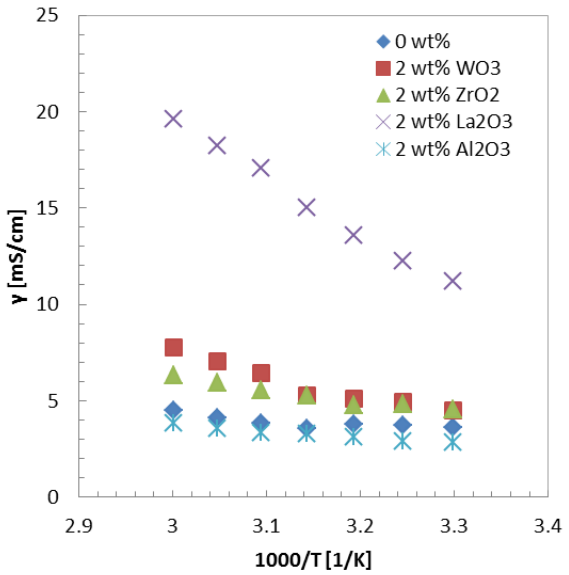

Figure 2 Arrhenius electrical conductivity plot of gel polymer electrolytes.

Conclusion

Current development of this work is focused on improving the electrochemical properties of gel electrolytes based on methacrylate, which will replace liquid electrolytes in electrochemical power sources. The main goals were to increase ion conductivity, and to extend potential window for improving electrochemical stability of the polymer and the

 ISBN 978-80-8152-941-2

solvent. Nanoparticles were added to gel polymer electrolytes in the amount of 2 wt% to achieve these goals. The electrical conductivity depending on temperature and potential windows was measured.

In Figure 1, we can see that the addition of nanoparticles increases the electrical conductivity of gel electrolytes. The highest conductivity has the sample with 2 wt% of La_2O_3. With increasing the temperature from 30 °C to 60 °C, the electrical conductivity of gel samples increases as well. It means that the electrical conductivity of gel electrolytes with nanoparticles has the Arrhenius behaviour. It supports the idea that ions move mainly through the liquid electrolyte phase in these gel electrolytes.

Acknowledgements

This work was supported by the specific graduate research of the Brno University of Technology No. FEKT-S-20-6206.

References

[1] A.M. Stephan, European Polymer Journal. 42 (2006) 21-42.

[2] D.-W. Kim, J. of Power Sources. 87 (2000) 78-83.

[3] Y. Wang, J. Qiu, J. Peng, J. Li, M. Zhai, J. Mater. Chem. A. 5 (2017) 12393-12399.

[4] M. Tripathi, A. Kumar, Ionics. 24 (2018) 3155-3165.

[5] I. Veselkova, M. Jahn, M. Sedlaříková, Nanomaterials: Fundamentals and Applications. (2017) 55-57.

[6] I. Veselkova, M. Sedlaříková, G. Fafilek, C. Gierl-Mayer, ECS Transaction. 1 (2019) 47-55.

 ISBN 978-80-8152-941-2

Atomic layer deposition: basic principles and preparation of thin films for energy applications

K. Fröhlich[a,b]*

[a] Institute of Electrical Engineering, SAS, Dúbravská cesta 9, 841 04 Bratislava, Slovakia
[b] Centre for Advanced Materials Application, SAS, Dúbravská cesta 5807/9, 845 11 Bratislava, Slovakia
*karol.frohlich@savba.sk

Basic principles of atomic layer deposition

Atomic layer deposition (ALD) is chemical method based on a sequential introduction of chemical precursors and reactants. Compared to chemical vapour deposition distinctive and clear feature of ALD lies in the self-limiting nature of precursor adsorption and reaction. ALD growth consists of the four steps: 1) precursor adsorption, 2) purging, 3) reactant exposure and 4) purging. These steps constitute an ALD cycle. ALD takes place in conditions where precursor adsorption is the self-limiting step, i.e. only 1 molecular layer is adsobed at the surface. Theoretically, exposure to reactant gives rise to formation of 1 atomic layer of the reaction product. Consequently, ALD is a surface-controlled process, where parameters other than reactants, substrate and temperature have little influence. ALD cycle for growth of Al_2O_3 film is schematically depicted in the Fig. 1.

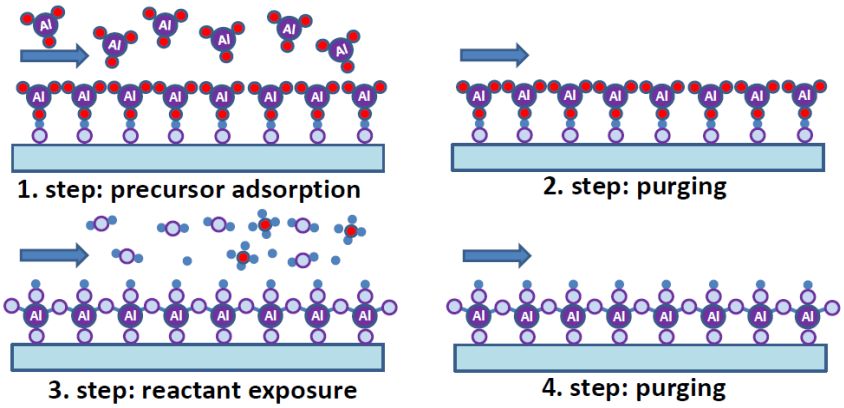

Figure 1 ALD cycle for Al_2O_3 film growth.

Repeating of the ALD cycle results in precise control of thin film thickness. Fig. 2 shows linear dependence of the film thickness on number of cycles. Furthermore, ALD films can be grown at low temperatures, the films are of very good quality without defects such as pinholes. As ALD is surface-controlled process, the films are uniform in thickness on large planar surfaces and highly conformal on 3 dimensional substrates. Excellent analysis of growth of Al_2O_3 films by ALD can be found in ref. [1]. Overview of deposition of various films by ALD was published in 2013 [2].

 ISBN 978-80-8152-941-2

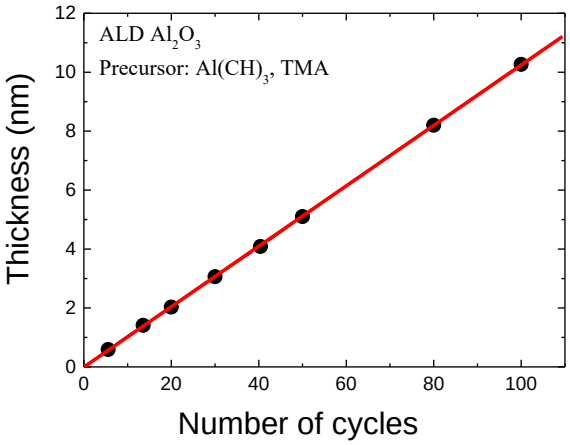

Figure 2 Thickness as a function of number of ALD cycles for Al_2O_3 film growth.

ALD application in microelectronics

ALD prepared films found broad application in microelectronics, in particular in preparation of high-k dielectrics as replacement of SiO_2 gate oxide in CMOS technology [3]. Similarly, ALD was used for growth of high-k thin films in dynamic random access memory (DRAM) applications. We have shown, that dielectric constant of ALD grown TiO_2 can achieve values higher than 100 due to en epitaxial growth of the rutile structure on RuO2 electrode [4]. Another application of ALD in microelectronics includes thin films in resistive switching structures [5, 6]. In vertical structures, resistive switching using ultra-fast pulse of 10 ns was demonstrated. In insulating films in GaN-based metal-oxide-semiconductor high electron mobility transistors substantial suppression of gate leakage current was achieved using 10 nm of ALD grown Al_2O_3 film [7]. ALD films are used in microelectronics due to their high quality, capability to cover large surface with high homogeneity and conformal growth on non-planar substrates.

ALD films for energy application

ALD was employed for preparation of ZnO-based transparent conducting electrodes used in solar cells. Deposition of the Al-doped ZnO films was carried out at temperatures between 150 and 250 °C on Si and quartz substrates. Diethyl zinc and trimethyl aluminium were used as precursors and water vapours as reactant. Al-doping was performed by inserting Al_2O_3 cycles in ZnO growth. Deposition of 1 Al_2O_3 layer per 7 deposited ZnO layers gave the best results. Resistivity of the Al-doped ZnO films depended on the deposition temperature and film thickness. Transition electron microscopy revealed typical columnar growth of the films with fine grained polycrystalline region close to the substrate. The films prepared at 250 °C exhibited 002 texture and for the thickness above 100 nm showed resistivity of 1 mΩcm. This corresponds to the sheet resistance of 40 Ω/square. Fig. 3 displays resistivity of the Al-doped ZnO films deposited at temperatures from 100 up to 250 °C as a function of thickness. Hall measurement revealed electron concentration up to $4*10^{20}$ cm^{-3} and mobility in the range of 10-20 cm^2Vs^{-1}. Optical transmittance of the films was higher than 80% in the wavelength range between 400 and 900 nm for the thickness up to 350 nm.

Inorganic-organic hybrid perovskite solar cells suffer from poor stability in ambient atmosphere. Oxygen and moisture are supposed to be reason for the solar cell degradation. Encapsulation of solar cells using ALD thin films has potential to improve their stability in ambient atmosphere. ALD prepared Al_2O_3 films were employed for encapsulation. Trimethyl aluminium was used as a precursor while water vapours were applied as reactant. Deposition of the Al_2O_3 films was performed at 50°C [8].

 ISBN 978-80-8152-941-2

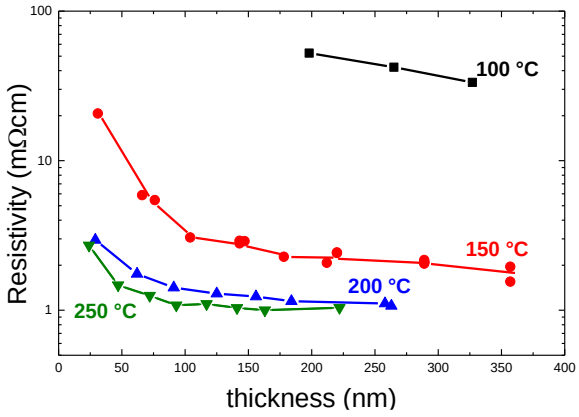

Figure 3 Resistivity of Al-doped ZnO transparent films as a function of thickness for various deposition temperatures.

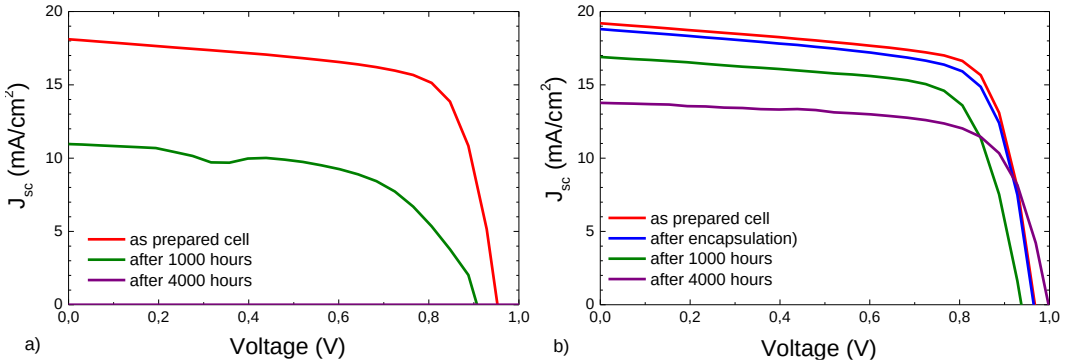

Figure 4. Current-voltage characteristics for a) unprotetected and b) Al_2O_3 encapsulated perovskite-based solar cell.

Power conversion efficiency of the solar cell encapsulated by 25 nm Al_2O_3 thin film decreased after 4000 hours in ambient atmosphere from 13.4 to 9.2%, while unprotected solar cell was completely degraded. Degradation of the unprotected cell was found to be related to the short circuit current density decrease. This indicates degradation of the perovskite layer. Such the perovskite layer deterioration was confirmed by X-ray diffraction.

Potential application of ALD layers emerged recently in improved performance of batteries with electrodes covered by thin films. For Li-S batteries coverage of the sulfur cathode by ultrathin ALD films can effectively suppress the well-known “shuttle effect” rooted in the formation of soluble polysulfides during charge/discharge of the battery [8]. Ultrathin ALD film on grafite anode protects effectively the surface and result in highly durable and safe Li-ion battery [10]. Utilization of thin films in batteries opens another possibility for ALD application in materials for energy.

Acknowledgements

This study was performed during the implementation of the project Building-up Centre for advanced materials application of the Slovak Academy of Sciences, ITMS project code 313021T081 supported by Research & Innovation Operational Programme funded by the ERDF. The financial support of the VEGA project 2/0136/18 is acknowledged.

References

 ISBN 978-80-8152-941-2

R. L. Puurunen, J. Appl. Phys. 97 (2005) 121301.

V. Miikkulainen, M. Leskelä, M. Rittala, R. L. Puurunen, J. Appl. Phys. 113 (2013) 021301.

G. D. Wilk, R. M. Wallace, J. M. Anthony, J. Appl. Phys. 89 (2001) 5243.

K. Fröhlich, M. Ťapajna, A. Rosová, E. Dobročka, K. Hušeková, J. Aarik, A. Aidla, Electrochem. Solid-State Lett. 11 (2008) G19.

P. Jančovič, B. Hudec, E. Dobročka, J. Dérer, J. Fedor, K. Fröhlich, Appl. Surface Science 312 (2014) 112.

B. Hudec, I-T. Wang, W-L. Lai, C. C. Chang, P. Jančovič, K. Fröhlich, M. Mičušík, M. Omastová, T-H. Hou, J. Phys. D: Appl. Phys. 49 (2016) 215102.

D. Gregušová, M. Jurkovič, Š. Haščík, M. Blaho, A. Seifertová, J. Fedor, M. Ťapajna, K. Fröhlich, P. Vogrinčič, J. Liday, J. Derluyn, M. Germain, J. Kuzmik, Appl. Phys. Lett. 104 (2014) 013506.

K. Fröhlich, M. Mikolášek, R. Subair, V. Nadáždy, A. Rosová, E. Dobročka, M. Precner, M. Jergel, E. Majková, 20^{the} Int. Conf. on Atomic Layer Deposition, 29.6-1.7. 2020.

B. Yan, X. Li, Z. Bai, X. Song, D. Xiong, M. Zhao, D. Li, S. Lu, J. Power Sources 338 (2017) 34.

Y. S. Jung, A. S. Cavanagh, L. A. Riley, S-H. Kang, A. C. Dillon, M. D. Groner, S. M. George, S-H. Lee, Adv. Mater. 22 (2010) 2172.

 ISBN 978-80-8152-941-2

Preparation and characterization of the screen printed carbon electrodes modified by zinc nanoparticles for electrochemical insulin determination

F.Chovancová[a*], I. Šišoláková[a], J. Shepa[a], R. Oriňaková[a]

[a] Department of Physical Chemistry, Faculty of Science, Pavol Jozef Šafárik University, Moyzesova 11, 04011 Košice, Slovak Republic
[*]frederika.chovancova1@gmail.com

Insulin is a peptide hormone produced by β cells of small spherical structures called Islets of Langerhans located in the endocrine pancreas [1, 2]. The main function of insulin in the body is to regulate the concentration level of the blood glucose. Insulin also plays role in the regulating the metabolism of fats and proteins. After increasing the glucose concentration in the blood, insulin is produced in the Islets of Langerhans and transported to the cell membranes. Subsequently, insulin activates the insulin receptors located on the cell membrane mainly brain, liver, and muscle cells. This step resulting in a series of other processes, including the activation of GLUT4 transporters, which provide glucose uptake into cells and its subsequent conversion to ATP [3]. Insufficient production of insulin or failure to provide the mentioned mechanism leads to worldwide known disease called diabetes mellitus (DM). Diabetes mellitus is severe and chronic disease represented by hyperglycaemia caused by insulin insufficiency or insulin resistance. In the present several types of diabetes are known. There are three main forms of DM – type 1 DM, type 2 DM, and gestational DM [4]. Type 1 DM is the result of the destruction of β cells and insulin deficiency. It is typical for childhood period because of genetic predisposition. Type 2 DM is typical by insulin resistance or insufficient secretion of insulin [5]. Type 2 DM is caused especially unhealthy lifestyle, obesity and strong family history [6]. Since it is not possible to cure DM completely, it is necessary to focus on the early and rapid diagnosis of this disease, which will be followed by treatment based on insulin administration.

Nowadays, third generation of enzymatic glucose sensors is commercially used of DM diagnosis. The first generation of glucose sensors faced several complications like as high operating potential and oxygen dependents. The second generation of glucose sensors used organic redox mediator for immobilisation of glucose oxidase (GOx) on the sensor surface. The third generation of sensors is based on the direct transport of electrons between GOx and the electrode surface. Nevertheless, third generation of enzymatic glucose sensors are currently used for DM diagnosis they faced various deficiencies like temperature and pH instability arising from the presence of used enzyme [7]. Therefore, research is currently focused on the development of an electrochemical sensor without a biological component. Since the amount of insulin in the blood indirect depends on the amount of glucose, the electrochemical sensor for insulin determination can be considered as the new approach in the diabetes diagnosis.

Currently different analytical methods are used for the detection of insulin. Immune methods include luminescent immunoassay (LIA), radioimmunoassay (RIA), and enzyme immunoassay [7, 8]. High-performance liquid chromatography (HPLC) and capillary electrophoresis (CE) are non-immune methods [7] Unfortunately, these methods are expensive, slow, and time-consuming [1, 2]. Therefore, the electrochemical methods are the most appropriate methods for insulin determination because of their unique properties like high sensitivity, low limit of detection (LOD), good selectivity, low cost and, rapid response [1, 9].

Different studies consider carbon as the most appropriate electrode material for the construciton of electrochemical sensor for insulin determination. However, carbon can be considered as the best electrode material for insulin determination, bare carbon electrodes displayed some disadvatnages like high LOD, not appropriate sensitivity and stability. To improve the analytical characteristics of carbon electrodes various type of nanomaterials for electrode modification are used. Carbon nanotubes (CNTs) are the most often used modification of carbon electrodes because of their unique properties like high conductivity, and mechanical strenght [10]. CNTs are also used because of the

 ISBN 978-80-8152-941-2

enlargement of active surface area of working electrode leading to improvement of analytical characteristics of prepared electrode. Also, metla nanoaprticles like Zn, Ni, Cu or metal oxide nanoparticles (ZnO, CuO, CoO) are used for carbon electrode modification. These nanoaprticles catalyst the insulin oxidation on the carbon electrode surface and improve the characteristics of prepared electrode.

Zinc nanoparticle (ZnNPs) are one of the most suitable candidate for carbon electrode modification because of their low price, biocompatibility, and simple prepration. There is also assumption of covalent bond binding between ZnNPs and insulin leads to better sensitivity of prepared sensors. Therefore combination of MWCNTs, chitosan and ZnNPs was choosen to study the effect for insulin oxidation.

This work deals with the preparation and characterization of the screen printed carbon electrode (SPCE) modified by combination of multi walled carbon nanotubes (MWCNTs), chitosan, and ZnNPs. First, chitosan and activated MWCNTs were ultrasonicated for one hour. After that the 10 µl of this mixture was dropped on the working electrode. ZnNPs were electrochemically deposited on the SPCE modified by mixture of chitosan and MWCNTs using pulse deposition method. The deposition potential was chosen according to polarization curve as – 0.6 V and the deposition time was changed due to the study of the influence of the deposition time of Zn to the surface structure of the prepared electrode. Three different deposition times were used t_1 = 15 s, t_2 = 30 s, and t_3 = 60 s.

The surface morphology of the ZnNPs/chitosan-MWCNTs/SPCEs was characterized by scanning electron microscope (SEM) and the elemental composition of the electrodes surface was studied using EDX analysis. Figure 1 shows SEM images of ZnNPs/chitosan-MWCNTs/SPCE prepared with different deposition times (t_1 = 15 s, t_2 = 45 s, and t_3 = 60 s), respectively. Figure 1 shows that with increase deposition time of Zn a compact Zn layer was gradually formed on the surface of the MWCNTs-chitosan modified SPCE. As can be seen at the deposition time of 60 s, the Zn layer on the surface has already cracked.

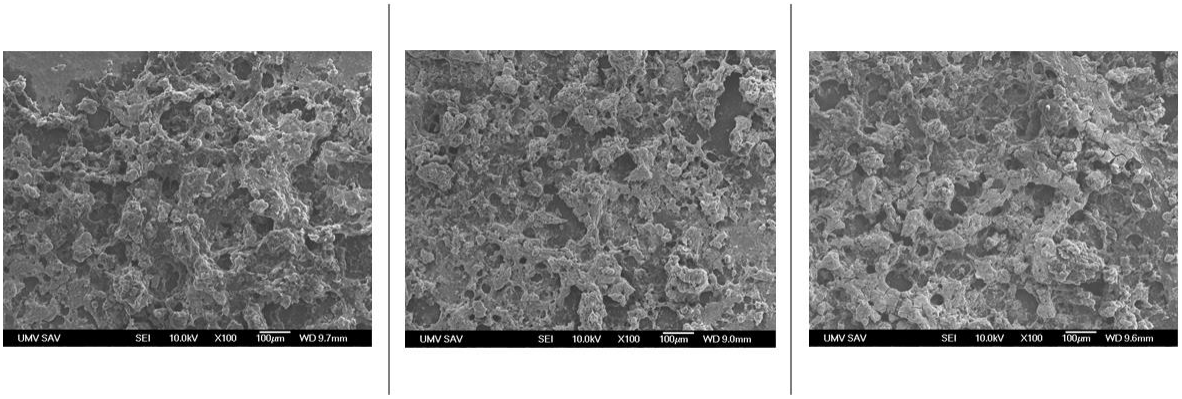

Figure 3 SEM images of ZnNPs/chitosan-MWCNTs/SPCE at 100 times magnification prepared with different deposition times of Zn t_1 = 15 s, t_2 = 30 s, and t_3 = 60 s.

Also the active surface areas of ZnNPs/chitosan-MWCNTs/SPCEs prepared with the different deposition times of Zn were determined electrochemically in solution consisting of 1 mM $K_4[Fe(CN)_6]$/1mM $K_3[Fe(CN)_6]$ and 1 M KCl via cyclic voltammetry method according to Randles-Ševčík equation. The results confirmed the increasement of active surface area with the increase of deposition time of Zn. The highest surface area (0.80 cm^2) was determined for ZnNP/chitosan-MWCNTs/SPCE with the deposition time of Zn t = 30s. The active surface area at the deposition time of t = 60s was lower than in the case of deposition t = 30s due to the formation of a compact Zn layer instead of Zn nanoparticles. Based on the previous results the ZnNPs/chitosan-MWCNTs/SPCE prepared with the deposition time t = 30s of Zn can be considered as the most appropriate for insulin determination. Therefore, stability and long-term stability of this electrode was studied. The current response towards insulin oxidation after 50 cycles decreased of

 ISBN 978-80-8152-941-2

only 3.2% and the current response towards insulin oxidation after one month of the electrode storage decreased of only 2.8% what represents the great value. The selectivity of the electrode was studied in the presence of interferences (glucose, uric acid, and lactic acid) with the same concentration as the concentration of these analysts in the human blood. Obtained results suggest that no significant effect of interferences on electrochemical determination of insulin at ZnNPs/chitosan-MWCNTs/SPCE in blood can be expected. Therefore, ZnNPs/chitosan-MWCNTs/SPCE prepared with the deposition time of Zn t = 30s can be considered after initial tests for electrode characterization as a suitable candidate for future electrochemical sesnor for the diagnosis of diabetes. Therefore, further tests and determined analytical characteristics of the electrode will be performed and a detailed study of insulin determination on the prepared electrode will be obtained.

Acknowledgements

This work has been supported by the projects VEGA 1/0074/17 of the Slovak Scientific Grant Agency, APVV-16-0029 and APVV-PP-COVID-20-0036 of the Slovak Research and Development Agency, and Visegradfund project number 22020140.

References

[1] I. Šišoláková, J. Hovancová, R. Oriňaková, A. Oriňak, L. Trnková, I. Třísková, Z. Farka, M. Pastucha, J. Radoňák, J.Electroanal. Chem. 860 (2020).

[2] I. Šišoláková, J. Hovancová, R. Oriňakova, A. Oriňak, L. Trnková, D. R. García, J. Radoňák, Bioelectrochemistry. 130 (2019).

[3] M. M. Qaid, M.M. Adbelrahman, Cogent Food Agric. 2 (2016) 1-18.

[4] A. M. Egan, S. F. Dinneen, Medicine (Baltimore). (2018) 1-4.

[5] S. M. Blackman, D. W. Cooke, Encycl. Biol. Chem. Second Ed. 1 (2013) 649-658.

[6] S.Y. Tan, J. L. M. Wong, Y. J. Sim, S. S. Wong, S. A. M. Elhassan, S. H. Tan, G. P. L. Lim, N. W. R. Tay, N. C. Annan, S. K. Bhattamisra, M. Candasamy, Diabetes Metab. Syndr. Clin. Res. Rev. 13 (2019) 364- 372.

[7] J. Hovancová, I. Šišoláková, R. Oriňaková, A. Oriňák, Biosens. Bioelectron (2017) 2147-2166.

[8] J. Hu, Y. Yu, M. Guo, M, Yuan, W. Liu, Biosens. Bioelectron. 77 (2016) 215-219.

[9] E. Martínez-Peri˜nán, M. Revenga-Parra, M. Gennari, F. Pariente, R. Mas-Ballesté, F. Zamora, E. Lorezo, Sensors Actuators B Chem. 222 (2015) 331-338.

[10] J. Xu, L. Wang, Elsevier Inc (2019).

 ISBN 978-80-8152-941-2

Electrochemical enzymatic glucose sensors with immobilized glucose oxidase

D. Kondrakhova[a]*, V. Latyshev[a], V. Tomečková[b], V. Komanický[a]

[a] Department of Condensed Matter Physics, Institute of Physics, Faculty of Science, P. J. Šafárik University in Košice, Košice, Slovakia
[b] Department of Medical and Clinical Biochemistry, Faculty of Medicine, P. J. Šafárik University in Košice, Trieda SNP , Košice, Slovakia
*kondrakhova.darya@gmail.com

Tear fluids are easily accessible sampling material which allow diagnostics of not only ophthalmological but also systemic diseases. The composition of tear fluid changes significantly during the presence of a disease. The various noninvasive diagnostic methods help to detect the disease from tear fluid. In our work was developed new noninvasive approaches and techniques in the analysis of tear fluid from patients by cyclic voltammetry using amperometric sensors. Amperometric biosensors are widely used due to their high selectivity and high efficiency. Amperometric glucose biosensors are obtained by immobilizing glucose oxidase molecules on sensor electrodes [1]. To improve the performance of sensors (Au-Pt) onto the sensor's working area, we carried out the immobilization by glucose oxidase and Nafion®. Improving sensor parameters lowers the threshold for glucose detection in tears, which may help identify diseases that are often asymptomatic in the early stages. Also was done the work to fabricate sensors to reduce the used volume of the tears fluid and optimize the geometrics scheme of their realization. This is a very important aspect since the volume of the analyte is limited (is 0,7 μL). In the manufacture of sensors was used, a combination of electron beam lithography and magnetron sputtering.

The cyclic voltammetry method, with the use of a standard three-electrode compound, was applied to test the performance of advanced sensors. Two types of sensors have been compared using the method of cyclic voltammetry: the commercial sensor Au-Pt and the sensor Ag-Pt of our own manufacture. From the measurement of 10 μL of 0.9% saline solution (NaCl) using a reagent-less method (Figure 1).

As can be seen the curves have strong differences. All three redox regions are clearly visible on the graph, obtained from measurements on sensor Ag-Pt. Besides this sensor also has a large working area, which can significantly increase the glucose detection limit. However, it should be noted, that besides the visible advantages, the sensor has very low stability and is deactivated after two or three cycles of work. So, fabricated sensor Ag-Pt can be used for further application only after the improvement electrode adhesion to the glass substrate. Au-Pt sensors have shown correct results in the necessary working areas, and stable performance within several cycles of work. All further measurements were carried out on this sensor.

 ISBN 978-80-8152-941-2

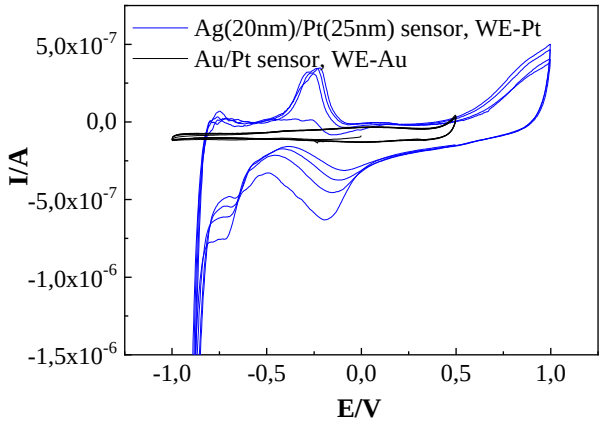

Figure 1 Comparison of CV curves between the commercial sensor Au-Pt and sensor Ag-Pt in measurement of 10 µL 0,9 % NaCl (scan rate: 50 mV s^{-1}).

Also, to evaluate the effect of saline solution on the results of CV measurements the following solutions were measured (Figure 2). The glucose concentration chosen for two cases was: 0,3 mM D - glucose concentration observed in the tears of a healthy person; 9 mM and higher - observed in the tears of patients with diabetes mellitus. Two anodic reaction peaks are observed at -0,1 V and +0,1 V, respectively, for two concentrations of glucose in the NaCl solution, which may indicate that the reagentless method is not informative to measure these samples and requires further improvements.

In this regard, at the second stage, measurements were performed using the Glucose oxidase and Nafion®. Comparative CV curves measured in the presence of Glucose, on standard and modified sensors with GOx, presented in Figure 3. Comparison plots obtained from CV curves from standard and modified sensors show the dependence of the value of glucose concentration. Namely, the effect of glucose concentration on the potential of the anodic peak. In the first case, the peak shifts to the right, in the second case, its value increases.

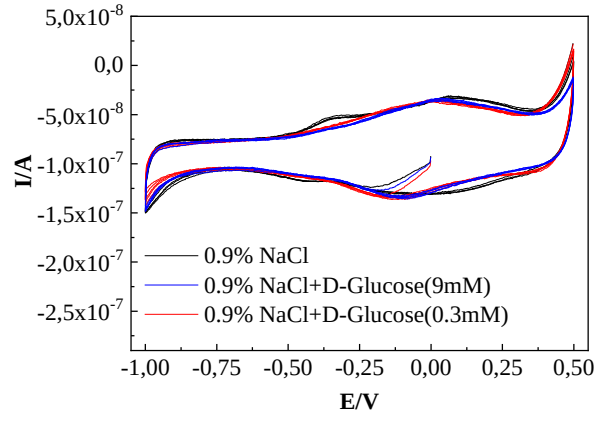

Figure 2 Comparison between CV measured of clear 0,9% s.s. and combined with the presence of 0,3 mM of glucose (healthy people) and 9mM of glucose (people with DM) on the Au-Pt sensor (scan rate: 50 mV s^{-1}).

ISBN 978-80-8152-941-2

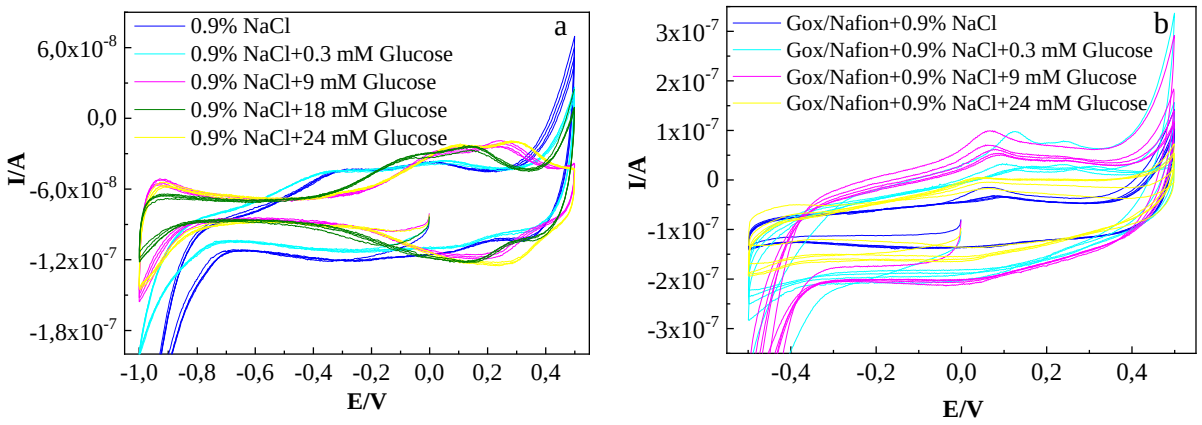

Figure 3 Comparison of CV curves between the commercial sensor Au-Pt (a) and sensor Au-Pt with modified WE (b) in 0,9 % NaCl as the solvent in the presence of 0 - 24 mM glucose (scan rate: 50 mV s^{-1}).

Study of electrochemical measurement of sensor Au-Pt by cyclic voltammetry confirmed the possibility of detecting glucose in solutions at rather low concentrations, which corresponds to the glucose concentrations in human tears. Taking into account the results of cyclic voltammetry, we can assume the possibility of the further use of Au-Pt sensors to study the presence of glucose in tear fluids in various diseases, after their modification using Glucose oxidase and Nafion®.

Acknowledgements

This work has been supported by grant VEGA No. 1/0204/18, the grant of the Slovak Research and Development Agency under contract No. APVV-17-0059 and grant VEGA No. 1/0333/20.

Reference

[1] Artigues M., Abellà J., Colominas S., Sensors (2017) 17 (11), 2620.

ISBN 978-80-8152-941-2

Fabrication of combinatorial materials libraries by flow cell electrodeposition technique

V. Latyshev[a], S. Vorobiov[a], O. Shylenko[a], V. Komanicky[a]*

[a]Department of Condensed Matters Physics, Faculty of Science, P. J. Safarik University,
Park Angelinum 9, 041 54 Kosice, Slovak Republic
*vladimir.komanicky@upjs.sk

High-throughput discovery of electrocatalysts require development both fabrication techniques of materials libraries as well as approaches for their activity screening. Scanning flow cell is a technique which is widely used for rapid screening of electrocatalysts libraries [1-4] but not for their fabrication. Here we propose for the first time to apply the flow cell technique to fabrication of materials libraries on example of Pt-Ni alloy. The idea is to use electrolyte for electrodeposition which contains Pt and Ni salts, instead of electrolyte used for measurements in the flow cell system. In this case, application of the standard electrodeposition technics makes possible the fabrication of the deposits of variable compositions on one substrate.

Electrochemical flow cell was designed with 3D modeling software and then printed from polylactide (PLA) via Prusa i3 3D printer. 3D printing technology is extremely appropriate for the flow cells fabrication because the cells contain small connected channels and openings which are difficult to form by convectional drilling and grinding techniques. The three-electrode configuration of the flow cell was used. The reference electrode was placed in the flow cell as close as possible to the working electrode. Platinum wire, acted like counter electrode, was immersed into a container with an electrolyte. As working electrode, the glassy carbon substrate with dimensions of 5×50 mm was used. The electrolyte for the electrodeposition was a mixture of 0.003 mol/l K_2PtCl_4 + 0.1 mol/l $NiCl_2$ + 0.5 mol/l NaCl (pH = 2.5).

The electrodeposition was performed in the potentiostatic mode. Fig. 1 shows fabricated Pt-Ni combinatorial library consisted of 7 points on a glassy carbon substrate. These 7 points was deposited at different fixed potentials from 0.2 V (vs. Ag/AgCl) to 0.8 V with a potential step of 0.1 V. The concertation of Ni changes from 3 at. % for the first point to 61 at. % for the last point with increasing of Ni content from point to point. Thus, the fabrication of the Pt-Ni material library by the flow cell electrodeposition technique was successfully demonstrated.

 ISBN 978-80-8152-941-2

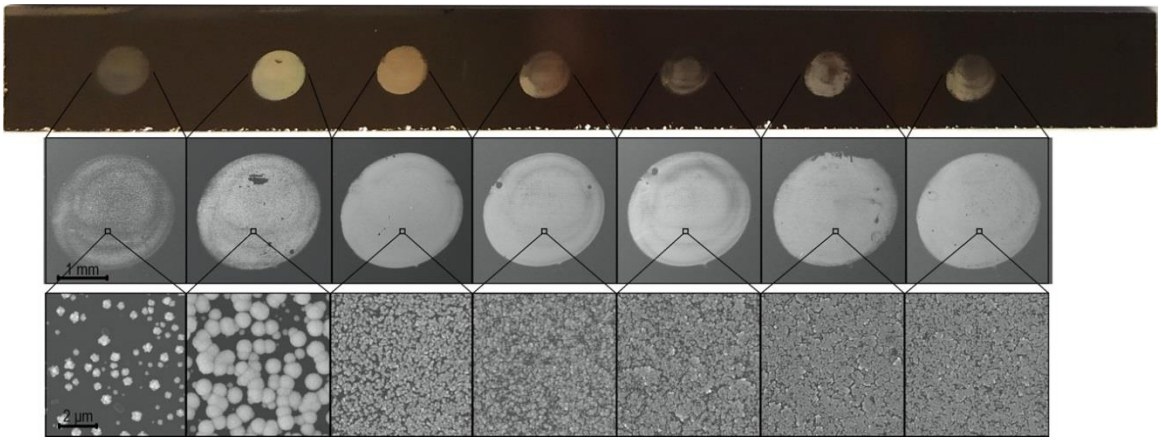

Figure 1 Pt-Ni combinatorial library on glassy carbon substrate fabricated by flow cell electrodeposition technique.

Acknowledgements

This work has been supported by grant 313011V334, Innovative Solutions for Propulsion, Power and Safety Components of Transport Vehicles.

References

[1] S.O. Klemm, J.C. Schauer, B. Schuhmacher, A.W. Hassel, Electrochim. Acta. 56 (2011) 4315–4321.

[2] A.W. Hassel, M.M. Lohrengel, Electrochim. Acta. 42 (1997) 3327–3333.

[3] I. Pötzelberger, C.C. Mardare, L.M. Uiberlacker, S. Hild, A.W. Hassel, Electrocatalysis. 9 (2018) 359–369.

[4] A.K. Schuppert, A.A. Topalov, I. Katsounaros, S.O. Klemm, K.J.J. Mayrhofera, J. Electrochem. Soc. 159 (2012) 670–675.

 ISBN 978-80-8152-941-2

Investigation of changes in AsxSe100-x amorphous thin films after irradiation with visible light and electron beam

O. Shylenko[a], B. Bilanych[b], V. Komanicky[a*]

[a]Faculty of Science, Safarik University, Kosice 04001, Slovakia
[b]Faculty of Physics, Uzhgorod National University, Uzhgorod 88000, Ukraine
*vladimir.komanicky@upjs.sk

Abstract

Chalcogenide glasses have been traditionally used as elements of IR optics devices, optoelectronics, electronic equipment, fiber optic communication devices, and sensitive infrared systems. Irradiation of these materials with light can modify their optical and physicochemical properties. Recently, the possibilities of modifying the surface of chalcogenide films by laser and electron irradiation for the manufacture of diffraction, waveguide, and other elements of integrated optics, optoelectronics, as well as for photo and electron lithography have been demonstrated [1-4]. The modification of the surface of chalcogenide films by a laser beam, based on polarization-dependent photoplastic phenomena, is caused by directional mass transfer. The formation of a photo-induced relief is preceded by the appearance of a periodically ordered charge on the film surface [5]. Similar phenomena of the appearance of a relief on the surface of chalcogenide films are observed upon irradiation with an electron beam [6-8]. It was found that the main role in the modification of the surface of chalcogenide films by the electron beam is played by the processes of charge formation and its transport in the irradiated region [9]. In this work the sensitivity of binary AsxSe100-x systems to irradiation with electrons and light were systematically studied to establish correlations between observed phenomena and structure of these systems. Structural changes in these systems after electron beam irradiation were carefully studied by X-ray absorption fine-structure (XAFS) and extended X-ray absorption fine structure (EXAFS). We also investigated reliefs formed after electron beam irradiation with atomic force microscopy and kelvin force microscopy.

We find that film sensitivity to electron beam irradiation correlates with electrical conductivity of films. We also find that there is a correlation between sensitivity to electron beam and sensitivity to light.

Acknowledgements

This work has been supported by the grant of the Slovak Research and Development Agency under contract No. APVV-17-0059.

References

[1] J.L. Adam, X. Zhang. Chalcogenide glasses: preparation, properties and applications. Woodhead publishing, 2014.

[2] A.S. Glebov. Semiconducting Chalcogenide Glass III: Applications of Chalcogenide Glasses, 2004.

[3] A. Zakery, S.R. Elliott. Optical nonlinearities in chalcogenide glasses and their applications. Berlin, Springer, 2007.

[4] G.B. Hoffman, W.C. Liu, W. Zhou, R. Sooryakumar, P. Boolchand, R.M. Reano, J. Vac. Sci. Technol. B Microelectron. Nanom. Struct. 26 (2008) 2478–2483.

 ISBN 978-80-8152-941-2

[5] M.L. Trunov, P.M. Lytvyn, P.M. Nagy, A. Csik, V.M. Rubish, S. Kökényesi, Phys. Status Solidi Basic Res. 251 (2014) 1354–1362.

[6] G.B. Hoffman, R.M. Reano, J. Vac. Sci. Technol. B, Nanotechnol. Microelectron. Mater. Process. Meas. Phenom. 30 (2012) 06F301.

[7] K. Tanaka, Appl. Phys. Lett. 70 (1997) 261–263.

[8] G. B. Hoffman et al., Journal of Vacuum Science & Technology B: Microelectronics and Nanometer Structures Processing, Measurement, and Phenomena, 26, 6, 2478-2483, 2008.

[9] V. Bilanych, V. Komanicky, M. Kozejova, A. Feher, A. Kovalcikova, F. Lofaj, V. Kuzma, V. Rizak, Thin Solid Films. 616 (2016) 86–94.

 ISBN 978-80-8152-941-2

Numerical model of multiphase catalytic reactions

M. Mačák[a]*, P. Vyroubal[a], J. Maxa[a]

[a] Department of Electrical and Electronic Technology, Brno University of Technology, Brno 616 00, Czech Republic
*xmacak00@vutbr.cz

Introduction

The catalytic hydrogenation of nitrobenzene (NB) is still one of the most important chemical processes in the synthesis of aniline (AN), which is an important material for production of polyurethanes, rubbers, dyes, or pharmaceuticals [1]. The production can be carried out either in gaseous or liquid phase. The hydrogenation of NB in gaseous phase occurs at higher temperatures and due to worse heat transfer conditions and large volumes of the steam phase, the process is very demanding. These conditions make this process not favourable for current industrial production [1]. On the other hand, gas-liquid-solid systems, which consist of three or four phases offer simpler process due to lower operating temperature and higher heat transfer coefficients, while being able to offer higher volume productivity [2, 3]. Gas and solid phases generally consist of a reacting gas and fine catalyst particles (Pt, Pl, Ru or Ni [1, 2, 3]). The liquid phase acts as a continuous phase, in which solid particles and gas phases are dispersed [3]. This process usually occurs in slurry reactors with suspended catalyst as the fixed bed reactors suffer from uneven flow and heat distribution and local temperature increases [2].

Even though this technology is established, the properties of reactors and are usually only characterised experimentally, which makes it difficult or even impossible to study internal processes. The use of numerical simulations is surprisingly very sparse and limited. Usually, the simulations only investigate the reaction kinetics [4], or they are focused on small-scale applications [5].

This work presents a custom 3D numerical model implemented into Ansys Fluent. The model describes a hydrogenation of NB using a particle catalyst in a gas lift reactor. The model is able to study the effects of the multiphase flow, heat transfer coupled with chemical reactions occurring on the catalyst particle surface.

Chemistry

The reaction mechanism itself is quite complex but can be simplified into two parts. In the first step, AN reacts with H_2, which produces AN and water, which is subsequently evaporated. The second step involves a deep hydrogenation of AN which produces various side products [4, 6]. In this study a production of cyclohexylamine (CHA) has been considered. The ratio between the reactions depends on the temperature and on the concentration of NB, which can adsorb on the catalyst surface and slow down the reaction. As the temperature rises, the side reactions overtake the main reaction, and the quality of the product is decreased.

 ISBN 978-80-8152-941-2

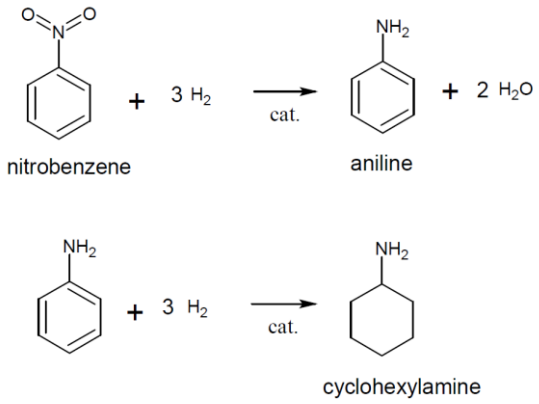

Figure 4 Reaction mechanism. First equation describes the production of AN. Second reaction describes the side production of CHA.

Simulation

In the presented numerical model, the hydrogenation of a liquid nitrobenzene is described as a multiphase reacting turbulent flow. The fluid flow is described by a Eulerian approach in which the transport of every compound (NB, H_2, AN, H_20 and CHA) is governed by an individual Navier-Stokes equation [7]. The effects of turbulence are defined by a two-equation SST k-ω turbulence model. The surface tension between AN and H_2 is also considered, as it can significantly influence the behaviour of the flow. The transport of catalyst particles is defined through a Lagrangian discrete element method, which is governed by an equation of motion [8]. As the active surface of the catalyst particles is much larger than a surface of a discrete sphere with the same diameter, the interaction between the continuum flow and discrete particles is carried out by integrating the number of particles in a control volume to obtain the macroscopic concentration. Then, the influence of the active surface can be incorporated directly into reaction rates, so it is not necessary to model it explicitly. The reaction rates were based on the kinetic model presented by Turek et al. [4], in which the kinetic rate is defined by Arrhenius equation. Additionally, the effects of NB adsorption on the catalyst surface were also considered. The presented simulation studies the governing chemical reactions (Figure) at the injection site of a gas lift reactor. The computational domain consists of a main pipe, in which the bottom opening acts as an inlet for AN with a temperature of 440 K. and a small percentage of NB. Additional NB and H_2 are injected from the side (NB-lower, H_2-higher). The pipe is cooled (wall temperature was set to 373 K), so the temperature does not increase dramatically. The velocity distribution and catalyst particle trajectories are shown in Figure 2.

 ISBN 978-80-8152-941-2

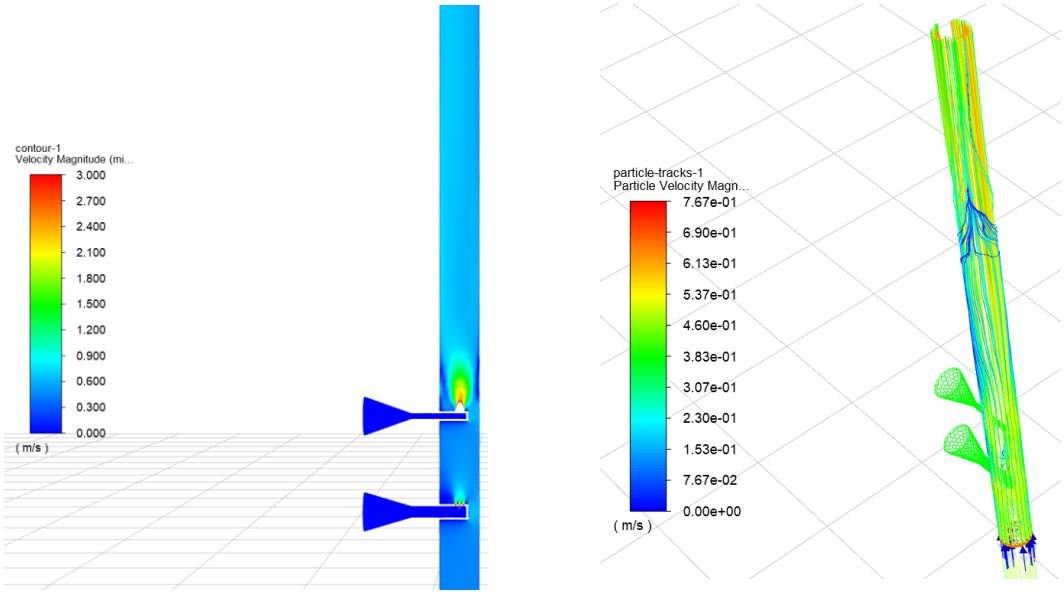

Figure 5 Velocity distribution of the mixture (left). Velocity and trajectory of catalyst particles (right).

The influence of the chemical reaction on temperature distribution in the reactor is shown in Figure 3. Without the reaction, the temperature of AN cools down to 400 K. When the reaction occurs, the temperature of the mixture rises to 440 K.

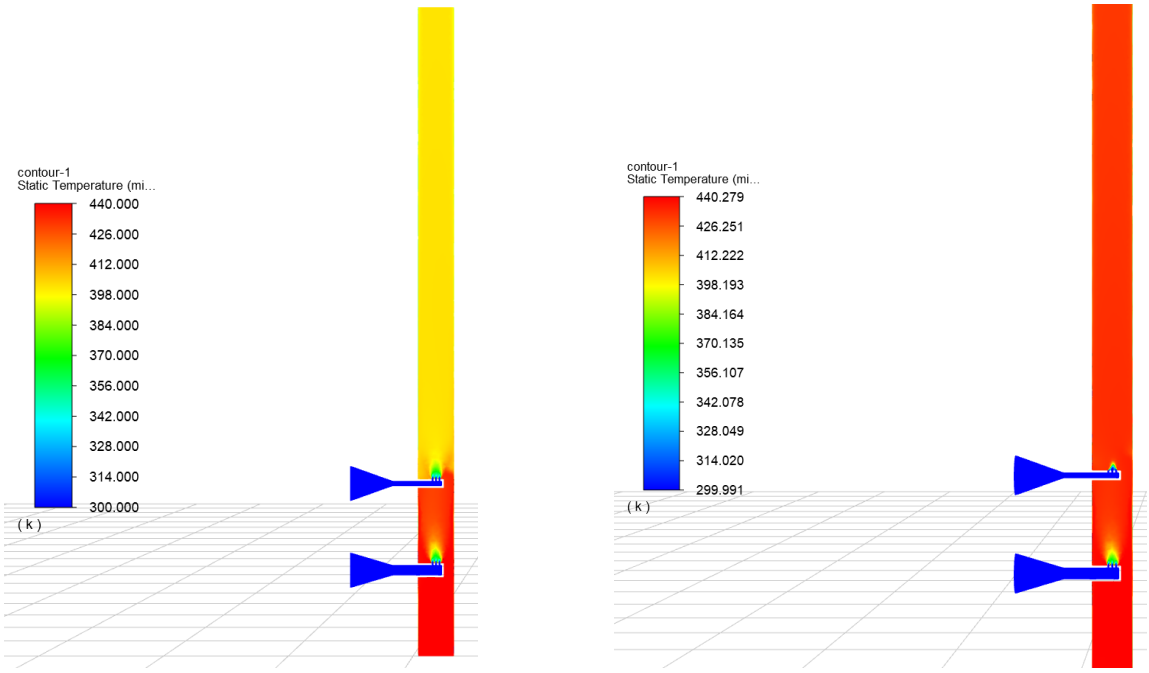

Figure 6 Temperature distribution without the reaction (left) and with the reaction (right).

ISBN 978-80-8152-941-2

Conclusions

The flow characteristics in reactors can influence the mixing of reacting compounds as well as the heat transport and in result, the quality of the final product. The presented numerical model is able to describe the fluid flow as well as the catalytic hydrogenation of liquid nitrobenzene. The model might bring valuable information about the process as these characteristics are difficult to observe experimentally. The application of numerical simulations might lead to improving the design of reactors as well as to improving the quality and efficiency of the production. Additionally, this model can be adjusted and used for any process with catalytic reactions.

Acknowledgements

This work was supported by the BUT specific research program (project No. FEKT-S-20-6206).

References

[1] V. Y. Doluda, A. E. Filatova, E. M. Sulman, V. G. Matveeva, S. P. Mikhailov, A. I. Sidorov, and Y. Y. Kosivtsov, Catalysis in Industry, 11(2) 147-153 (2019).

[2] M. Turáková, T. Salmi, K. Eränen, J. Wärnå, D. Y. Murzin, and M. Králik, Applied Catalysis A: General, 499 66-76 (2015).

[3] D. V. Sharma, A. W. Patwardhan, and V. V. Ranade, Industrial & Engineering Chemistry Research, 56 (6) 1404-1415 (2017).

[4] F. Turek, R. Geike, and R. Lange, Chemical Engineering and Processing: Process Intensification, 20 (4) 213-219 (1986).

[5] Y. Mo, J. Imbrogno, H. Zhang, and K. F. Jensen, Green Chemistry, 20 (16), 3867-3874 (2018).

[6] C. S. Couto, L. M. Madeira, C. P. Nunes, and P. Araújo, Chemical Engineering & Technology, 38 (9) 1625-1636 (2015).

[7] A. Mühlbauer, M. W. Hlawitschka, and H. -J. Bart, Chemie Ingenieur Technik, 91 (12) 1747-1765 (2019).

[8] L. Gallen, A. Felden, E. Riber, and B. Cuenot, Proceedings of the Combustion Institute, 37 (4) 5429-5436 (2019).

 ISBN 978-80-8152-941-2

Catalytic pyrolysis of cellulose catalysed by nanoporous ZnO and ZnO-CuO nanoparticles

N. Podrojková[a]*, J. Patera[b], A. Oriňak[a], R. Oriňaková[a]

[a] Department of Physical Chemistry, Faculty of Science, P.J. Šafárik University, Moyzesova 11, 041 54 Košice, Slovakia

[b] Department of Organic Technology, University of Chemistry and Technology Prague, Technická 5, Prague 6 – Dejvice, 16628 Prague, Czech Republic

*natalia.podrojkova@student.upjs.sk

With rising concerns about energy supply and pollution emerging from the burning of fossil fuels, the attention now is being drifted towards the importance of usage of renewable and clean fuels which include biomass. As an energy source biomass can be used in promising alternative route that includes processes of pyrolysis, gasification, and combustion. Pyrolysis with the use of appropriative catalyst can provide mainly high yields of bio-oils [1,2] at moderate temperatures and shorter vapor residence time, biofuels and various chemicals. Bio-oil as a liquid fuel has many great aspects, which includes low cost and clearly positive CO_2 balance, possibility of utilisation in small-scale power generation systems as well as use in large power stations, storability and transportability, high-energy density compared to biomass gasification fuel and potential of using pyrolysis liquid in existing plants [3-5]. However, bio-oil also has physical and chemical disadvantages such as containment of high oxygen levels which causes instability of bio-oil, corrosiveness, etc. Therefore, appropriative catalysts for production of desirable bio-oil fractions are studied.

In our previous results (Podrojková et al. 2018), we have studied the effect of the crystallinity and morphology of ZnO/2%Cu and ZnO/7%Cu catalysts on the bio-oil composition. Our results showed that different structure of catalyst highly affects the bio-oil yield and composition. Therefore, in this study we focused on the solvothermal synthesis of the porous ZnO nanoparticles doped with CuO and examined prepared nanocatalyst in the catalytic pyrolysis of cellulose with comparison to our previous results.

The pyrolytic degradation of cellulose using Py-GC/MS unit has been studied over nanoporous ZnO and ZnO-CuO nanocatalysts at the temperature range 400–800 °C. Kinetic parameters using differential and integral methods were calculated. The activation energy of ZnO-CuO was lower by 30 kJ/mol from the activation energy of clean ZnO and calculated rate constants showed that cellulose pyrolytic reaction is faster using ZnO-CuO catalyst. Comparison of these results our previous studies of ZnO/2% Cu and ZnO/7% Cu nanocatalysts showed that nanoporous ZnO doped with CuO highly enhanced overall product composition and porous structure of ZnO nanocatalysts has significant effect on the reaction pathways fragmentation and transglycosylation of cellulose degradation.

 ISBN 978-80-8152-941-2

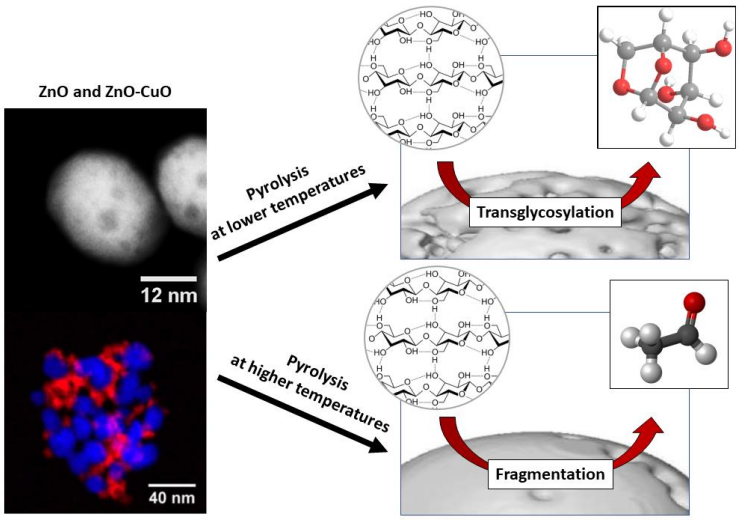

Figure 1 ZnO and ZnO-CuO nanocatalysts and its effect on cellulose pyrolysis at different temperatures.

Acknowledgements

This work was supported by the Internal Scientific Grant System of Faculty of Science of Pavol Jozef Šafárik University in Košice, Slovak republic project no. VVGS-PF-2019-1052 and by Scientific Grant Agency of the Ministry of Education, Science, Research, and Sport of the Slovak Republic project no. VEGA 1/0074/17.

References

[1] J. Grams, A. M. Ruppert, Energies 10 (2017) 1-25.

[2] J. S. Kim, G. G. Choi, Pyrolysis of Lignocellulosic Biomass for Biochemical Production; in: Waste Biorefinery: Potential and Perspectives, Vol. 1 (Bhaskar T., ed.). Elsevier B. V., Amsterdam, page 323.

[3] D. Chiaramonti, A. Oasmaa, Y. Solantausta, Renew. Sustain. Energy Rev. 11 (2007) 1056-1086.

[4] M. Balat, M. Balat, E. Kirtay, H. Balat, Energy Convers. Manag. 50 (2009) 3147-3157.

[5] M. G. Rasul, M. I. Jahirul, W. Science, Recent Developments in Biomass Pyrolysis for Bio-Fuel Production: Its Potential for Commercial Applications Pyrolysis Process Description Pyrolysis classification; in: Recent Researches in Environmental and Geological Sciences, Vol. 1. (Altawell, N., ed.). WSEAS Press, Athens, page 256.

 ISBN 978-80-8152-941-2

DFT calculations of CO_2 activation and conversion on CuO surfaces during heterogeneous catalytic hydrogenation of CO_2

N. Podrojková[a]*, E. Szlapa[b], K. Honkala[b], R. Oriňaková[a]

[a] Department of Physical Chemistry, Faculty of Science, P.J. Šafárik University, Moyzesova 11, 041 54 Košice, Slovakia

[b] Nanoscience Center, Department of Chemistry, University of Jyväskyla, Survontie 9 C, 40500 Jyväskylä (YNC, Ylistörinne), Finland

* natalia.podrojkova@student.upjs.sk

To decrease the carbon dioxide concentration in the atmosphere and reduce its negative effect on the Earth's temperature, various chemical methods are being developed to employ CO_2 as an abundant C1 building block for production of chemicals, materials, fuels or carbohydrates. One of them is hydrogenation, where one of the main products is methanol. To obtain high level of methanol, high chemical stability and activation energy of CO_2 molecule must be overcome. This may be accomplished using efficient catalysts. The main catalysts used in the synthesis of methanol are catalysts based on Cu, ZnO and Al_2O_3 (CZA). ZnO increases life of the catalyst by removing acidic sites in the alumina phase, thereby preventing the conversion of methanol to dimethyl ether. However, CZA catalysts show low activity in the hydrogenation of CO_2 due to the formation of water and the strong hydrophilic character of alumina [1]. The selectivity still needs to be enhanced and the mechanism pathway is not well known either.

The experimental findings can be supported by computational studies to better understand the reaction mechanism and enrich experimental results. Catalyst modelling with computational simulations using quantum mechanics theory has great potential to contribute to the development of highly efficient CO_2 conversion catalysts. At the present, density functional theory (DFT) studies for catalytic CO_2 hydrogenation are becoming very popular. DFT calculations of the CO_2 behaviour on the catalyst surface provides valuable insight into the activation of the C = O bond, information about adsorption and dissociation of CO_2. It can also help to understand the basic steps involved in the hydrogenation mechanism of CO_2, the nature of chemical reaction deeply from the molecular level, study the reaction including every primitive step, then find the pathway of chemical reaction, and eventually find out the key points affecting the reaction rate [2].

For DFT calculations the structure of CuO was used to observe how the oxygen atoms affect the reaction. DFT+U methodology was implemented using GPAW program to describe the CuO cell, calculate the value of the U parameter and to determine the structural parameters and the magnetic moment. For the CuO cell the calculated U parameter value was 8.0 eV which differed slightly from the literature for CuO. Geometry of CO_2 adsorption on the surface of CuO (111) was performed with correction of long-range dispersion interactions, and the results were compared with the literature. It was found that the most energy stable surface of CuO(111) shows a strong adsorption (-95.038 kJ / mol) and compared to the literature this adsorption is stronger. In the case of adsorption of the H_2 molecule, it was found that the whole H_2 molecule is not adsorbed on the surface of CuO(111), the molecule is first cleaved and then hydrogen atoms are adsorbed separately. This structure shows strong adsorption (-91.38 kJ / mol).

Current and future obtained results from DFT calculations will be used and compared with our experimental results of CO_2 hydrogenation using ZnO-CuO core-shell nanoparticles.

 ISBN 978-80-8152-941-2

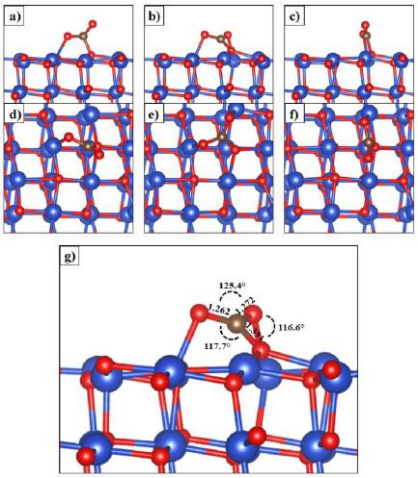

Figure 1 CO_2 molecule adsorbed on CuO (111) surface. The upper figures (a, b, c, g) show side views, while the top view is shown in figures d, e, f. Blue and red colored spheres indicate the surface atoms of Cu and O, while the C atom of the CO_2 molecule is represented by a brown sphere. Figure g shows the bond length values in Angstroms of the structure with the lowest adsorption energy.

Acknowledgements

This work was supported by the Internal Scientific Grant System of Faculty of Science of Pavol Jozef Šafárik University in Košice, Slovak republic project no. VVGS-PF-2019-1052 and by Scientific Grant Agency of the Ministry of Education, Science, Research, and Sport of the Slovak Republic project no. VEGA 1/0074/17.

References

[1] S. Sharamun, et al., Sains Malaisia 47 (2018) 207-214.

[2] D. Weijing et al., Energy Procedia 152 (2018) 997-1002.

 ISBN 978-80-8152-941-2

Thermal decomposition of methane using Pd as a catalyst - Theoretical study

K. Sisáková[a]*, E. Szlapa[b], K. Honkala[b], R. Oriňaková[a]

[a] Pavol Jozef Šafárik University in Košice, Šrobárova 2, 041 80 Košice
[b] Nanoscience Center, Department of Chemistry, University of Jyväskyla, Survontie 9 C, 40500 Jyväskylä (YNC, Ylistörinne), Finland
Slovak Republic
*k.sisakova@gmail.com

Introduction

The use of hydrogen in fuel cells is one of the most energy efficient technologies for the production of hydrogen of the 21st century. Thermal decomposition of methane is one of the most promising and ecological methods for the production of hydrogen, because no carbon oxides are formed.

$$CH_4(g) \rightarrow C(s) + H_2(g) \qquad \Delta H_{298K} = 74.52 kJ/mol \qquad (1)$$

A great advantage of this reaction is also the possibility of using a by-product, which is solid carbon. Depending on the type of catalyst used and the reaction conditions, it is possible to prepare different forms of carbon by this way [1]. However, the thermal decomposition of methane to produce COx-free hydrogen entails several obstacles that need to be overcame. One of the disadvantages of the process is the high temperature at which the reaction takes place. Decomposition of methane without the use of a catalyst takes place at temperatures higher than 1200 ° C. The development of high-efficiency catalysts and the optimization of reactors are essential for the industrial production of TCDs. Catalysts can reduce activation energy and shorten reaction times. Therefore, the selection of a suitable catalyst plays a crucial role in the TCD catalyzed process. Currently, research is mainly focused on Ni-based catalysts, noble metal doped catalysts, carbon catalysts and iron-based catalysts [2]. Another disadvantage is that the carbon formed is adsorbed on the active sites of the catalyst and causes the catalyst to be deactivated. At present, many industrial catalysts consist of Ni or Ni alloys of another metal supported on a suitable support. The main reason for this support is to keep the catalytically active phase in a highly dispersed state. The most important factors influencing carbon deposition during metal-catalyzed methane decomposition are particle size, dispersion, and stabilization of the metal catalyst particles, which can be controlled by selecting a suitable support. In recent years, special attention has been focused on the use of SiO_2 as a support for a suitable catalyst for the process of thermal decomposition of methane. The addition of a noble metal to a nickel-based catalyst, such as palladium, leads to a significant increase in stability and overall hydrogen yields, but modification with other noble metals reduces nickel activity [3].

Due to the complexity of the experimental study of the mechanism of the decomposition reaction at the atomic level and the study of the catalytic activity of various promoters, the theoretical study using the DFT method provides a unique opportunity to examine catalysts without experimental measurements. Currently, most DFT studies of the mechanism of thermal decomposition of methane focus on the study of catalysts based on transition metals - especially palladium. Several articles have been published that focus on comparison of different forms of nanostructured palladium [4]. Some DFT studies of catalysts for the TCD process indicate that defects such as steps are always preferred in the process of TCD dissociation reactions compared to flat surfaces. In other words, dissociation reactions are structurally sensitive. The structural sensitivity, i.e. where the reaction should take place, is largely related to the binding competitive effect, which is determined by the reactant and the metallic valence bond. Also, reactions with high valence reactants are more sensitive to structure compared to reactions with low valence reactants [5, 6].

Material and methods

 ISBN 978-80-8152-941-2

For simulations and modeling of thermal decomposition of methane, it was necessary to prepare and optimize the surfaces of H_2, CH_4, methane radicals and palladium. The general gradient adjustment (GGA), which modifies the functional, is commonly used in catalysis and is referred to as the revised Perdew-Burke-Ernzerhof (rPBE), which uses double numerical plus polarization (dnp). This functional was used in conjunction with FD mode. The basis set was used to balance electron exchange and correlation. The most stable crystallographic surface of palladium (fcc 111) was studied. The basal cell achieved relaxation when the forces applied to each atom were less than 0.05 eV / Å. If the energy after relaxation reached a value > ~ 0.05 eV, a new iteration of the "StrainFilter" relaxation cycle was performed. Monkhorst-Pack k-node lattice with values for x, y and z axes - 4, 4, 1 were used for simulations. To ensure the complete disappearance of the wave function in front of the cell edges, the vacuum is 10 Å on both sides. To allow the relaxation of the two atomic layers, the lower 2 atomic layers were fixed. The grid parameter before optimization was set to a = 3.93Å, which corresponded to the literature. The grid distances were set to 0.18 Å. The base cell was modeled using the ASE program. This basic surface cell (3x3x4) consisted of 36 palladium atoms and four layers. When optimizing the structure, the symmetry constraints were turned off so that the CH4, methane radical and Pd molecules could move in all directions, reorient and thus find their structure with minimal adsorption energy. When modeling the interactions of the adsorbing methane molecule on the palladium surface, the methane molecules and the two palladium surface layers were allowed to relax indefinitely until the residual forces on all atoms reached less than 0.05 eV / Å.

The adsorption energy per 1 molecule can be calculated from the relation:

$$E_{ads} = E_{surface+mol} - (E_{surface} + E_{mol}) \quad (2)$$

where $E_{surface+mol}$ is the total energy of the adsorbate-substrate system; $E_{surface}$ is the energy of the surface cell; E_{mol} is the energy of the isolated CH_4 molecule. CH_4 adsorption was studied taking into account long-range dispersion forces, to correctly describe the interaction between the methane molecule and the palladium surface, where the PBE functional and Tkatchenko-Scheffler correction for long-range interactions were used. The "Nudged elastic band" (NEB) method is a method used to find transit states (and corresponding energy barriers) between given initial and final states. The method involves assembling a "chain" of "replicas" or "images" of a system and releasing them to some extent. This method was used to simulate the cleavage of C-H covalent bonds from a CH_4 molecule. The initial and final structures were optimized as in the case of surface formation.

Results and Discussion

The first step in the calculations and simulations of the TCD process using the DFT method was to optimize the surface of hydrogen and methane and calculate their adsorption energies. The adsorption energy of optimized methane is -23.973 eV and the adsorption energy of hydrogen is -6.704 eV, which corresponds to the literature [5].

The adsorption energy of Pd is -138,815 eV. In order to achieve the most accurate energy value, the grid parameter was also optimized in the values of 3.933 to 3.945 Å. The lowest value of adsorption energy was reached at the lattice parameter a = 3.942 Å. This value was used for surface creation and subsequent optimization. The distance between Pd atoms after optimization was 2.779 Å.

In order to find out how the methane molecule is rotated during adsorption on the Pd surface, several possibilities have been optimized, as can be seen in fig. 1. It was shown that the lowest adsorption energy was achieved by methane, which was placed on the surface of the Pd atoms turned with one hydrogen downwards - towards the surface of Pd. This location corresponds to the literature [5]. The lowest value of adsorption energy was -162.914 eV.

 ISBN 978-80-8152-941-2

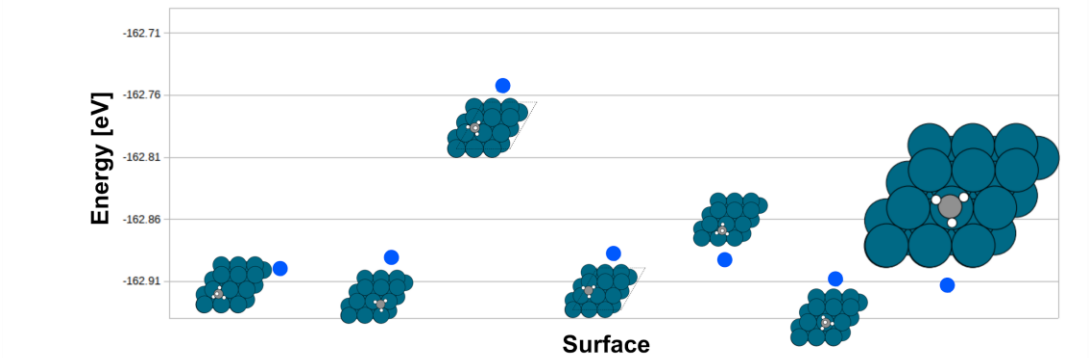

Figure 1 Comparison of the method of rotating the methane molecule during adsorption on the palladium surface.

The activation barrier required to dissociate the first hydrogen bond from the methane molecule was calculated using the NEB calculation method. A comparison of the energies before and after the cleavage of the bond can be seen in fig. 2.

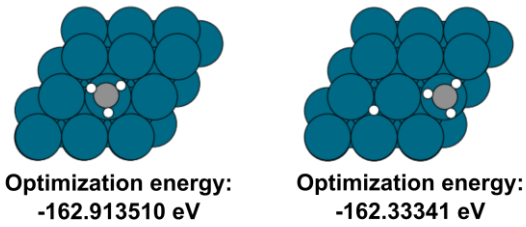

Figure 2 Comparison of energies before and after bond breaking.

The adsorption energy of the system before the cleavage of the hydrogen bond from the methane molecule on the palladium surface was -162.914 eV and after the cleavage of the bond was -162.333 eV. The calculated activation barrier is 0.581 eV for the palladium surface, indicating that from a thermodynamic point of view, this step does not require a large activation energy for dissociation. Arevalo et. al. studied TCD of methane on the surface of nickel and ruthenium, using NEB simulation of DFT calculations [6]. The activation barrier they calculated for the nickel surface was 0.49 eV, while for the ruthenium surface it was 1.10 eV. From the given results we can see that while, from a thermodynamic point of view, the surface of ruthenium requires a high activation energy, on the contrary, the surfaces of palladium and nickel do not need a large activation energy for dissociation. Liu et. al. studied thermal decomposition of methane on the surface of palladium and ruthenium [5]. They calculated activation barrier for the dissociation of the first hydrogen bond from a methane molecule on the palladium surface of 0.3 eV. Compared to the values presented in this work, their value is half lower. Such different values may be due to the use of other calculation methods than in the case of the simulations of Liu et. al., where they used the VASP program with the PW method and in the case of the DFT method they used PBE functional with Dudareva correction instead of the Tkatchenko-Scheffler correction.

Similar to the first methane dissociation reaction on the palladium surface, the structures and adsorption energy were optimized for the other dissociation reactions. The adsorption energy calculated in this work for the CH_3 radical was 1.258 eV, for the CH_2 radical 3.198 eV, for the CH radical 5.655 eV. Kozlov kol. studied various palladium structures

 ISBN 978-80-8152-941-2

for the TCD process. They calculated a value of 1.316 eV for the CH_3 radical, 3.234 eV for the CH_2 radical and 5.731 eV for the CH radical [4]. As already mentioned, these small differences in values can be caused by the use of another calculation program or a different Van der Waals correction.

Conclusion

Using the DFT method, we studied Pd nanoparticles for the TCD process. We used the GPAW program for calculation and simulation, and the ASE program for surface modeling. The implementation of a given program for the study of TCD process brings new possibilities for the study of catalytic surfaces. The results are comparable to current research. Surfaces of methane, hydrogen, palladium and methane radicals were modeled and optimized. In addition, we implemented NEB calculations. We found that activation barrier for the first hydrogen dissociation reaction from the methane molecule on the palladium surface is 0.581 eV. This value is higher than stated in the articles, but these minor differences were due to the use of other calculation methods. The adsorption energy calculated in this work for the CH_3 radical was 1.258 eV, for the CH_2 radical 3.198 eV and for the CH radical 5.655 eV.

Acknowledgements

This work was supported by the Scientific Grant Agency of the Ministry of Education, Science, Research, and Sport of the Slovak Republic Projects No. VEGA 1/0074/17, and the Internal Scientific grant system PF UPJŠ VVGS 2019/1061.

References

[1] J. Qian, T. Chen, L. Enakonda, D. Liu, G. Mignani, J. Basset, L. Zhou, International Journal of Hydrogen Energy 45 (2020) 7981-8001.

[2] S. Takenaka, Y. Shiget, E. Tanabe, K. Otsukaa, Journal of Catalysis 220 (2003) 468-477.

[3] L. Zhou, L. Enakonda, M. Harb, Y. Saih, A. Aguilar-Tapia, S. Ould-Chik, J. Hazemann, J. Li, N. Wei, D. Gary, P. Del-Gallo, J. Basset, Applied Catalysis B: Environmental 208 (2017) 44-59.

[4] S. Kozlov, K. Neyman, Journal of Catalysis 337 (2016) 111-121.

[5] Z. Liu, P. Hu, Journal of the American Chemical Society 125 (2003) 1958-1967.

[6] R. Arevalo, S. Aspera, M. C. Escaño, H. Nakanishi, H. Kasai, Scientific Reports 7 (2017) 2045-2322.

 ISBN 978-80-8152-941-2

Liquid organic hydrogen carriers (LOHC)

K. Sisáková[a]*, A. Oriňak[a], R. Oriňaková[a]

[a] Pavol Jozef Šafárik University in Košice, Šrobárova 2, 041 80 Košice
Slovak Republic
*k.sisakova@gmail.com

Principle of Liquid organic hydrogen carriers

Hydrogen, as a secondary clean energy source, is becoming an efficient energy carrier for wide applications, especially for a future fuel-cell-based automotive industry. Due to the flammable and explosive nature of hydrogen, its storage and transportation with high capacity and energy efficiency under ambient conditions have become one of the technical problem for the development of a "hydrogen economy" [1].

Liquid organic hydrogen carriers (LOHCs) are an interesting option for the storage of hydrogen. Hydrogen storage and release by liquid organic hydrogen carriers (LOHCs) are achieved by a reversible catalytic hydrogenation and dehydrogenation process. Generally, catalytic hydrogenation and catalytic dehydrogenation require different noble metal catalysts. The concept of LOHC is based on the reversible hydrogenation of an unsaturated, usually aromatic, compound. This reaction forms a saturated compound, which is the hydrogen-rich form of the carrier. In a dehydrogenation reaction, the hydrogenated (i.e., hydrogen rich) form releases the hydrogen for further utilization. The hydrogen uptake in the hydrogenation reaction requires elevated pressures of about 30 to 50 bar. The dehydrogenation on the other hand can be operated at ambient pressure but necessitates high temperatures of up to 300 °C. However, during storage time, ambient conditions can be applied to the carrier, without any negative influence on storage density or losses during storage time. This is one of the most important advantages compared to the majority of other hydrogen storage technologies [2].

Several different substances such as toluene, N-ethylcarbazole or other carbazole derivatives have been studied as Liquid Organic Hydrogen Carriers. Due to specific advantageous properties, such as excellent commercial availability, high thermal stability and good hydrogen capacity, dibenzyltoluene (H0-DBT)/perhydro-dibenzyltoluene (H18-DBT) LOHC system is of special relevance for practical and industrial applications [3].

 ISBN 978-80-8152-941-2

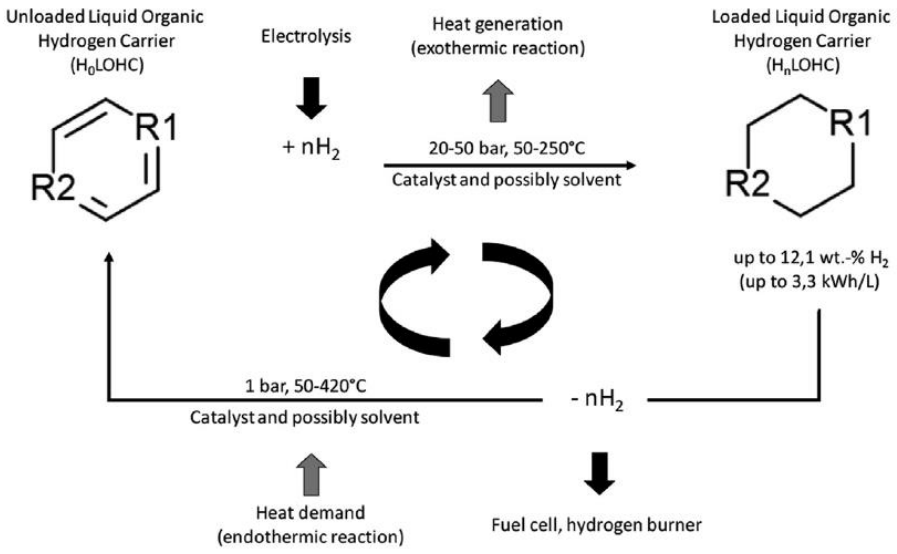

Figure 1 Concept of Liquid organic hydrogen carriers [4].

The design of a LOHC system is dependent on reliable data for substance properties. Important values are for example the enthalpies of the hydrogenated and dehydrogenated form, since the enthalpy of reaction along with heat capacity determines a major part of the energy demand of the process. Data concerning evaporation behaviour can also be crucial since evaporation during hydrogen release influences the energy balance. Furthermore, knowledge about the vapor pressure of the LOHC compounds is important for the removal of traces of LOHC from the hydrogen gas leaving the release unit [5].

The use of catalyst in Liquid hydrogen carriers

Catalysis plays a crucial role within the underlying reaction processes. Hydrogenation of the unloaded LOHC (H_0LOHC) as well as dehydrogenation of the loaded LOHC (H_nLOHC) is typically catalysed. A heterogeneous catalysis is beneficial for such LOHC-storage systems because there is no need to separate the catalyst from the reaction mixture. Thus, it is possible to operate the reactor and the storage tank separately; this might have advantages especially for large systems. Using the right type of catalyst reduces not only the temperature but also the pressure required for the reaction. For example, dehydrogenation temperature for benzene is 300–350 °C (one aromatic ring), for naphthalene 250–300 °C (two fused aromatic rings) and for N-containing heteroaromatics 50–200 °C (from one to three rings). Heterogeneous metal catalysts assist hydrogenation and dehydrogenation in the LOHC systems [17]. For example, hydrogenation of LOHCs with Ru or Ni catalysts takes place at temperatures of 100–250 °C and pressures of 10–50 bar. Hydrogenation of LOHCs is exothermic, and thus excess heat can be recovered, or cooling is needed. Endothermic dehydrogenation is typically catalysed by heterogeneous Pt or Pd catalysts at temperatures of 150–400 °C and pressures below 10 bar. Support is also important for the activity and stability of a heterogeneous catalyst. Homogeneous catalysts typically operate at lower temperatures than heterogeneous catalysts. However, they often require a solvent, and their durability may be modest [6].

Liquid Organic Hydrogen Carriers are able to store hydrogen in a dense and safe form at ambient conditions. While storage of electrical energy in these carrier systems is possible and attractive application, the dynamics of the load profile has been believed to represent a major challenge for this storage technology.

During the past few years, great efforts have been made to promote heterogeneous catalytic dehydrogenation. Screening of different reaction conditions, catalysts, and support materials are attempted to obtain targeted reaction

 ISBN 978-80-8152-941-2

rate and desired product. As heterogeneous catalysts, special attention should be paid to the catalytic stability, which is still poor. Aggregation, leaching, poisoning, as well as the structural change of the nanoparticles and support materials are the main concerns regarding the catalyst deactivation. From the economical viewpoint, the search of nonprecious metal or nonmetal catalysts with comparable catalytic activity to substitute the noble metals, which have shown great performances is required.

Acknowledgements

This work was supported by the Scientific Grant Agency of the Ministry of Education, Science, Research, and Sport of the Slovak Republic Projects No. VEGA 1/0074/17, and the Internal Scientific grant system PF UPJŠ VVGS 2019/1061.

References

[1] K. Müller, K. Stark, V. Emel'yanenko, M. Varfolomeev, D. Zaitsau, E. Shoifet, Ch. Schick, S. Verevkin, W. Arlt, Industrial and Engineering Chemistry Research 54 (2015) 7967-7976.

[2] D. Teichmann, K. Stark, K. Müller, G. Zottl, P. Wasserscheid, W. Arlt, Energy Environ. Sci. 5 (2012) 9044-9054.

[3] G.W. Crabtree, M.S. Dresselhaus, M.V. Buchanan,Phys. Today 57 (2004) 39-44.

[4] M. Niermann, A. Beckendorff, M. Kaltschmitt, K. Bonhoff, Int. J. of Hydrogen Energy 44 (2019) 6631-6654.

[5] T. Sinigaglia, F. Lewiski, M.E.S. Martins, J.C.M. Siluk, Int. J. Hydrogen Energy 42 (2017) 24597-24611.

[6] P. T. Aakko-Saksa, Ch. Cook, J. Kiviahob, T. Repo, Journal of Power Sources 396 (2018) 803–823.

 ISBN 978-80-8152-941-2

Modelling of gamma-valerolactone conversion to hydrocarbons over the metallic surface

E. N. Szlapa[a*], M. M. Kauppinen[a], K. Honkala[a]

Nanoscience Center, Department of Chemistry, University of Jyväskylä, Finland
*ewa.n.szlapa@jyu.fi

Biomass-derived molecules have been receiving a lot of attention as an alternative source of building blocks for organic synthesis. Among them gamma-valerolactone (GVL) has been identified as a platform for production of value-added chemicals due to many possibilities of catalytic functionalization and upgrade [1]. Recently it has been shown that a similar molecule, gamma-nonalactone (GNL) may be converted to desirable biofuel preferentially over Ru/ZrO2 catalysts [2]. The selectivity pattern of GNL conversion hints towards complex reaction mechanism that could be resolved with the support from computational modelling. Our density functional theory calculations, employed to investigate the reaction mechanism of analogous GVL transformation over Ru(0001), suggest that hydrocarbons might be produced preferably following the pathway involving ketone intermediate (yellow route on the figure below). Subsequently microkinetic modelling is used to simulate the reaction rates of a complex GVL transformation and to compare the selectivity towards the three products: ketone, alcohol and alkane, which depends on the temperature, coverage and the effect of co-catalyzing water molecule.

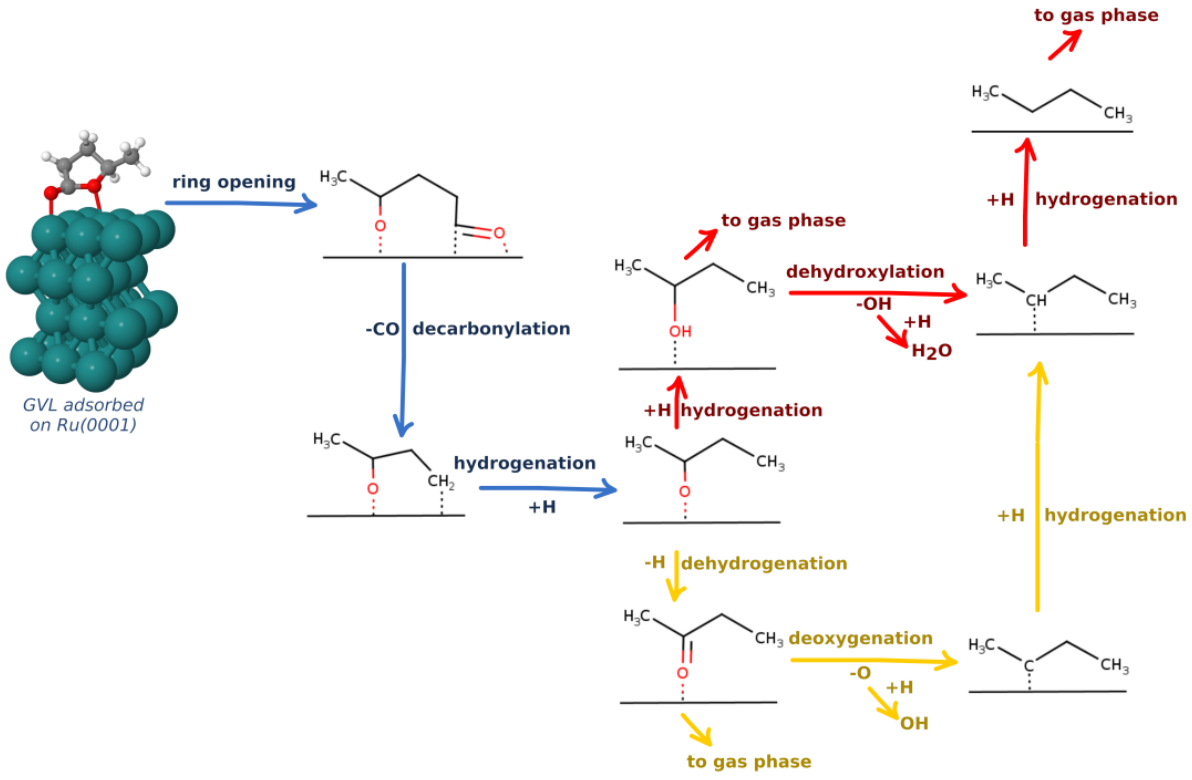

Figure 1 Reaction network of gamma-valerolactone transformation over ruthenium terrace surface towards butane.

 ISBN 978-80-8152-941-2

References

[1] K. Yan, Y. Yang, J. Chai, Y. Lu, Appl. Catal., B ,179, 292–304 (2015).

[2] J. L. González Escobedo, E. Mäkelä, A. Braunschweiler, J. Lehtonen, M. Lindblad, R. L. Puurunen, R. Karinen, Top Catal 62: 724 (2019).

 ISBN 978-80-8152-941-2

The 4th International Conference on Nanomaterials: Fundamentals and Applications

Book of Abstracts

Edited by: Jana Shepa, Ivana Šišoláková

Publisher: Pavol Jozef Šafárik University in Košice
ŠafárikPress

Year: 2020

Pages: 91

Author's sheets: 4,35

Edition: first

ISBN 978-80-8152-941-2

ISBN 978-80-8152-941-2